Available online at www.sciencedirect.com
ScienceDirect
Biochimica et Biophysica Acta 1778 (2008) 1545–1575
Biochimica et Biophysica Acta BBA
www.elsevier.com/locate/bbamem

Review

Protein modulation of lipids, and *vice-versa*, in membranes ☆

Derek Marsh *

Max-Planck-Institut für biophysikalische Chemie, Abt. Spektroskopie, 37070 Göttingen, Germany

Received 19 November 2007; received in revised form 17 January 2008; accepted 19 January 2008
Available online 7 February 2008

Abstract

This review describes: (i) perturbations of the membrane lipids that are induced by integral membrane proteins, and reciprocally, (ii) the effects that the lipids may have on the function of membrane-associated proteins. Topics of the first category that are covered include: stoichiometry and selectivity of the first shell of lipids associated at the intramembranous perimeter of transmembrane proteins; the chain configuration and exchange rates of the first-shell lipids; the effects of transmembrane peptides on transbilayer movement of lipids (flip-flop); the effects of membrane proteins on lipid polymorphism and formation of non-lamellar phases; and the effects of hydrophobic mismatch on lipid chain configuration, phase stability and selectivity of lipid–protein association. Topics of the second category are: the influence of lipid selectivity on conformational changes in the protein; the effects of elastic fluctuations of the lipid bilayer on protein insertion and orientation in membranes; the effects of hydrophobic matching on intramembrane protein–protein association; and the effects of intrinsic lipid curvature on membrane integration, oligomer formation and activity of membrane proteins.

Keywords: Hydrophobic matching; Intrinsic curvature; Elastic bending fluctuations; Non-lamellar lipid; Boundary lipid; Annular lipid

Contents

☆ This review is dedicated to the memory of my colleague László I. Horváth, who passed away on the 29th September 2006.

* Tel.: +49 551 201 1285; Fax: +49 551 201 1501.
E-mail address: dmarsh@gwdg.de.

0005-2736/$ - see front matter © 2008 Elsevier B.V. All rights reserved.
doi:10.1016/j.bbamem.2008.01.015

1. Introduction

This review of the interactions of lipids with integral membrane proteins is concerned not only with the effects of the transmembrane protein on the membrane lipid, but also with reciprocal effects of the membrane lipid environment on the incorporated proteins, particularly their functional activities. A central role is played by the lipid–protein interface, the properties of which are studied extensively by spin-label EPR and fluorescence methods. Protein activities respond to, and are modulated by, the hydrophobic thickness and intrinsic curvature of the lipids at the intramembranous surface of the protein. Reciprocally, the affinities of lipids for the protein depend upon the hydrocarbon chainlength. Protein–lipid interactions that are of longer range also exist, propagated by cooperative lipid–lipid interactions within the bilayer. Embedded proteins extend or modulate the coexistence of gel and fluid domains of membrane lipid, in regions of lateral phase separation. Likewise transmembrane proteins can suppress or control the formation of non-bilayer lipid phases, and correspondingly modulate the tendency to surface curvature of asymmetric membranes. Reciprocally again, elastic lipid bending fluctuations may modulate protein orientation and control incorporation of proteins into the membrane.

The approach given here is principally thermodynamic, but relevant structural and dynamic aspects are also considered. The properties of the lipid–protein interface are considered first, followed by considerations both of longer range effects and functional modulations at the protein–lipid interface.

2. First-shell lipids: stoichiometry and selectivity

Fig. 1 shows the first shell of lipids surrounding the mitochondrial ADP–ATP carrier from a molecular modeling study [2]. These first-shell lipids exchange with those in the surrounding fluid bilayer but are resolved on the timescale of conventional spin-label EPR spectroscopy because their rotational mobility is perturbed significantly at the intramembranous surface of the protein (for reviews see: [3–17]). Thermodynamically, the first shell of lipids is characterised by the number of lipid sites, (i.e., the lipid/protein stoichiometry, N_b), and by the affinities (or relative association constants, K_r) of these sites for different lipids. Both of these quantities can be determined by EPR difference spectroscopy, and the values of K_r may be obtained alternatively by fluorescence quenching methods [18–20].

2.1. Lipid Stoichiometry

Table 1 gives the stoichiometries, N_b, of lipids interacting with a wide variety of transmembrane proteins of different sizes, both

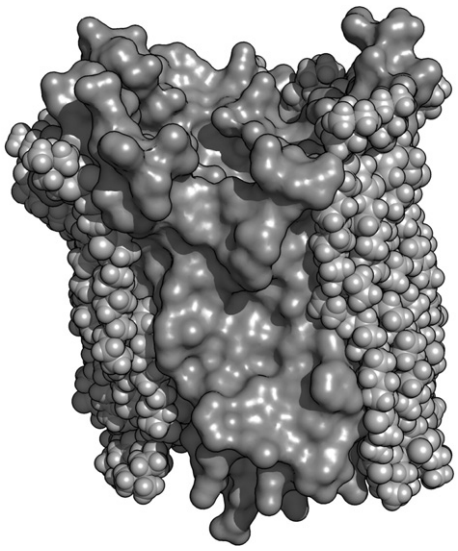

Fig. 1. Van der Waals surface from the crystal structure of mitochondrial ADP–ATP carrier ([1]; PDB: 1OKC), surrounded by a single bilayer shell of N_b energy-minimised di$C_{14:0}$PC lipids [2]. For clarity, only part of the lipid shell is shown — in space-filling representation.

Table 1
Stoichiometries, N_b, of motionally restricted lipids associated with different transmembrane proteins or peptides, including molecular masses, M_r, and predicted or actual number of transmembrane helices, n_α, of the protein

Protein	N_b (mol/mol)	M_rx10^{-3}	n_α	Ref.
Cytochrome *c* oxidase	56±5	204	28	[21]
	55±4	204	28	[22]
Nicotinic acetylcholine receptor	40±7	250	20	[23]
	42±7	268	20	[24]
Cytochrome *c* reductase	38±3	230	13	[25]
Na,K-ATPase, kidney	31.5±1.5	157	12	[26]
Na,K-ATPase, shark	33±3	147	12	[27,28]
Ca-ATPase	22±2	115	10	[29]
	24±5	115	10	[30]
Rhodopsin, bovine	25±3	39	7	[31]
	22±2	39	7	[32]
Rhodopsin, frog	23±2	39	7	[33]
ADP–ATP carrier	25	32.8	6	[34]
Myelin proteolipid	10±2	25	4	[35]
16-kDa proteolipid	5–6	17.5	4	[36]
M13 phage coat protein	4–5	5.2	1	[37]
Phospholamban (PLB)	5.7±0.7	6.12	3.5±0.4[e]	[38]
PLB-A[37]	11.8±0.6	6.08	1 . 1 5 ±0.15[e]	[38]
PLB-A[36,41,46]	7.1±0.2[a]	6.11	1.9±0.1[e]	[39]
	4.0±0.1[b]	6.11	4.9±0.1[e]	[39]
	11.3[c]	6.11	1.0[e]	[39]
	7.8±0.3[d]	6.11	2.2±0.5[e]	[40]
PLB-Δ[1–25]A[36,41,46]	4.0±0.2[a]		5.1±0.6[e]	[39]
	4.0±0.2[b]		5.0±0.5[e]	[39]
	10.1±1.3[c]		1.2±0.2[e]	[39]
	6.0±0.6[d]		3.3±0.4[e]	[40]
Gramicidin A	3.6±0.3	1.88	β[6.3-helix]	[41]
K27, K-channel peptide	2.2	3.16	β-sheet	[42]
K27-Δ[2]	2.5	3.04	β-sheet	[43]
M13 phage coat protein	4	5.2	β-sheet	[44]
OmpA	11	18.90	β-barrel	[45]
OmpG	20	32.78	β-barrel	[46]
FomA	23	40.28	β-barrel	[47]
FhuA	32	80.09	β-barrel	[45]

All values are given per protein monomer.
[a] In diC$_{14:0}$P.C
[b] In C$_{16:0}$C$_{18:1c}$PC.
[c] In diC$_{14:0}$PG.
[d] In diC$_{18:1c}$PC.
[e] Deduced from N_b by using Eq. (3).

α-helical and β-sheet. All of these values are determined from EPR spectra of spin-labelled lipids, mostly phosphatidylcholine.

For an integral protein whose transmembrane sector consists of α-helices, the number of perimeter lipids is related to the total number, n_α, of transmembrane helices. Simple geometrical estimates for helical sandwiches or regular polygons predict the following linear dependence [48,49]:

$$N_b = \pi(D_\alpha/d_{ch} + 1) + n_\alpha D_\alpha/d_{ch} \quad (1)$$

where D_α and d_{ch} are the diameters of an α-helix and a lipid chain, respectively, ($D_\alpha/d_{ch} \approx 2.1$), and $n_\alpha > 1$. Transmembrane α-helical assemblies that are less compact than a regular helical sandwich have larger lipid stoichiometries, corresponding to their relatively larger intramembranous perimeter. For a linear array of helices, for example, instead of Eq. (1), one finds [48]:

$$N_b = \pi(D_\alpha/d_{ch} + 1) + 2(n_\alpha - 1)D_\alpha/d_{ch} \quad (2)$$

which is valid also for $n_\alpha = 1$. In the latter case of a single bitopic transmembrane helix, the number of perimeter lipids is $N_b \approx 10$.

The stoichiometry per monomer is reduced in oligomeric proteins, because lipids are excluded from the monomer–monomer interfaces within the oligomer. Eq. (1) or (2) also applies approximately to protein oligomers, if the monomers are roughly circular in cross-section and are packed in a manner similar to that assumed above for α-helices. Then D is the diameter of the protein monomer and n is the aggregation number. If the oligomer packing is tighter than this and preserves the helical sandwich motif throughout the oligomer, the number of perimeter lipids per protein monomer is given from Eq. (1) by:

$$N_b^{(1)} = (\pi/n_{agg})(D_\alpha/d_{ch} + 1) + n_\alpha D_\alpha/d_{ch} \quad (3)$$

where n_{agg} is the number of monomers per oligomer. This latter equation is used to estimate the degree of oligomerisation of phospholamban, a single transmembrane helix, in Table 1. Another example of reduced lipid stoichiometry arising from protein aggregation is afforded by cephalopod rhodopsin in squid photoreceptor membranes [50].

Fig. 2 compares the lipid stoichiometries determined by spin-label EPR (solid circles) with predictions from molecular modeling that uses the crystal structures of the proteins (open squares), as in Fig. 1. For reference, the geometric predictions of Eqs. (1) and (3) for monomers and hexamers, respectively, are shown by the solid and dotted lines in Fig. 2. Phospholambam is monomeric only for certain mutants, e.g., L37A which disrupts the leucine zipper motif, in which case the stoichiometry of motionally restricted lipid corresponds with that predicted for $n_\alpha = 1$ in Eq. (2). Examples in which a single transmembrane helix appears to present an insufficiently extensive intramembranous surface to produce a

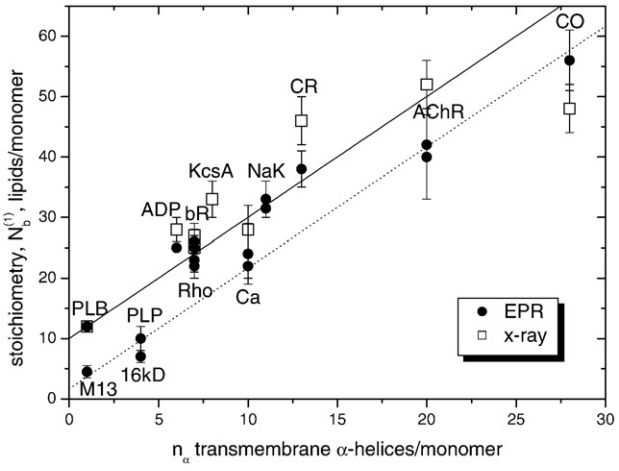

Fig. 2. Stoichiometry, N_b, of first-shell lipids associated with integral proteins as a function of the number, n_α, of transmembrane helices per monomer. Solid circles are the numbers of motionally restricted lipids that are resolved by EPR spectroscopy (see Table 1 for references). Open squares are the numbers of first-shell lipids surrounding the X-ray structure of the protein from model building, as in Fig. 1 [2]. Solid line: prediction of Eq. (1) for helical sandwiches. Dotted line: prediction of Eq. (3) for hexamers ($n_{agg} = 6$). M13, M13 phage coat protein; PLB, L37A mutant of phospholamban; PLP, myelin proteolipid protein; 16 kD, 16-kDa proteolipid from *Nephrops norvegicus*; ADP, ADP-ATP carrier; Rho, rhodopsin; Ca, Ca-ATPase; NaK, Na,K-ATPase; CR, cytochrome *c* reductase; AChR, nicotinic acetylcholine receptor; CO, cytochrome *c* oxidase.

motionally restricted component in conventional EPR include the hydrophobic lung surfactant protein SPC [51], and the synthetic Leu–Ala WALP and KALP peptides [52,53].

For an integral protein with β-sheet transmembrane structure, the lipid stoichiometry can be considerably smaller than that for an α-helical protein of comparable size. This is because the β-strand is a much more extended polypeptide structure than is an α-helix. The number of phospholipids per monomer that can be accommodated at the perimeter of a transmembrane β-barrel protein is given by (cf. [54]):

$$N_b = n_\beta D_\beta / \left(d_{ch}\cos\gamma_\beta\right) \tag{4}$$

where $D_\beta = 0.47$ nm [55] is the interstrand separation, γ_β is the tilt of the β-strands relative to the membrane normal, and n_β is the number of β-strands per protein monomer. Because of the extended structure of the β-strand, a tilt of $\gamma_\beta = 60°$ is required for the same number of apolar residues to be accommodated within the membrane as for an α-helix [12,56]. Noting that $D_\beta \approx d_{ch}$, it is predicted from Eq. (4) that $N_b \approx n_\beta$ for untilted strands and that $N_b \approx 2n_\beta$ for 60°-tilted strands (or β-hairpins) in a β-barrel structure. The lipids are assumed to cover only the outer surface of the β-sheet, in all these cases.

The EPR method, with spin-labelled lipids, can be used also to detect partial penetration of surface-binding proteins into the hydrophobic membrane core. In these cases, the stoichiometry of motionally restricted lipid affords a means to estimate the extent of membrane penetration or insertion. Notable examples are: the cytochrome *c* precursor, apocytochrome *c* [57–61]; myelin basic protein [62–64]; prePhoE and SecA from *Escherichia coli* [65,66]; the presequence of cytochrome *c* oxidase subunit IV [67]; the molten globule form of α-lactalbumin [68]; diphtheria toxin at low pH [69]; and the bovine seminal plasma protein PDC-109 [70,71]. In addition, the effects of surface-binding proteins on the stoichiometry of motionally restricted lipids interacting with transmembrane proteins also have been studied [16,72]. Surface binding of cytochrome *c* increases the stoichiometry of motionally restricted lipids for cytochrome *c* oxidase reconstituted in $diC_{14:0}PG$ [22], as does that of melittin for SERCA Ca-ATPase in sarcoplasmic reticulum membranes [73]. On the other hand, binding of the partially penetrating myelin basic protein reduces the amount of motionally restricted lipid associated with the myelin proteolipid protein in $diC_{14:0}PG$ [72]. Lipid chains of biotin-PE conjugated to avidin [74–77] display an increased stoichiometry of interaction with myelin proteolipid protein, relative to that with the free biotin-PE lipid [78].

Examples of surface-associated proteins that do not penetrate the membrane and therefore exhibit no motionally restricted spin-labelled lipid component are: α-synuclein [79,80], pentalysine [81], melittin [82], avidin [75,77,83], human serum albumin [84,85], creatine kinase [86], and cytochrome *c* and polylysine [87–90].

2.2. Lipid Selectivity

The exchange equilibrium for labelled, L*, and non-labelled, L, lipids competing for the N_b sites in the first shell at the intramembranous surface of the protein, P, can be depicted as:

$$\mathrm{P{\bullet}L}_{N_b} + \mathrm{L}^* \overset{K_r}{\longleftrightarrow} \mathrm{P{\bullet}L}_{N_b-1}\mathrm{L}^* + \mathrm{L}$$

The equilibrium constant for association of lipid L* at first-shell sites, relative to that of the background lipid L, is given by:

$$K_r = \frac{[\mathrm{L}^*\mathrm{P}][\mathrm{L}]}{[\mathrm{LP}][\mathrm{L}^*]} \tag{5}$$

This is related to the free energy of association, $\Delta G_{ass}(\mathrm{L}^*)$, by:

$$\Delta\Delta G_{ass} = \Delta G_{ass}(\mathrm{L}^*) - \Delta G_{ass}(\mathrm{L}) = -k_B T \ln(K_r) \tag{6}$$

where T is the absolute temperature and k_B is Boltzmann's constant.

Values for the free energy of association of different spin-labelled lipids with a wide range of different integral membrane proteins are given in Table 2. In most cases, phosphatidylcholine (PC) is the reference lipid (but see also [101,102]). In addition to the data given in Table 2, the selectivity of interaction of spin-labelled gangliosides [103] has been studied with Na,K-ATPase [104], and of diacyl glycolipids with plant photosystems I and II [105–107]. Also, the interaction of both lyso and acyl derivatives of CL with cytochrome *c* oxidase [108], and with the Na, K-ATPase [109], has been investigated by spin-label EPR. For Na,K-ATPase, it was also demonstrated that the selectivity for fatty acids was independent of the nature of the spin-label group [110]. It should be noted that the relative association constants obtained from EPR are measured with spin-labelled lipids at probe concentrations. Therefore, the values of K_r that are reported represent an average over all first-shell sites, *i*:

$$K_r = \frac{1}{N_b}\sum\nolimits_{i=1}^{N_b} K_{r,i} \tag{7}$$

where $K_{r,i}$ is the relative association constant at site *i*. Under these circumstances, a small number of highly specific sites cannot be distinguished from a smaller, but generalized, specificity for all N_b first-shell sites. In the case of cardiolipin (CL) interacting with cytochrome *c* oxidase, higher concentrations of cardiolipin were used, but no saturation of highly specific sites was observed [111]. Thus, cytochrome *c* oxidase displays a generalized specificity for all CL sites that are detected by spin-label EPR. This is in spite of the fact that all endogeneous CL was substituted by PC [112], whereas non-annular, intersubunit sites for cardiolipin are detected in the crystal structure of cytochrome *c* oxidase [113,114], and CL is able to enhance the activity of PC-substituted cytochrome oxidase [115].

Heterogeneity of binding affinities has been found in the lipid quenching of fluorescence from site-specific tryptophans in the MscL mechanosensitive channel [116], and in the KcsA potassium channel [117]. Differences in affinity are not only between annular and non-annular lipid sites; also transbilayer asymmetries occur in the affinity for annular sites. The values of K_r that are reported in Table 2 for SERCA Ca-ATPase, OmpF, KcsA and MscL are obtained from competitive inhibition of fluorescence quenching by brominated PC. Thus, they correspond only to

Table 2
Free energies of association $\Delta\Delta G_{ass}/k_BT$, relative to phosphatidylcholine, of various spin-labelled phospholipids interacting with different transmembrane proteins or peptides[a]

Protein	CL[b]	PA	SA	PS	PG	PE	PC	Ref.
PLP	–	−2.34	−1.87	−0.79	−0.59	–	0.00	[91]
DM-20	–	−0.83	−0.69	−0.10	0.00		0.00	[91]
myelin proteolipid[c]	−0.41[d]	−1.06[d]	−1.95[d]	−0.34[d]	−0.10[d]	+0.69[d]	0.00	[35]
	−1.10[e]	−0.88[e]	−1.06[e]	−0.34[e]	−0.69[e]	−0.53[e]	0.00	[72]
Na,K-ATPase	−1.34	−0.41	−0.53	−0.53	+0.11	+0.11	0.00	[27]
Na,K-ATPase-trypsinised	–	–	−0.41, −1.03[f]	−0.64	–	–	0.00	[92]
SERCA Ca-ATPase	–	0.0	+0.7[k]	0.0	–	+0.8	0.00	[93,94]
cytochrome *c* oxidase	−1.69	−0.64	–	0.00	0.00	0.00	0.00	[95]
ADP-ATP-carrier	−1.34	−1.46	−1.41	−0.88	+0.22	–	0.00	[34]
nicotinic acetylcholine receptor	–	−0.99	−1.41	+0.36	–	−0.10	0.00	[23]
	–	−0.10	−0.41,−0.92[f]	−0.79	–	–	0.00	[96]
	−1.63	–	−1.59	−0.99	−0.53	+0.69	0.00	[24]
M13 phage coat protein	−1.44[g]	−1.44[g]	−0.83[g]	−0.74[g]	−0.47[g]	+0.11[g]	0.00	[97]
	–	−0.47[h]	−0.18[h]	−0.18[h]	−0.10[h]	0.00[h]	0.00	[37]
cytochrome *c* reductase	−0.34	−0.88	−0.92	−0.59	−0.53	−0.26	0.00	[25]
16-kDa proteolipid	–	–	−0.88	−0.41	−0.34	–	0.00	[36]
K27, K-channel peptide[i]	–	−1.19	−0.69	−0.69	−0.10	–	−0.10	[42]
K27-Δ^2	–	−1.46	−1.46	−0.92	0.00	–	0.00	[43]
phospholamban-$A^{36,41,46}$	–	−0.26	−1.03	0.00	0.00	+0.11	0.00	[39]
phospholamban-$\Delta^{1-25}A^{36,41,46}$	–	−0.10	−0.59	0.00	0.00	+0.22	0.00	[39]
GalP	–	0.00,−1.06[f]	−0.64,−1.46[f]	−0.01	+0.11	0.00	0.00	[98]
Rhodopsin	0.00	0.00	0.00	0.00	0.00	0.00	0.00	[31,4]
Gramicidin A	–	−0.18	+0.36,−0.34[f]	−0.10	+0.22	+0.22	0.00	[41]
OmpA[j]	–	−0.92	~+1.6	+.60	0.00	+0.69	+0.51	[45]
OmpG	–	−0.17	+0.4	–	−0.13	+0.09	0.00	[46]
FomA	–	−0.19	−1.41	−0.46	−0.13	−0.06	0.00	[47]
FhuA[j]	–	−0.41	−1.10	−0.34	0.00	+0.51	−0.10	[45]
OmpF	–	–	–	–	+0.6	+0.2	0.00	[99]
KcsA	+0.9	−0.3	–	+0.2	−0.23	+0.6	0.00	[100]
MscL	−0.6	−0.6	–	−0.8	−0.6	−0.1	−0.00	[247]

[a] Derived from the relative association constants, K_r, measured by spin-label EPR or fluorescence quenching: see Eq. (6).
[b] CL, cardiolipin; PA, phosphatidic acid; SA, stearic acid; PS, phosphatidylserine; PG, phosphatidylglycerol; PE, phosphatidylethnolamine; PC, phosphatidylcholine.
[c] Natural mixture of the proteolipid protein and the DM-20 isoform.
[d] In $diC_{14:0}PC$.
[e] In $diC_{14:0}PG$.
[f] Values for protonated and charged forms, respectively.
[g] β-sheet form of the protein in $diC_{14:0}PC/diC_{14:0}PG$ (80:20 mol/mol).
[h] α-helical (partly) form of the protein in $diC_{14:0}PC$.
[i] Sequence: KLEALYILMVLGFFGFFTLGIMLSYIR. Values are referred to PC association with the K27-Δ2 deletion mutant.
[j] Relative to PG.
[k] oleic acid.

annular or first-shell sites on the protein, assuming that non-annular sites are inaccessible to PC. All other values of K_r that appear in Table 2 are obtained from specifically spin-labelled lipids, relative either to unlabelled PC or to spin-labelled PC. They therefore include contributions from any non-annular sites that are accessible to the specifically labelled lipids. Binding constants for the non-annular sites on KcsA have been determined with fluorescence quenchers, by combining results from unlabelled specific lipids in brominated PC with those from brominated specific lipids in unlabelled $diC_{18:1c}PC$ [100], or by using tryptophan deletion mutants [117]. Absolute values of the association constant for the non-annular sites are given simply by:

$$K_B = \frac{[PL^*]_{NA}}{[P]_{NA}[L^*]} \tag{8}$$

where the subscript *NA* represents non-annular sites. Values for non-annular sites are given in Table 3, for which concentrations are expressed as mole fraction units (see [118]).

The dependence of lipid association constants on acyl chainlength is dealt with later, in the Section on hydrophobic

Table 3
Association constants, K_B, and free energies of association, $\Delta G_{ass}^{NA}/k_BT$, of phospholipids with the non-annular sites of KcsA [117]

Lipid	K_B (mole fraction)$^{-1}$	$\Delta G_{ass}^{NA}/k_BT$
CL	7.3±1.2	−2.0±0.2
PA	4.6±2.1	−1.5±0.5
PS	7.1±2.7	−2.0±0.4
PG	3.0±0.7	−1.1±0.2

matching. Here, we note that lipid headgroup selectivity is modulated additionally by manipulations of the aqueous phase, particularly pH titration of the polar groups and electrostatic screening by increasing ionic strength [34,39,108,110,119,120].

The EPR method can also be applied to determination of the selectivity of interaction of hydrophobic drugs or anaesthetics at the intramembranous perimeter of the protein. Examples are the association of spin-labelled aminated local anaesthetics [121] with the nicotinic acetylcholine receptor [122], and that of spin-labelled indolyl-pentadienamide inhibitors [123,124] with the vacuolar H-ATPase [125].

2.3. Energetics of lipid–protein interaction and conformational change

Here we consider how changes in lipid composition, which determine the energetics of the lipid–protein interface via changes in the free energy of association $\Delta\Delta G_{ass}$, might affect protein conformational equilibria. Let $g_{LP}(z)$ be the excess free energy of interaction per unit area of lipid–protein interface at distance z from the membrane mid-plane (see Fig. 3). An appropriate reference state is the free energy of interaction between lipid molecules in the protein-free membrane. At depth z in the membrane, the free energy profile of lipid–protein interaction is $\Delta G_{LP}(z).dz = 2\pi r_P(z) g_{LP}(z).dz$, where $r_P(z)$ is the radius of the cross-section of the protein at vertical position z in the membrane. The change in chemical potential, $\Delta\mu_b$, when a conformational change takes place in the protein, is then given simply by the product of the excess free energy density of the lipid–protein interaction and the change in area of the lipid–protein interface:

$$\Delta\mu_b = -2\pi \int g_{LP}(z)\Delta r_p(z).dz \qquad (9)$$

where $\Delta r_P(z)$ is the difference in cross-sectional radius of the protein in the two conformations.

The profile of the free energy density, $g_{LP}(z)$, can be partitioned into contributions from the lipid headgroups and the lipid chains. A term involving the exposure of hydrophobic groups to a polar environment (Δg_{mis}) enters only in the case of mismatch between the transmembrane hydrophobic spans of lipid and protein (see later, in Section 8). Conformational changes can be effected by differences in the free energy density of lipid–protein interaction, which depend on lipid composition of the host membranes. The excess free energy of interaction with the lipid chains has been measured to be: $0.12 \pm 0.01 \times k_BT$ per CH_2 group for rhodopsin reconstituted in disaturated PCs [126,127] and approximately half this for the SERCA Ca-ATPase reconstituted in 9-*trans*-monounsaturated PCs ([128]; see [14]). (See also Section 8.1 on hydrophobic matching.) These values correspond to a contribution from the chains to the excess free energy density of lipid–protein interaction of $g_{LP}^{(ch)} \approx 1.1$ to $2.2 \times k_BT$ per nm^2, assuming a transverse area per CH_2 group of 0.053−0.061 nm^2 (see, e.g., [129]). Relative association constants of phospholipid species with different polar headgroups typically correspond to differential free energies of lipid–protein interaction of $\Delta\Delta G_{ass} \sim +0.7$ to $-2.3 \times k_BT$, relative to phosphatidylcholine (see Table 2). Assuming an effective transverse area per phospholipid headgroup of ca. 0.85 nm^2 from crystal structures (see, [130]), yields estimates of $g_{LP}^{(HG)} \approx +0.8$ to $-2.7 \times k_BT$ per nm^2 for the average contribution of the lipid polar groups to the excess interaction free energy density.

For a protein of mean cross-sectional radius $r_P \approx 2$ nm, such as rhodopsin [131], a change in cross-sectional area by 1 nm^2 would correspond to a change in cross-sectional radius of $\Delta r_P \approx 0.1$ nm. A change of 1 nm^2 is comparable in size to the change in asymmetry of protein cross-section that is estimated for the meta-I to meta-II transition of rhodopsin (see [132] and Table 8, given later below). A change of this magnitude would involve the displacement, or incorporation, of effectively just one lipid in the first shell at the perimeter of the transmembrane protein. Correspondingly, experiments with spin-labelled lipids do not detect a significant change in the number of first-shell lipids on mild bleaching of rhodopsin to the meta-II state [133]. Because rhodopsin displays very little selectivity between different lipid headgroups [4,31,33,133], the influence of lipid–protein interactions should be felt primarily in the lipid chain regions. With a change in excess free energy density of $\Delta g_{LP}^{(ch} \approx 2.2 \times k_BT$ per nm^2 (see above) and a hydrophobic span for rhodopsin of 3.2 ± 0.2 nm

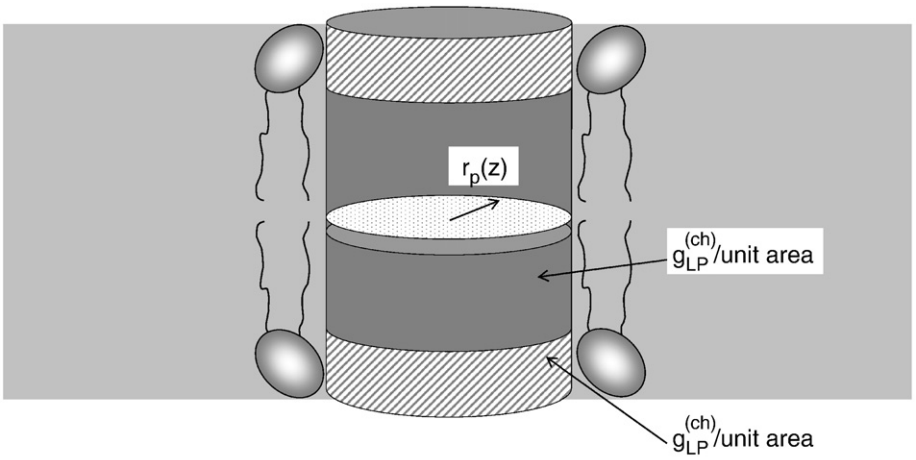

Fig. 3. Energetics of the lipid–protein interface: the free energy of lipid–protein interaction, per unit area of interface, is $g_{LP}(z)$ at distance z from the membrane mid-plane. Contributions of the lipid polar headgroups and hydrocarbon chains to the free energy density are $g_{LP}^{(HG)}$ and $g_{LP}^{(ch)}$, respectively.

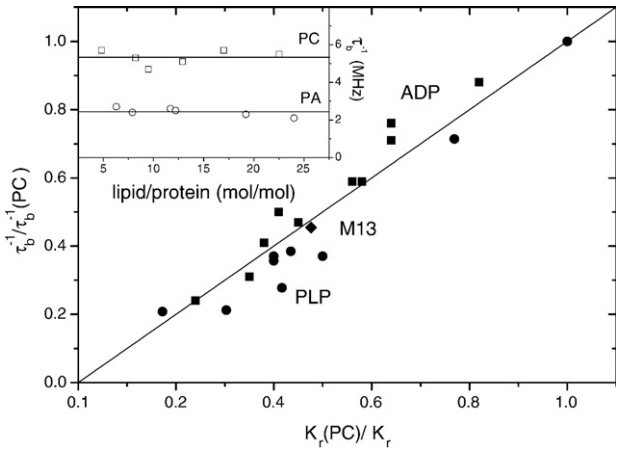

Fig. 4. Correlation of the off-rate constant, τ_b^{-1}, for exchange of spin-labelled lipids associated with myelin proteolipid protein PLP (solid circles; [119,141]), M13 coat protein (diamond; [44]) and ADP-ATP carrier (solid squares; [34]) with the corresponding inverse relative association constants, $1/K_r$. Both sets of values are normalized to those for spin-labelled PC. Inset: shows the off-rate constants for spin-labelled PC (open squares) and PA (open circles) at 30 °C as a function of lipid/protein ratio in lipid recombinants with the M13 coat protein [44].

[134], Eq. (9) then predicts a change in chemical potential on changing lipid composition of $4.4\pm0.3\times k_BT$, for a conformational change with $\Delta r_P\approx0.1$ nm. This would shift relative conformational equilibrium populations, e.g., of the meta-I and meta-II states, by 80-fold. In fact, the meta-I to meta-II transition is accompanied by a change in volume of rhodopsin of 0.18 nm^3 [135], but this does not exclude larger changes in cross-sectional area that are compensated by changes in thickness of the protein. Similar estimates, but based on the selectivity of lipid headgroup interactions with other integral proteins, yield changes in chemical potential of the protein that are in the range of $+1.6$ to $-4.6\times k_BT$, relative to PC, for a protein of the same size as rhodopsin. This demonstrates that changing lipid polar headgroup potentially can cause appreciable shifts in conformational equilibria.

Note that the treatment of lipid–protein energetics in terms of the pressure difference across curved surfaces (i.e., the Laplace equation), which was introduced originally by Baldwin and Hubbell [136], is formally equivalent to the above approach, where g_{LP} plays the role of an interfacial tension [132].

3. Dynamics of protein–lipid shells

Resolution of two distinct components in the EPR spectra of spin-labelled lipids in lipid–protein systems implies that exchange between the two lipid populations is slower than the difference in their spectral frequencies [137]. The critical rate is $\sim5\times10^8$ s^{-1} (see, e.g., [138]), which exceeds that for translational diffusion of free lipids in fluid bilayer membranes [139,140].

3.1. Lipid exchange rates

The exchange rates can be estimated by simulating the EPR lineshapes and linewidths (which depend upon T_2-relaxation rates) with a two-site exchange model for lipid L* [137,141]:

$$P\bullet L_{N_b}+L^*\underset{\tau_b^{-1}}{\overset{\tau_f^{-1}}{\rightleftharpoons}}P\bullet L_{N_b-1}L^*+L$$

where τ_f^{-1} is the on-rate and τ_b^{-1} is the off-rate for lipid L*. If f is the fraction of L* associated with the protein, then material balance requires that:

$$f\tau_b^{-1}=(1-f)\tau_f^{-1} \tag{10}$$

where τ_b^{-1} is the intrinsic exchange rate that depends on the affinity of L* for the protein (i.e., on K_r), and is independent of the lipid–protein ratio (see inset to Fig. 4). The on-rate, on the other hand, is diffusion-controlled and depends on the size of the free pool of lipid according to Eq. (10). The intrinsic off-rates of lipids A and B reflect their relative selectivities for the protein and depend inversely on their relative association constants [141]:

$$\frac{\tau_b^{-1}(A)}{\tau_b^{-1}(A)}=\frac{K_r(B)}{K_r(A)} \tag{11}$$

This reciprocal relation is illustrated by data for myelin proteolipid protein (PLP), M13 phage coat protein, and the ADP–ATP carrier, in Fig. 4.

The intrinsic off-rate constants for exchange of phosphatidylcholine, a lipid that does not express specificity for the protein, at the interface with different membrane proteins are listed in Table 4. In general, the off-rates for PC and α-helical proteins are in the region of $1-2\times10^7$ s^{-1}, which are of the same order as, but significantly slower than, lipid–lipid exchange in fluid bilayers ($\sim8\times10^7$ s^{-1}, [139,140]). For lipids displaying selectivity, the off-rates are correspondingly slower, according to Eq. (11).

3.2. T_1-sensitive measurements

More sensitive assessment of the exchange rate comes from EPR saturation experiments (which depend upon T_1-relaxation) that are sensitive to motions in the microsecond time regime and

Table 4
Phosphatidylcholine off-rate constants (τ_b^{-1}) and activation energies (E_a) for lipid exchange at the intramembranous surface of different integral membrane proteins

Protein/Lipid	T (°C)	τ_b^{-1} (s^{-1})	E_a (kJ/mol)	Ref.
Myelin proteolipid protein/$diC_{14:0}$PC	30	1.6×10^7	20	[119,137,141]
Myelin DM-20 protein/$diC_{14:0}$PC	30	1.5×10^7	–	[91]
Rhodopsin/$diC_{14:0}$PC	30	1.6×10^7	20	[32]
M13 coat protein(α-helix)/$diC_{14:0}$PC	30	2.3×10^7	–	[37]
M13 coat protein(β-sheet)/$diC_{14:0}$PC	30	5.3×10^6	–	[44]
M13 coat protein(α-helix)/$diC_{18:1c}$PC	24	3.0×10^7	–	[37]
ADP-ATP carrier/egg PC	10	1.4×10^7	–	[34]
Ca-ATPase/$diC_{18:1c}$PC	37	$1–2\times10^7$	–	[142]

therefore optimally matched to lipid exchange processes (see, e.g., [61,143–146]). Saturation is effectively relieved by exchange at the lipid interface with myelin PLP in the fluid phase, but not in the gel phase where exchange is extremely slow [147,148]. The increase in spin-lattice relaxation rate of the protein-associated lipids that arises from exchange with the fluid lipid population is given by [147]:

$$\Delta\left(\frac{1}{T_{1,b}}\right) = \frac{\tau_b^{-1}}{1 + T_{1,f}^{o}\tau_f^{-1}} \tag{12}$$

where T_{1f}^{o} is the spin-lattice relaxation time of the fluid lipids in the absence of exchange, and an analogous expression holds for the relaxation enhancement of the fluid lipids. From Eq. (10), and Eq. (12) and its equivalent, it is found that the exchange rate lies in the range $\tau_b^{-1} = (0.7-5)\times(T_{1,b}^{o})^{-1}$, depending on the affinity of the exchanging lipid for PLP [147]. This means that the exchange rate is of the same order as the T_1-relaxation rate, i.e., the lifetimes of the lipids on the protein are in the immediately sub-microsecond to microsecond regime. Exchange at these rates readily explains why protein-associated lipids are not resolved by NMR (see, e.g., [149]): all lipids are in fast exchange on the NMR timescale in fluid bilayers.

4. Ordering of protein–lipid shells

At least three approaches provide information on the configuration of the lipid chains in the first or annular boundary shell at the protein perimeter. These are: order parameter measurements by ^{2}H-NMR, angular dependent spin-label EPR measurements on aligned membranes, and direct structural resolution of lipids contacting the protein in crystals. Of these, only ^{2}H-NMR is a dynamic measurement evincing motional averaging. The other two are static or quasi-static measurements, and order parameters must be calculated by averaging over the orientational distribution (see Fig. 5).

4.1. ^{2}H-NMR order parameters

Order parameters of lipid chains that are obtained from quadrupolar ^{2}H-NMR are an average over all lipid environments, because of the fast exchange referred to in the previous Section 3.2. Assuming that the chain order of only the first shell is perturbed by the protein, the mean segmental order parameter of this shell is given by (see, e.g., [52,150]):

$$\langle S_{CD}\rangle_b = \left(\langle S_{CD}\rangle - \langle S_{CD}\rangle_o\right)\frac{N_t}{N_b} + \langle S_{CD}\rangle_o \tag{13}$$

where N_t is the total lipid/protein ratio, $\langle S_{CD}\rangle$ is the mean order parameter of chain CD segments in the protein-lipid sample and $\langle S_{CD}\rangle_o$ is that in membranes of the lipid alone. A general feature found from ^{2}H-NMR experiments on systems for which the protein is well integrated in the membrane is that $\langle S_{CD}\rangle$ does not differ greatly from $\langle S_{CD}\rangle_o$ [149,151–154]. Thus the mean orientational order of the lipid chains at the protein interface, $\langle S_{CD}\rangle_b$, is similar in magnitude to that in fluid lipid bilayer regions of the membrane, i.e., $\langle S_{CD}\rangle_o$. This is a condition for good hydrophobic matching between lipid and protein, and for the protein to be well integrated in the lipid bilayer. Systematic changes in lipid chain order parameters are found with varying degree of hydrophobic matching in peptide systems ([52] and see Section 8.5 later).

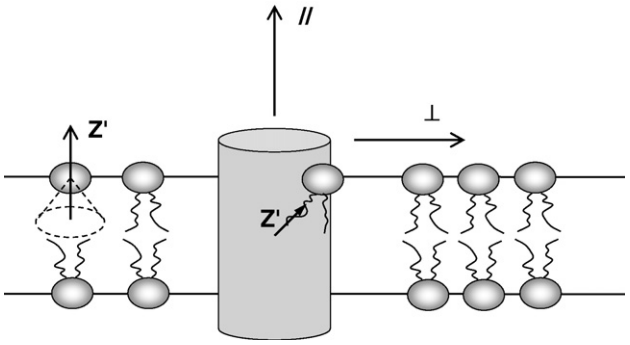

Fig. 5. Ordering of lipid chains in fluid bilayer regions and at the protein interface, in aligned membranes. Rapid lipid rotation in fluid bilayers gives partial averaging of the angular anisotropy in spin-label EPR and ^{2}H-NMR spectra, resulting in axial symmetry with respect to the membrane normal (//). A quasi-static (i.e., crystal-like) distribution of chain orientations, Z′ , is obtained in the EPR spectrum of motionally restricted spin-labelled lipids at the protein interface. In a quadrupolar ^{2}H-NMR spectrum, both environments are averaged by translational exchange.

Whereas the mean segmental order parameter changes relatively little, the spread in order parameters might be expected to differ, however, reflecting the more heterogeneous chain environment at the protein interface than in bulk fluid lipid bilayers. Table 5 gives results for rhodopsin in fluid-phase bilayers of di$C_{14:0}$PC with perdeuterated chains [155]. The mean chain order parameter, $\langle S_{CD}\rangle$, averaged over all chain segments decreases only slightly with increasing protein content, but the spread of segmental chain order parameters, $\langle(S_{CD} - \langle S_{CD}\rangle)^2\rangle^{1/2}$, increases progressively with increasing amount of rhodopsin in the membrane. This can be attributed variously to the irregular intramembranous surface of the protein, or to a statistical heterogeneity of protein–lipid contacts on the ^{2}H-NMR timescale [155]. Analysis of chain order for the lipids resolved at the surface of membrane proteins in crystals reveals a large distribution width about the average over the entire chain ([16]; and see Section 4.3, below).

4.2. Spin-label EPR angular distributions

Unlike the fluid bilayer lipids, the EPR spectra of the first-shell lipids lie close to the limits of motional sensitivity of spin-label spectroscopy. Information on the chain ordering of the protein-associated lipids can therefore be obtained only from aligned membranes (see Fig. 5). The configurational disorder of the chains is then depicted by a static orientational distribution, $\rho(\theta_i)$, which will have a characteristic mean value and distribution width. The segmental chain order parameters, $S_{mol,i}$, are then obtained by integration over the axial orientational distribution, $\rho(\theta_i)\sin\theta_i$:

$$S_{mol,i} = \langle P_2(\cos\theta_i)\rangle = \frac{\int_0^{\pi}\frac{1}{2}(3\cos^2\theta_i - 1)\rho(\theta_i)\sin\theta_i d\theta_i}{\int_0^{\pi}\rho(\theta_i)\sin\theta_i d\theta_i} \tag{14}$$

where θ_i is the inclination of the C_{i-1}–C_{i+1} vector to the membrane normal. Note that this is perpendicular to the C–D bond of a CD_2 group. Therefore, the CD order parameters of Section 4.1 are related to those of the chain axis by: $S_{CD,i} = (-1/2)S_{mol,i}$,

Table 5
Distribution of chain segmental order parameters, $\langle S_{CD}\rangle$, in rhodopsin/diC$_{14:0}$PC membranes of different lipid/protein ratios, L/P, at 23 °C. (Data from [155])[a]

L/P (mol/mol)	$\langle S_{CD}\rangle$	$[\langle S_{CD}^2\rangle - \langle S_{CD}\rangle^2]^{1/2}$
∞	−0.19	±0.06
150:1	−0.19	±0.08
50:1	−0.15	±0.08
30:1	−0.15	±0.11
12:1	−0.18	±0.14

[a] $\langle S_{CD}\rangle$ is the mean order parameter of the different chain segments, and $\langle S_{CD}^2\rangle - \langle S_{CD}\rangle^2 = \langle (S_{CD} - \langle S_{CD}\rangle)^2\rangle$ is the mean squared width of the order parameter distribution.

assuming axial symmetry (see e.g., [156,157]). EPR experiments with macroscopically aligned rod outer segment discs reveal a wide orientational distribution of the lipid chain segments that are associated with rhodopsin [158]. These results are therefore in accord with the ^{2}H-NMR results on randomly oriented reconstituted rhodopsin membranes that are summarized in Table 5 [155].

4.3. Crystal structures

Segmental ordering of the lipid chains in protein crystals can be determined from the orientations of the C_{i-1}–C_{i+1} vectors, $\theta_{i,m}$ for chain m [16]. These chain directions are likely to be specified more reliably by the electron densities than are the individual torsional angles of the phospholipid structures which exhibit many conformational violations [159,160]. The order parameter of segment i requires averaging over the chain sites, m, on the protein:

$$S_{mol,i} = \frac{3}{2n_{ch}} \sum_{m=1}^{n_{ch}} \cos^2\theta_{i,m} - \frac{1}{2} \tag{15}$$

where n_{ch} is the number of chains included in the average. The mean segmental order parameters are then given by averaging over the length of the lipid chain:

$$\langle S_{mol}\rangle = \frac{1}{n_c - 1} \sum_{i=2}^{n_c} S_{mol,i} \tag{16}$$

where $n_C - 1$ is the number of chain segments that are averaged over.

Averaging over the lipid chains in crystals of cytochrome c oxidase, cytochrome c reductase, cytochrome b_6f and photosynthetic reaction centres, produces in each case mean segmental order parameters, $\langle S_{mol}\rangle \equiv -2\langle S_{CD}\rangle$, that are less than those for rhodopsin in membranes (cf. Table 5), and are also less than those in fluid lipid bilayers [16]. Also, the distribution widths, $\langle (S_{mol} - \langle S_{mol}\rangle)^2\rangle^{1/2}$, are considerably larger than that corresponding to the limiting value at high/protein ratio in Table 5. Only the phytanyl chains in bacteriorhodopsin crystals produce higher mean order parameters, but nonetheless large distribution widths.

Apparently, the spread in disorder of the lipid chains that are resolved in protein crystals is greater than that for the full population of lipid chains at the intramembranous surface of the protein. With the exception of bacteriorhodopsin, the average degree of disorder is also greater. Presumably those lipids that mediate optimal hydrophobic matching at the protein perimeter in membranes are not resolved, or not present, in the crystals.

5. Lipid flip-flop in protein–lipid shells

The intrinsic rate of exchange of phospholipids between the endo- and exo-facial leaflets of a fluid bilayer:

$$[lipid]_{endo} \overset{k_{flop}}{\longleftrightarrow} [lipid]_{exo}$$

is extremely slow, with half-times ($t_{1/2} = 0.6931/k_{flop}$) of many hours or even days (see e.g., [161–163]). By contrast, transbilayer movement of phospholipids in biogenic membranes, such as the bacterial cytoplasmic membrane or that of the endoplasmic reticulum, is fast with half-times in the range of minutes or less (see [164] for a review).

Transbilayer transport of fluorescent, NBD-caproyl, phospholipids is found to be rapid in large unilamellar vesicles (LUVs) of *E. coli* lipids that contain α-helical transmembrane peptides of the type, $GX_2L(AL)_mX_2A$, where X is an interfacial anchoring residue [165]. As seen from Fig. 6, the rate of outward lipid transport depends linearly on the mole fraction of peptide present. This fixed stoichiometry suggests that the lipid–protein interface plays a major role in the transbilayer movement. At a $GK_2L(AL)_{12}K_2A$/lipid molar ratio of 1/250 the half-time for lipid translocation is ~10 min at 25 °C, whereas translocation is negligible on this timescale in the absence of peptide. The flop rate for 23-residue peptides is modulated by the type of anchoring residue in the order X=K>H>W with rate constants of k_{flop}=3.2, 1.2 and 0.6 h^{-1}, respectively, at 25 °C. Translocation rates are similar for the 23- and 31-residue X=K peptides (KALP23 and KALP31, respectively). Rapid transbilayer movement of lipids is also induced by the bitopic protein glycophorin A from red blood cells [166], and a peptide corresponding to transmembrane helix-1 of the leader peptidase from *E. coli* [167].

Investigation of the effects of lipid composition on translocation induced by $GX_2L(AL)_8X_2A$ peptides reveals a clear dependence on lipid headgroup and a strong suppression by cholesterol [168]. Translocation rates of C$_6$NBD-PG by the X=W peptide (WALP23) in diC$_{18:1}$PC are 7-fold faster than in *E. coli* lipids

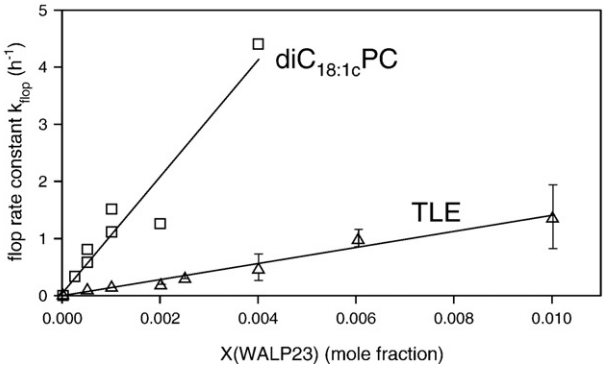

Fig. 6. Dependence of the rate of outward movement, k_{flop}, of C$_6$NBD-PG in LUVs of diC$_{18:1c}$PC (squares) and of *E. coli* lipids (triangles) on content of the Ac-$GW_2L(AL)_8W_2A$-amide peptide (WALP23). T=25 °C [168].

(see Fig. 6); they are reduced slightly by admixture of $diC_{18:1}PG$ and to a greater extent by admixture of $diC_{18:1}PE$. Cholesterol has a much greater effect than the phospholipids, admixture of 40 mol% reduces the flop rate by 6-fold. For the X=K peptide (KALP23), translocation rates are increased by admixture of $diC_{18:1}PG$ in $diC_{18:1}PC$, and are reduced only slightly by admixture of $diC_{18:1}PE$. The flop rates for different headgroups of NBD-labelled lipids in $diC_{18:1}PC$ are in the order: PA ≈ PG >> PE > PS ≈ PC ≈ 0 with both WALP23 and KALP23 peptides.

Experiments with different prokaryotic transmembrane proteins reveal that only a subset are capable of promoting transbilayer movement of phospholipids [167]. Monomeric *E. coli* leader peptidase (Lep), which contains two helical TM segments, and the tetrameric KcsA potassium channel from *S. lividans*, which contains two TM segments per monomer, mediate lipid translocation with comparable efficiencies (see Table 6). By contrast, the ABC transporter from *E. coli* MsbA, a suggested flippase, does not facilitate phospholipid translocation, nor does the *E. coli* outer membrane β-barrel protein OmpT.

It is consequently proposed that phospholipid translocation is mediated only by those transmembrane segments of small integral proteins that are in a dynamic configuration, as in the single-spanning TM peptides [164]. In this connection, it is important to remember that the monomeric translocation-promoting WALP and KALP peptides do not motionally restrict lipids in the manner characteristic of larger integral proteins (see Section 2.1). Thus translocation is not a general feature of the protein-lipid interface, but is confined to a few specially dynamic transmembrane segments. The strong suppression by cholesterol is also of considerable significance, in view of the well-established lipid asymmetries in eukaryotic plasma membranes.

6. Membrane elastic fluctuations

Lipid membranes are subject to elastic, out-of-plane bending fluctuations (see Fig. 7), which are excited thermally [169–171]. These fluctuations are manifested by flickering phenomena in erythrocytes and giant lipid vesicles [172,173], by undulation forces between membranes [174,175], and by a low-frequency dispersion in NMR relaxation rates that scales as ω^{-1} [176,177]. The energy scale for the fluctuations is set by the elastic bending modulus: $k_c \sim (1/4) K_A d^2$, where K_A is the modulus for area dilation and d is the membrane thickness [178,179]. The effects of bending fluctuations are therefore expected to be particularly pronounced for thin membranes.

Table 6
Rates of outward translocation of C_6NBD-PG in proteoliposomes or LUVs of *E. coli* lipids that contain different peptides or proteins [167]

Protein/peptide	Molar ratio	k_{flop} (h^{-1})		
		Proteoliposomes 37 °C	LUVs 37 °C	LUVs 25 °C
–	0	0.056	0.050	0.031
WALP23	1:1000	0.35	0.80	0.17
WALP23	1:250	ND	ND	0.60
Helix-1/Lep	1:250	ND	ND	1.61
Lep	1:1000	0.16		
KcsA (tetramer)	1:1000	0.21		

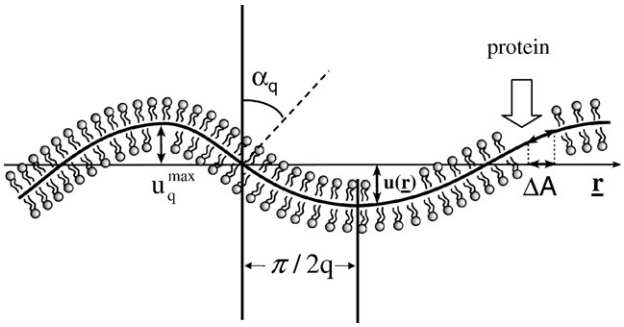

Fig. 7. Thermal elastic fluctuations of a lipid membrane. The amplitude of the deviation from a flat membrane is $u(r)$, and the wavevector of one of the constituent modes is q. Protein insertion causes compression of the lipid area by an amount ΔA, projected on the flat membrane. The local director tilt is α_q, which is equal to the angle that the local membrane plane makes with the horizontal. For small angular amplitudes: $\sin \alpha_q \approx 2u_q^{max} q/\pi$.

Membrane incorporation and folding of β-barrel outer membrane proteins occurs spontaneously in small unilamellar lipid vesicles that are produced by limit sonication. Spontaneous incorporation in fluid LUVs, however, occurs only for phosphatidylcholine lipids with chainlengths less than $C_{14:0}$ [180–182]. Correspondingly, the tilt of the β-barrel in aligned membranes increases abruptly for phosphatidylcholines with chainlengths shorter than this critical value [46,183]. It is suggested that both these phenomena can be accounted for by elastic membrane fluctuations because of the highly non-linear dependence on lipid chain length. Note that, in several (but not all) cases, the local tilt of transmembrane peptides relative to the bilayer normal, is found to be relatively small [184–187]. This suggests that large effective tilts in aligned systems might arise preferentially from undulations in the membrane surface, i.e., bending fluctuations.

6.1. Protein insertion

Insertion of proteins in the membrane depends on the lateral compressibility of the lipid, $\tilde{K}_A$. This is effectively renormalized by the membrane fluctuations (cf. Fig. 7), to an extent that depends on the square of the bending rigidity [170,171,188]:

$$\tilde{K}_A \approx \frac{8\pi^3 k_c^2}{k_B T A} \approx \frac{\pi^3 K_A^2 d^4}{2 k_B T A} \tag{17}$$

where K_A is the intrinsic area dilation modulus, and A is the total membrane area. The partition coefficient, K_P, for protein insertion is related by a Boltzmann factor to the free energy of lipid compression [189]:

$$K_p \propto \exp\left(\frac{-\tilde{K}_A(\Delta A)^2}{k_B T A_P}\right) \tag{18}$$

where ΔA is the lipid compression and A_P is the membrane area per protein (see Fig. 7). This exponential dependence, together with the extremely steep dependence on membrane thickness in Eq. (17), could possibly account for the high sensitivity of spontaneous insertion of OmpA to lipid chainlength. Numerical estimates and further refolding experiments with OmpA support this view [188].

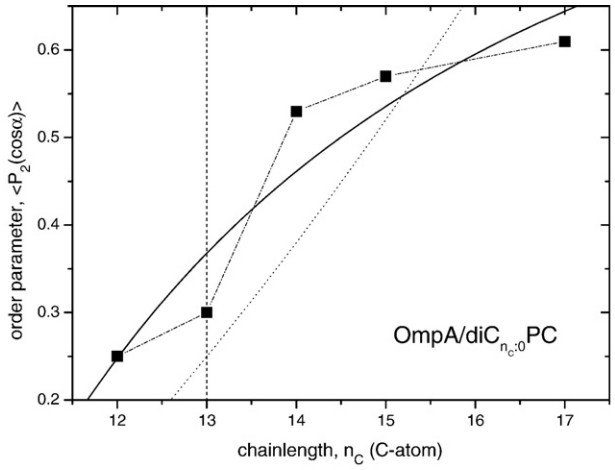

Fig. 8. Dependence of the order parameters, $\langle P_2(\cos\alpha)\rangle$, of the β-barrel domain of OmpA on chainlength, n_C, of fluid-phase di$C_{n_C:0}$PC bilayers in which OmpA is incorporated [183]. Solid line is the fit of a chainlength dependence: $P_2 \sim 1 - B/(n_c - 1)^2$, according to Eq. (20). The vertical dashed line indicates the chainlength for approximate hydrophobic matching. Dotted line is a fit for simple geometrical hydrophobic matching [188].

6.2. Protein tilt

Bending fluctuations give rise to a time-average net tilt, alpha, of the protein (relative to an orienting substrate) that depends upon the amplitude of transverse displacement of the membrane (see Fig. 7). An inverse dependence on bending rigidity is predicted for the power spectrum of mean-square displacement amplitudes, $\overline{u_q^2}$, by the equipartition theorem [174,179]:

$$\overline{u_q^2} = \frac{k_B T}{A k_c q^4} \tag{19}$$

This is related to the mean-square angular fluctuations of the director, as indicated in Fig. 7. Summation over all q-modes then leads to the following approximate result for the order parameter associated with the director fluctuations [188]:

$$\langle P_2(\cos\alpha)\rangle = \frac{1}{2}\left(3\langle\cos^2\alpha\rangle - 1\right) \approx 1 - \frac{3k_B T}{\pi^3 k_c}\ln\frac{A}{A_L} \tag{20}$$

where A_L is the area per lipid molecule. Fig. 8 shows the dependence of the order parameters of the OmpA β-barrel domain on lipid chainlength in aligned membranes [183]. The steep increase between $n_C = 13$ and 14 is evident. The solid line is a fit with the functional dependence predicted by Eq. (20). Clearly there are contributions other than lipid director fluctuations, most notably hydrophobic matching, to the chainlength dependence of the β-barrel ordering. Nonetheless, the fit in Fig. 8 suggests that bending fluctuations can make an appreciable contribution to the dependence of OmpA tilt on lipid chainlength, including that in the region of hydrophobic matching [188].

7. Modulation of lipid polymorphism

In addition to lamellar bilayer membranes, depending on environmental conditions and molecular structure, lipids dispersed in water may alternatively assume various non-lamellar phases (see, e.g., [190,191]). According to the shape concept of lipid polymorphism [192], single-chain lipids, such as lysolipids, tend to form normal micelles, M_I, in which the lipid hydrocarbon is surrounded by water (i.e., oil-in-water configuration). On the other hand, lipids with two long, or *cis*-unsaturated, chains tend to form inverted phases, e.g., H_{II} or Q_{II}, in which water is surrounded by lipid hydrocarbon (i.e., water-in-oil configuration). The extent of lyotropic polymorphism that can be exhibited by biological lipids is indicated in Fig. 9, as a generalized temperature-composition phase diagram for the high temperature region (see, e.g., [193]). Lipid phase designations are as defined in Marsh [194].

7.1. Lipid packing parameters

The phase preference of a particular lipid can be expressed in terms of a lipid packing parameter, $V_L/A_L l_L$, where V_L and l_L are the volume and length of a lipid molecule, and A_L is the area per lipid molecule at the lipid–water interface [195]. Lamellar phases are expected for $V_L/A_L l_L \approx 1$, whereas normal phases are favoured for $V_L/A_L l_L < 1$, and for $V_L/A_L l_L > 1$ inverted phases are preferred (see Fig. 9). An experimental means to quantify nonlamellar phase propensity is via the spontaneous or intrinsic curvature, c_o, which is measured from relaxed lipid H_{II} phases, in the presence of excess hydrocarbon [196]. This will be shown later to be an important parameter for characterising functional lipid–protein interactions (see Section 9). It is related to the packing parameter by [197,198]:

$$c_o = \frac{1}{R_o} = \frac{2}{l_L}\left(1 - \frac{V_L}{A_L l_L}\right) \tag{21}$$

where R_o is the radius of curvature for a cylindrical system, and is defined as negative for inverted structures and positive for normal structures (see Fig. 10). The intrinsic curvature of lipid mixtures

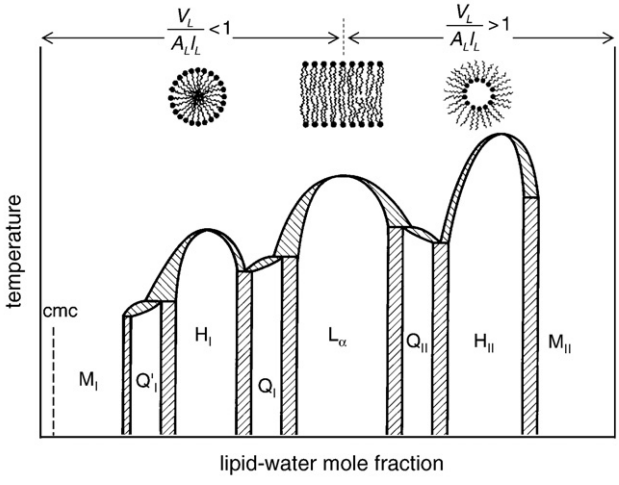

Fig. 9. Schematic lipid–water phase diagram for phospholipid amphiphiles. Hatched areas indicate two-phase regions. The left-hand side of the diagram is representative of single-chain lipids ($V_L/A_L l_L < 1$), and the right-hand side is representative of long two-chain lipids ($V_L/A_L l_L \geq 1$). Subscripts I and II represent normal and inverted phases, respectively. M = micellar; Q = cubic; H = hexagonal; L_α = fluid lamellar.

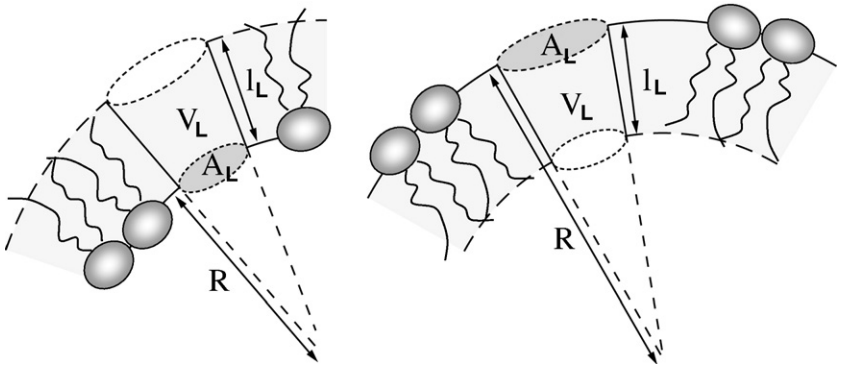

Fig. 10. Topology of: inverted (left, water-in-oil), and normal (right, oil-in-water), curved lipid monolayer structures. Characteristic dimensions of a lipid molecule, volume V_L, cross-section A_L, and length l_L, specify the lipid packing parameter and the monolayer curvature $\pm 1/R$ (+ for normal; − for inverted).

may be predicted from Eq. (21), by assuming linear additivity of component volumes and surface areas (and lipid lengths) [132,197,198]. Alternatively, in several cases, linear additivity of the component curvatures is found to be a reasonable approximation [132,197–200]:

$$c_o = c_{o,A}X_A + c_{o,B}X_B \tag{22}$$

where $c_{o,A}$ and $c_{o,B}$ are the intrinsic curvatures, and X_A and X_B are the mole fractions, of the two lipids in the mixture, e.g., di$C_{18:1c}$PE and di$C_{18:1c}$PC.

7.2. Influence of lipid shape and environment

As an example of varying the lipid packing parameter, Fig. 11 shows the ^{31}P-NMR powder spectra of different derivatives of cardiolipin (CL; diphosphatidylglycerol), an anionic tetraacyl phospholipid which in eukaryotes is unique to mitochondrial membranes. Cardiolipin from beef heart has highly unsaturated chains, approximately 90% of which are linoleate, $C_{18:2}$. (The lyso-derivatives are produced by the progressive action of phospholipase A_2, which cleaves at positions equivalent to the *sn*-2 chain in a diacyl lipid.) The various CL derivatives display a rich range of lyotropic polymorphism, depending on the number of acyl chains and the ionic strength [201], and interestingly differ considerably in their ability to activate cytochrome *c* oxidase [115]. In the absence of salt, the two-chain dilysoCL derivative forms micelles, M_I. The three-chain monolysoCL derivative forms lamellar structures, L_α, as does also the parent 4-chain CL. However, CL bearing a fifth chain acylated on the centre -OH of the glycerol moiety forms an inverted hexagonal phase, H_{II}.

High salt concentrations screen electrostatic repulsion between the lipid headgroups, and the resulting electrostatic neutralisation favours formation of inverted hexagonal phases for CLs with unsaturated chains [202,203]. As seen from Fig. 11, dilysoCL converts from a micellar to an L_α phase in 3 M NaCl. MonolysoCL remains in an L_α phase, whilst CL itself converts from the L_α phase to an H_{II} phase. Acyl CL, on the other hand, undergoes no transition and remains in the H_{II} phase in 3 M NaCl. High salt concentrations also favour H_{II} phase formation in zwitterionic lipids because of their effect on headgroup hydration [190,191,204,205].

Headgroup size also plays an important role in lipid polymorphism, particularly for mixtures containing large amounts of lipids that alone do not form lamellar phases. Protonated fatty acids and diacylglycerols, both of which have small and relatively apolar headgroups, tend to form inverted non-lamellar phases when mixed at high levels with PCs or other phospholipids [157,204,206–209]. On the other hand, mixtures of *N*-acyl ethanolamines, which have a larger and more polar headgroup, with PCs or PEs maintain a lamellar phase up to high mole fractions of the *N*-acyl ethanolamine [210,211]. Going even further, covalent addition of biotin to the headgroup of PEs produces biotinylated phospholipids that, on chain melting, can undergo a transition to an isotropic non-lamellar phase of normal rather than inverted curvature [212–214].

7.3. Thermotropic transitions

In excess water, thermotropic transitions may take place between fully hydrated lipid phases: from lamellar to non-lamellar phases with increasing temperature. Above the chain-melting transition, the generalized sequence for diacyl lipids is:

$$L_\alpha \xrightarrow{T_h} Q_{II} \longrightarrow H_{II} \xrightarrow{T_I} M_{II}$$

where T_h is the lamellar–nonlamellar transition temperature, and T_I is the temperature of isotropic melting. Such a progression, with an intervening cubic phase (Q_{II}) before the H_{II} phase, is observed, e.g., for medium-chain saturated PEs and PC:fatty acid 1:2 mixtures [191,206,207]. An isotropic phase (M_{II}), following the H_{II} phase, is observed for PCs mixed with high mole ratios of diacylglycerols [157,209,215]. A particularly rich range of polymorphic transitions is exhibited, for phases of normal curvature, by $C_{16:0}$lysoPC in solutions of polyethylene glycol (PEG) [216]. With increasing temperature, $C_{16:0}$lysoPC in 23 wt% aqueous PEG proceeds from an interdigitated lamellar gel phase (L_β^i) to a cubic phase (Q_I), followed by a hexagonal phase (H_I), and finally to a normal micellar phase (M_I). This undoubtedly arises from the ability of PEG to reduce water activity [217,218], which modulates the phase preference of lysolipids [219], as indicated schematically by the dependence on lipid–water mole fraction in Fig. 9 (left side). Increase in chainlength or introduction of

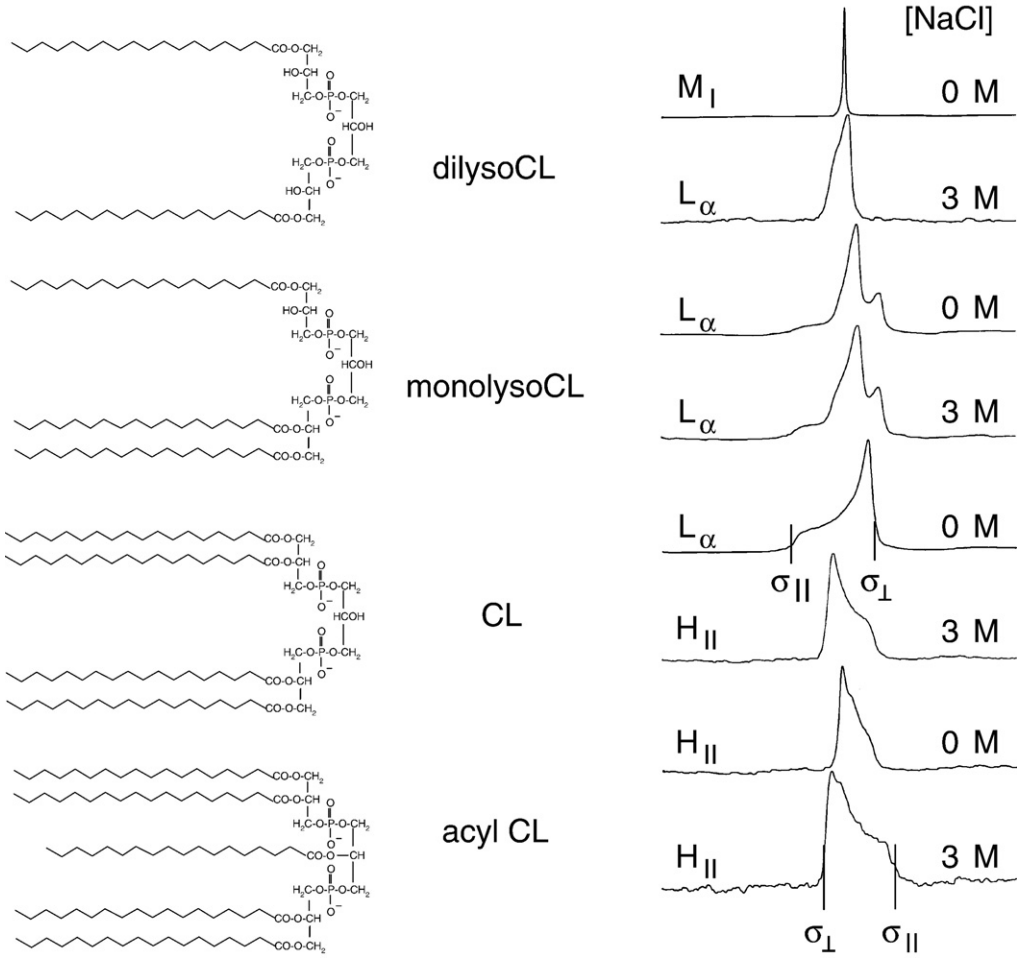

Fig. 11. Left: chemical structures of CL derivatives: (top to bottom) dilysoCL, monolysoCL, CL, and acyl CL. Right: broad-line ^{31}P-NMR spectra of CL derivatives in 0 (upper of each pair) and 3 M NaCl (lower of each pair) at 20 °C: (top to bottom) dilysoCL, monolysoCL, CL, and acyl CL. The two phosphates in monolysoCL are inequivalent. L_α phases have chemical shift anisotropy $\Delta\sigma=\sigma_{//}-\sigma_\perp<0$, for cylindrical phases (H_{II} and H_I) $\Delta\sigma>0$, and for cubic and isotropic phases $\Delta\sigma=0$. Phase identifications on the figure are established by x-ray diffraction [201].

double bonds decreases the nonlamellar transition temperature, T_h, of PEs, whereas increasing *N*-methylation of PE increases T_h [194].

7.4. Influence of integral proteins

Generally, transmembrane proteins tend to stabilize the lamellar phase in lipids which otherwise form the H_{II} phase (see, e.g., [220–222]). Fig. 12 shows the modulation of the salt-induced L_α to H_{II} transition in CL by the presence of cytochrome *c* oxidase [223]. In the absence of protein, bovine heart CL undergoes complete transition to the H_{II} phase at ~1.5–2.5 M NaCl, as seen also from Fig. 11. As protein content increases, the [NaCl] threshold for 50% conversion increases, and also the extent of conversion to the H_{II} phase decreases. Approximately 70–90 bilayer CLs per cytochrome oxidase are stabilized in high salt, at the different lipid/protein ratios. This corresponds to ~2–4 shells of CL surrounding cytochrome *c* oxidase, as deduced from the stoichiometry for diacyl lipids in Table 1. Freeze-fracture electron microscopy reveals phase separation between the domains of protein-containing bilayer CL and protein-free H_{II} CL domains, in 4 M NaCl [223].

Stabilization of the lamellar phase extends also to the natural lipid composition of biological membranes, if this is situated close to a nonlamellar phase transition, e.g., by rhodopsin in rod

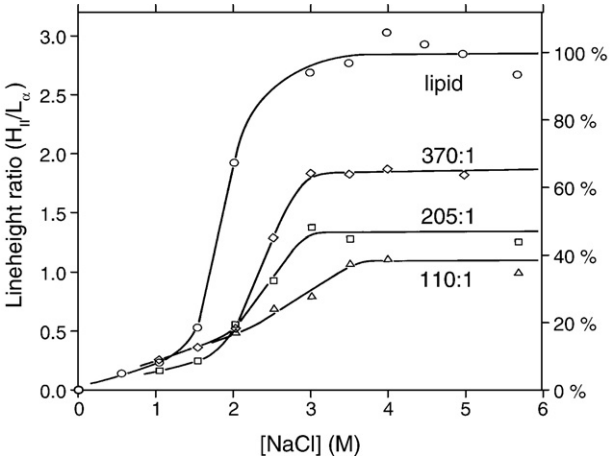

Fig. 12. Ratio of lineheights for the H_{II} and L_α components in the $\sigma_\perp$ region of ^{31}P-NMR spectra (at 20 °C, cf. Fig. 11) from cytochrome oxidase/CL complexes at the lipid/protein mole ratios indicated, as a function of salt concentration [223].

outer segment membranes [224,225], or by Na,K-ATPase in membranes from shark salt glands [226]. The diphytanyl lipids of the purple membrane from *Halobacterium cutirubrum*, on the other hand, remain in a lamellar state in both the presence and absence of bacteriorhodopsin [227]. Most likely, the lamellar phase is preferentially stabilized in nonlamellar-forming lipids because the hydrophobic span of the protein matches that of the lipid membrane in the lamellar phase (see, e.g., Section 8). This is potentially of functional relevance, because it implies that the natural lipids are in a state of curvature frustration, which can modulate protein activity via the inhomogeneous transverse profile of lateral pressure across the membrane (see Sections 9.2 and 9.3, below).

Systematic experiments with tryptophan-flanked WALPn_{res} transmembrane peptides of defined length, n_{res}, [228] reveal that the ability to promote formation of H_{II} phases depends on the direction and extent of hydrophobic mismatch (cf. also Section 8). Fig. 13 shows the fluid-phase preferences of saturated and *cis*-monounsaturated diC_{n_C}PCs that contain WALPn_{res} peptides of different lengths, at a mole ratio of 1:10. The extent of hydrophobic mismatch is given by the C^{α}–C^{α} distance between the outermost tryptophans of the α-helical peptide, minus the thickness of the hydrocarbon core of the lipid bilayer. In this case, all lipids prefer a lamellar phase in the absence of peptide, and the effect of negative mismatch is to induce the non-lamellar phase. It is presumed that the peptides join two cylinders of the H_{II} phase, along an intercylinder axis where the thickness of the lipid hydrocarbon core is considerably less than that in the L_{α} phase (see, e.g., [179]).

In a nonlamellar-forming lipid, WALPn_{res} peptides correspondingly promote formation of isotropic and/or H_{II} phases [229]. Incorporation of relatively short peptides, WALP14−17, at a level of 2 mol% in di$C_{18:1t}$PE lowers and broadens the temperature range over which the L_{α} to H_{II} transition takes place. All three peptides tested are equally efficient at promoting the H_{II} phase. Incorporation of longer peptides, WALP19−27, partially induces an inverse cubic phase (Pn3m); the proportion of this Q_{II} phase, relative to H_{II} phase, increases with increasing degree of hydrophobic mismatch between peptide and lipid. WALP27 does not stabilize the lamellar phase, despite its positive hydrophobic mismatch. Compared with integral proteins, this is probably because the WALP peptides are anchored solely by tryptophans. Peptides flanked by Trp, Tyr, Lys, or (at low pH) His residues are effective in inducing mismatch-relieving inverted cubic and H_{II} phases, whereas those flanked by Phe, Arg, or (at neutral pH) His residues cannot induce an H_{II} phase [230].

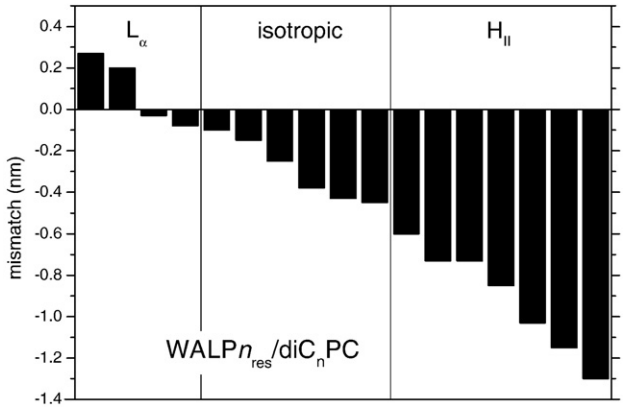

Fig. 13. Phase preference of saturated and unsaturated diC_{n_C}PCs containing 1:10 mole ratio of tryptophan-anchored WALPn_{res} peptides, according to the extent of hydrophobic mismatch between the $W_2L(AL)_mW_2$ peptide units and the lipid chains. The regions marked isotropic and H_{II} indicate that all or part of the lipid is in the corresponding phase. (Data from [228]).

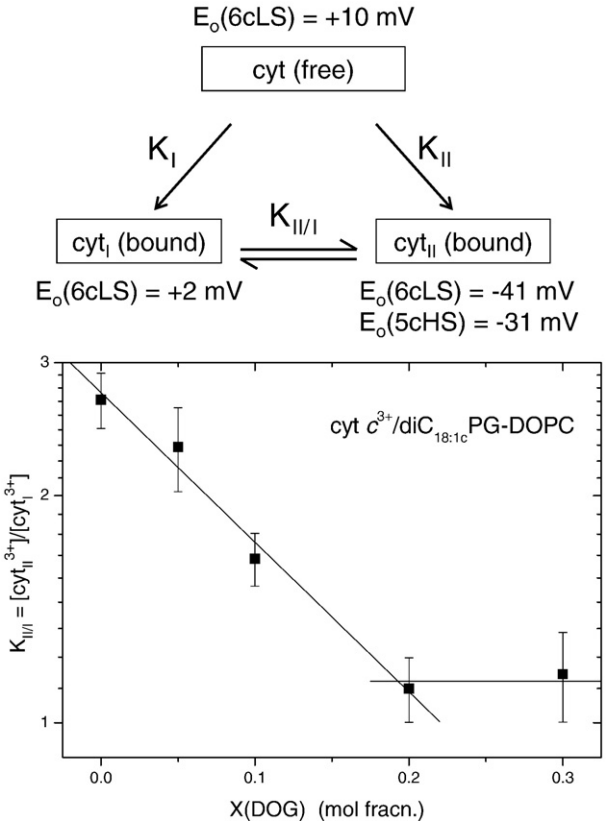

Fig. 14. Upper: binding and conformational equilibria for association of cytochrome *c* with anionic lipid membranes containing dioleoyl glycerol (DOG). Lower: dependence on membrane composition, [DOG], of the equilibrium constant, $K_{II/I}$, for the cyt c_{II}^{3+}/cyt c_I^{3+} conformational change of cytochrome c^{3+} bound to di$C_{18:1c}$PG-DOG bilayers. The ordinate is logarithmic. T=22.5 °C. Data from [233].

7.5. Influence of peripheral proteins

Surface association of cytochrome *c* with bilayers of CL induces either partially an H_{II} phase [231] or an isotropic lipid component [232], as judged by ^{31}P-NMR. An isotropic ^{31}P-NMR spectral component is also induced on binding cytochrome *c* to di$C_{18:1c}$PG and its mixtures with dioleoyl glycerol (DOG) or di$C_{18:1c}$PC, or to an oleic acid–di$C_{18:1c}$PC mixture [233]. In the absence of protein, these lipids are in a lamellar phase, although they have an intrinsic tendency to curvature because a 1:1 mixture of DOG with di$C_{18:1c}$PG forms an H_{II} phase. For di$C_{18:1c}$PG alone, the conversion to an isotropic component by cytochrome *c* is almost complete. Viscometry and negative stain electron

microscopy indicate that complexes of cytochrome *c* with di$C_{14:0}$PG form an extended network phase ([234; and see also [235]), whereas an inverse cubic phase was detected for aqueous dispersions of cytochrome *c* with monooleoyl glycerol [236]. These results indicate that an increase in surface curvature of the lipid lamellae can take place on binding the peripheral protein.

In the case of the electron-transfer protein cytochrome *c*, a reciprocal effect of the spontaneous curvature of the lipid is observed on the conformational state of the protein [233]. Two different states, I and II, are induced on binding cytochrome *c* to negatively charged lipids [237]. As indicated in Fig. 14, the conformation of cyt c_I^{3+} is very similar to that in solution and the native six-coordinate low-spin (6cLS) configuration of the haem is preserved, whereas in the cyt c_{II}^{3+} state the haem crevice opens and the Fe^{3+} exists in an equilibrium between a five-coordinate high-spin (5cHS) and a new 6cLS configuration. Although the secondary structure remains unchanged, these conformational changes on binding to anionic lipids are accompanied by a weakening of the tertiary contacts [238]. Fig. 14 shows that addition of the nonlamellar-favouring DOG to di$C_{18:1}$PG shifts the conformational equilibrium of the membrane-bound cytochrome *c*. Apparently, the tendency to nonlamellar curvature relaxes the conformation of the surface-associated protein in favour of the native-like 6cLS cyt c_I^{3+} state. This modulation can have functional significance because transition to the cyt c_{II}^{3+} state is accompanied by a large downward shift in the redox potential, E_o.

Interestingly, the high-specificity binding of avidin to biotinylated lipid headgroups also enhances the membrane surface curvature and induces isotropic ^{31}P-NMR lipid components [74], which could have implications for the lipid–protein interactions of proteins with covalently linked lipid chains.

8. Modulation by hydrophobic matching

Lipid chainlength is often found to modulate the function of integral transmembrane proteins. In numerous cases, the enzyme or transport activity reaches a maximum at a particular lipid chainlength and is reduced in membranes with either shorter or longer lipid chains [94,239–244]. Optimum activity is attained when the hydrophobic thickness of the lipid membrane matches the transmembrane hydrophobic span of the protein.

The effects on the membrane lipids of hydrophobic mismatch with embedded proteins are studied most directly from the equilibrium constants for association of lipids with the protein [20], and the segmental order parameters of the lipid chains associated with the protein [52]. Both of these indicate that the elastic distortion of the lipid chains is insufficient to compensate completely for the mismatch between the hydrophobic spans of the transmembrane protein and the lipid bilayer (see Fig. 15 and [245]).

The dependence of the association constants for the protein on lipid chainlength [246] can be described by an excess free energy, ΔG_{LP}, of lipid–protein interaction that consists of an elastic contribution from chain deformation, l_L–l_o, and a term that depends linearly on the residual mismatch, l_P–l_L. Here l_o is the length of the undistorted lipid molecule in free bilayers, l_L is the actual lipid length, and l_P is half the transmembrane length of the protein. The excess free energy of lipid–protein interaction, *per lipid molecule*, is then given by [245]:

$$\Delta G_{LP} = \frac{1}{2} K_t A_L \frac{(l_L - l_o)^2}{l_o} + \sigma_L \Delta g_{mis} |l_P - l_L| \qquad (23)$$

where K_t is the compressibility modulus for the thickness of lipid membranes (Young's modulus), A_L is the membrane surface area per lipid molecule, σ_L is the width of a lipid molecule at the lipid–protein interface, and Δg_{mis} is the free energy density of residual hydrophobic mismatch (per unit area of lipid–protein interface, cf. Section 2.3). On the basis of the lipid binding data to be given below, it is assumed that Δg_{mis} is the same for positive and negative mismatches. The condition for minimum free energy ($\partial \Delta G_{LP}/\partial l_L = 0$), then yields the

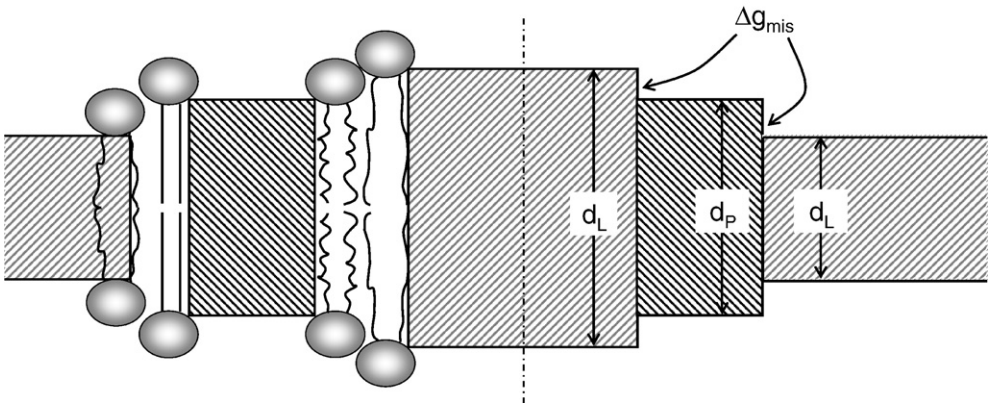

Fig. 15. Schematic indication of hydrophobic mismatch. On the left: the lipid chains extend or compress to compensate for the mismatch in hydrophobic spans of the lipid bilayer (d_L) and the protein (d_P). On the right: mismatch imposes an energy penalty from exposure of hydrophobic surfaces of the lipid or protein to a hydrophilic environment of the corresponding partner. The energy cost is equal to the product of the free energy density of exposure, Δg_{mis}, and the area of exposed interface. In the two outer regions ($d_L < d_P$), the hydrophobic thickness of the protein exceeds that of the lipid; in the central region ($d_L > d_P$), the hydrophobic thickness of the lipid exceeds that of the protein.

equilibrium length of the elastically distorted protein-associated lipids that is given by:

$$l_L = l_o\left(1 + \frac{(l_P - l_o)}{|l_P - l_o|}\frac{\sigma_L \Delta g_{mis}}{K_t A_L}\right) \tag{24}$$

for $l_o \neq l_P$. Substituting from Eq. (24) in Eq. (23) then yields the following dependence of the excess free energy of lipid–protein interaction on lipid chainlength, l_o:

$$\Delta G_{LP}(l_o, l_P) = \sigma_L \Delta g_{mis}\left(|l_P - l_o| - \frac{1}{2}\frac{\sigma_L \Delta g_{mis}}{K_t A_L} l_o\right) \tag{25}$$

at equilibrium. The free energy of lipid–protein interaction therefore depends linearly on lipid chainlength, with a slight asymmetry about the point of hydrophobic matching ($n_C = n_P$) that is determined by the ratio of the interfacial free energy density of mismatch to that of elastic extension, i.e., by $\Delta g_{\mathrm{mis}}/K_t$.

8.1. Lipid binding constants

Fig. 16 shows the chainlength dependence of the lipid association constants for different transmembrane proteins. This is taken from the work of East and Lee [19], O'Keeffe et al. [99], Williamson et al. [246], and Powl et al. [247]. The ordinate is plotted so as to yield the relative free energy of association, $\Delta\Delta G_{ass}/k_BT = -\ln(K_r)$, where K_r is the association constant relative to $\mathrm{diC}_{18:1c}\mathrm{PC}$. The free energy of association reaches a minimum at a particular lipid chainlength, $n_C = n_P$, that corresponds to hydrophobic matching with the transmembrane span of the protein. Outside this region, the chainlength dependence of $\Delta\Delta G_{ass}$ is linear over an appreciable range of n_C, as predicted by Eq. (25). With appropriate values of $K_t A_L/\sigma_L$, and the chainlength dependence of the bilayer thickness from the most recent X-ray refinements ([248]; see also [186]), it is then possible to determine the free energy density, Δg_{mis}, of mismatch. The values that are obtained from fitting Eq. (25) for the different transmembrane proteins are in the range $\Delta g_{\mathrm{mis}} \sim (0.5\text{–}1.2) \times k_BT\,\mathrm{nm}^{-2}$ [245].

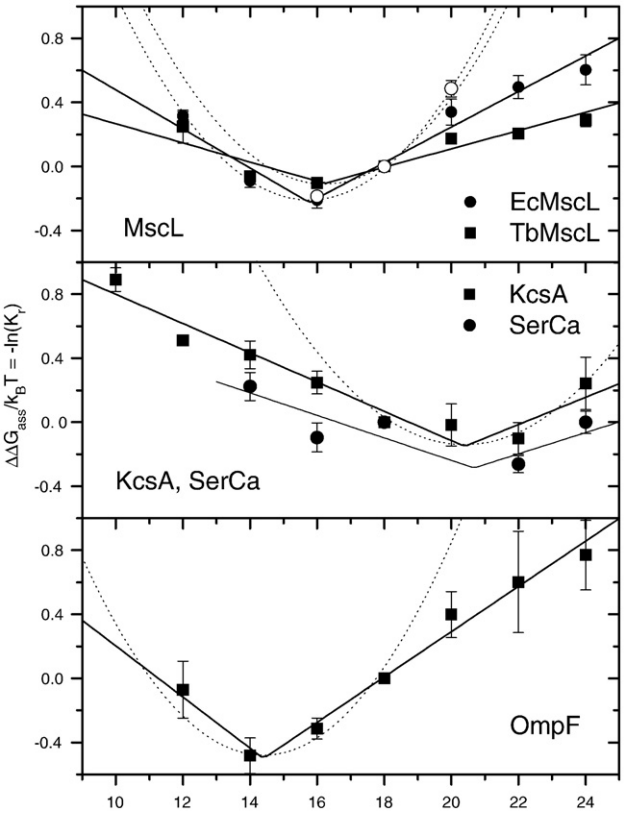

Fig. 16. Chainlength dependence of $\mathrm{diC}_{n_C:1c}\mathrm{PC}$ lipid association constants, K_r, relative to $\mathrm{diC}_{18:1c}\mathrm{PC}$, for association with (upper to lower panels): *E. coli* (solid circles) and *Mycobacterium tuberculosis* (squares) mechanosensitive channel of large conductance, EcMscL and TbMscL, respectively (data from [247]); *S. lividans* K^+-channel, KcsA (squares) (data from [246]) and Ca-ATPase, SERCA (circles) (data from [19]); and *E. coli* outer membrane porin, OmpF (data from [99]). The ordinate is plotted to yield the relative free energy of association $\Delta\Delta G_{ass}/k_BT = -\ln(K_r)$. Solid lines are least-squares fits of Eq. (25) [245]. Open circles in the top panel are the free energies of opening the *E. coli* MscL channel at zero tension (data from [244]), expressed per lipid with $N_L = 29$, and relative to $\mathrm{diC}_{18:1c}\mathrm{PC}$ bilayers as reference state.

8.2. Free energy of lipid–protein mismatch

The interfacial free energy densities, Δg_{mis}, for hydrophobic mismatch are found to be comparable in magnitude to those derived for lipid–protein interactions, g_{LP}, in Section 2.3. However, they are far less than the interfacial free energy for interaction of hydrocarbon chains directly with bulk water. The latter is characterized by a hydrophobic free energy density, $\gamma_{phob} \sim 8.5 \times k_BT\,\mathrm{nm}^{-2}$ [189,249,250], that is equivalent to an interfacial tension of 35 $\mathrm{mN.m}^{-1}$. This shows that hydrophobic groups are not exposed to water as a result of the mismatch between lipids and protein. As suggested by Sperotto and Mouritsen [251], the excess free energy density corresponds instead to the interaction of hydrophobic groups with a hydrophilic environment: either polar protein side chains or phospholipid headgroups. On this basis, the free energy density of hydrophobic–hydrophilic contact can be up to 17 times smaller than that of hydrophobic contact with bulk water.

An alternative explanation for these rather low free energies was proposed by Lee and coworkers [20,246]: that the protein distorts to alleviate mismatch with the hydrophobic span of the lipid chains. Of the transmembrane proteins in Fig. 16, the relatively rigid β-barrel protein OmpF has the steepest dependence of lipid association free energy on chainlength, whereas the α-helical mechanosensitive channel TbMscL has that which is least steep. Tilting of helices, as in the opening of mechanosensitive channels [252], is not expected to be very costly, compared with the energetics of distortion of protein secondary structure, as will be seen immediately below.

Under a membrane tension, $\overline{T}$, the free energy of opening a mechanosensitive ion channel is given by:

$$\Delta G_{open}(\overline{T}) = \Delta G_{open}(0) - \overline{T}\Delta A_P \tag{26}$$

where ΔA_P is the increase in cross-sectional area of the channel on opening. The probability, p_{open}, for channel opening is then given by the following two-state Boltzmann distribution:

$$p_{open} = \frac{1}{1 + \exp\left(\left(\Delta G_{open}(0) - \overline{T}\Delta A_P\right)/k_BT\right)} \tag{27}$$

Thus, the free energy of channel gating in the tension-free membrane can be determined from the dependence of the open probability on membrane tension according to:

$$\Delta G_{open}(0) = \overline{T}_{1/2}\Delta A_P \tag{28}$$

where $\overline{T}_{1/2}$ is the tension for 50% probability of channel opening.

The open circles in the top panel of Fig. 16 give the free energies of opening the EcMscL channel in di-monounsaturated phosphatidylcholines of different chainlengths that are derived from Eq. (28) by Perozo et al. [244]. So as to compare with the free energy of lipid association, these values are divided by the number of lipid molecules in the first shell surrounding MscL, N_L=29 (corresponding to a protein outer radius of 2.15 nm; [247]), and are referred to $\Delta\Delta G_{open}(0)$=0 for EcMscL in diC$_{18:1c}$PC bilayers. The agreement with the lipid binding data is quite good, indicating that the response to hydrophobic mismatch (by helix tilting) is responsible for the chainlength dependence in both cases.

Further, if it is assumed from Eq. (28) that the free energy is linear in the area change, then the value of $\overline{T}_{1/2} \approx$ 11.8±0.8 mN m^{-1} for EcMscL [253] determines the energy associated with changes in transmembrane thickness of the protein. With volume incompressibility, the change in protein thickness, d_P, is given by $\Delta A_P/A_P = -\Delta d_P/d_P$. This equals the fractional change in lipid length, $\Delta l_o/l_o$, for fully compensated hydrophobic matching. The free energy of protein deformation *per lipid* is then estimated as:

$$\Delta G_{def} \approx -T_{1/2}\frac{A_P}{N_L}\left(\frac{\Delta l_o}{l_o}\right) \tag{29}$$

where N_L~29 [247] for MscL. Eq. (29) predicts values of $\partial\Delta G_{def}/\partial n_C \approx (0.06–0.12)\times k_BT$ for di-monounsaturated phosphatidylcholines with chainlengths n_C=20 to 14, respectively [245]. These values correspond to free energy densities $\Delta g_{def} \approx (0.5–1.0)\times k_BT$ nm^{-2}, which are similar in magnitude to the experimental values derived from lipid binding. Thus, it appears that protein deformation, via helix tilting, is a quantitatively viable alternative to the exposure of hydrophobic groups to a polar membrane environment, for the free energy density of mismatch, Δg_{mis}.

8.3. Protein hydrophobic thicknesses

The minima in free energy of lipid association in Fig. 16 define the chainlength, n_P, corresponding to hydrophobic matching. Recent refinements of lipid bilayer thicknesses from X-ray diffraction [248,254,255] allow an improved estimate of the hydrophobic span of proteins for which the chainlength dependence of lipid binding, or other functional parameters, have been determined. Table 7 lists the values of n_P, and the hydrophobic thicknesses, d_c, which are deduced from them. For comparison, transmembrane hydrophobic spans that are derived from crystal structures of the proteins [20], and from theoretical estimates of free energies for partitioning the protein crystal structures [256] in a hydrophobic medium with an experimentally based boundary function [257], are also given in Table 7.

Table 7
Hydrophobic thickness (nm) of transmembrane proteins, and matching to lipid bilayers[a]

	OPM[b]	Structure[c]	n_P	d_c
OmpF	2.42±0.08	2.4	14.4±0.3	2.00±0.05
KcsA	3.31±0.10	3.7	20.4±0.5	3.13±0.10
TbMscL	2.65±0.38	1.8 or 3.4	16.2±0.6	2.34±0.11
EcMscL			15.8±0.3	2.25±0.06
SERCA	3.01±0.18	2.1	20.7±1.3	3.18±0.24
Rho	3.24±0.17		15	2.80
MelB	3.19±0.12[d]		16	2.30
Cyt. *c* Oxidase	2.54±0.18	2.9	18	2.68
F_1,F_o-ATPase	3.59±0.18		18	2.68
Na,K-ATPase			22	3.44

[a] n_P is the chainlength of the diC$_{n_C}$PC lipid with lowest free energy of association (Fig. 16) or highest activity (from [245]). d_c is the thickness of the hydrophobic core deduced from n_P by using refined X-ray data (see [186,245]).
[b] Hydrophobic thickness deduced from thermodynamic principles, as listed in the Orientation of Proteins in Membranes (OPM) database (http://opm.phar.umich.edu/).
[c] Hydrophobic thickness deduced from protein crystal structure as given by Lee [20].
[d] For *lac* permease from *E. coli*.

8.4. Lipid chain-melting transition shifts

The chain-melting transition temperature, T_t, of lipid bilayers is sensitive to the energetics of hydrophobic matching because the bilayer thickness differs between the gel ($T<T_t$) and fluid ($T>T_t$) phases. The preference of the protein for the fluid phase, relative to the gel phase, is given by the partition coefficient:

$$K_{f/g} = \exp\left(-\frac{\Delta G_{LP}(\mathrm{fluid}) - \Delta G_{LP}(\mathrm{gel})}{\mathrm{k_B}T_t}\right) \tag{30}$$

From Eq. (25), the difference, ΔG_{LP}(fluid)−ΔG_{LP}(gel), in free energy of lipid–protein interaction, *per lipid molecule*, at the chain-melting transition is given by:

$$\Delta\Delta G_{LP}(T_t) = \sigma_L\Delta g_{mis}\left(\frac{l_P - l_o}{|l_P - l_o|} + \frac{\sigma_L\Delta g_{mis}}{2K_tA_L}\right)(l_o(\mathrm{gel}) - l_o(\mathrm{fluid})) \tag{31}$$

where l_o(gel)−l_o(fluid) ($\approx \Delta l_{inc}\times n_C$) is the difference in length of the lipid molecules in gel and fluid phases. Eq. (31) applies in all regions except where the hydrophobic span of the protein lies between those of the gel- and fluid-phase bilayers.

For low mole fractions of protein, the difference in lipid chemical potential between fluid and gel phases is given by Henry's law [251]:

$$\mu_{L,f} - \mu_{L,g} = \mu^o_{L,f} - \mu^o_{L,g} - k_BT\left(x_{P,f} - x_{P,g}\right) \tag{32}$$

where $x_{P,f}$ and $x_{P,g}$ are the mole fractions of protein in the fluid and gel phases, respectively. The standard state for the lipid is the protein-free bilayer, and therefore:

$$\mu^o_{L,f} - \mu^o_{L,g} = \Delta H_t - T\Delta S_t = \Delta H_t\left(1 - \frac{T}{T_t}\right) \tag{33}$$

where ΔH_t and ΔS_t are the enthalpy and entropy, respectively, of chain-melting in the absence of protein. For binary mixtures with protein, the chemical potentials of gel and fluid lipids are equal

along a tie line at constant temperature, i.e., $\mu_{L,f} - \mu_{L,g} = 0$ in Eq. (32) (see Fig. 17). Thus the phase boundaries, T_f and T_g, at the *fluidus* ($x_{P,f} = X_P$) and *solidus* ($x_{P,g} = X_P$) ends of the tie line are given by, respectively:

$$T_f - T_t = \frac{k_B T_t^2}{\Delta H_t}\left(1/K_{f/g} - 1\right)X_P \tag{34}$$

and

$$T_g - T_t = \frac{k_B T_t^2}{\Delta H_t}\left(1 - K_{f/g}\right)X_P \tag{35}$$

where X_P ($= x_{P,f} + x_{P,g} << 1$) is the total mole fraction of protein. The dependence on hydrophobic mismatch of the shift in mid-point temperature, $(1/2)(T_f + T_g)$, of gel–fluid phase separation is therefore given by [251]:

$$\Delta T_t = \frac{k_B T_t^2}{\Delta H_t}\sinh\left(\frac{\Delta\Delta G_{LP}(T_t)}{k_B T_t}\right)X_P \tag{36}$$

where $K_{f/g}$ is substituted from Eq. (30).

Fig. 18 gives the shifts in chain-melting transition, on incorporation of the melibiose permease (MelB) from *E. coli* in di$C_{n_C:0}$PC bilayers [242]. The inset shows that the shift, ΔT_t, increases linearly with mole fraction of protein, as predicted for dilute solutions by Eq. (36). The solid line in Fig. 18 is a non-linear least-squares fit of Eq. (36) with the chainlength dependence given in Eq. (31) [245]. The fit is valid only in the regions outside that of hydrophobic matching, which must occur between $n_C = 14$ and $n_C = 16$ for saturated phosphatidylcholines. A fixed value of $n_P = 15$ is used for the fit shown in Fig. 18; values fixed in the range $n_P = 14.1$–15.9 do not change the fit at values of n_C outside this range.

The fit shown in Fig. 18 reproduces the essential features of the chainlength dependence of the transition temperature shift by MelB. It yields a value of $\Delta g_{mis}/k_B T_t = 2.5 \pm 0.5$ nm^{-2} for the free energy density of mismatch, which is comparable to direct estimates from lipid binding to other proteins. The fitted value for the difference in chainlength increments between gel and fluid phases is $\Delta l_{inc} = 0.10 \pm 0.02$ nm/CH_2. The maximum increment in the gel phase is l_{inc}(gel) = 0.127 nm/CH_2 for an all-*trans* chain, which yields an increment in the fluid phase of l_{inc}(fluid) = 0.03 ± 0.02 nm/CH_2. For comparison, correction of X-ray data for fluid-phase di$C_{n_C:0}$PC bilayers to the transition temperatures produces an effective increment of 0.061 ± 0.002 nm/CH_2 [245]. The description of the chainlength dependence of the transition temperature shifts by Eqs. (31) and (36) is therefore not quantitatively unreasonable.

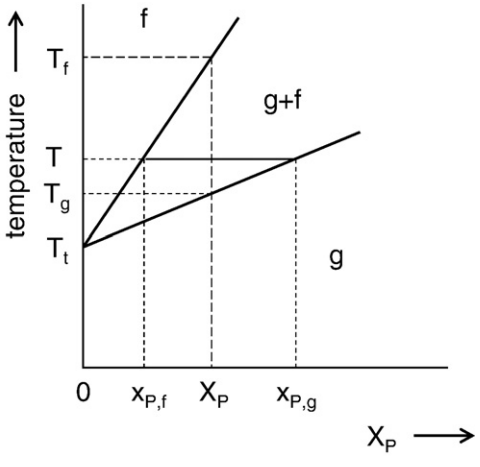

Fig. 17. Schematic phase diagram (T vs. X_P) for a binary mixture of a protein with a single lipid. Single-phase regions correspond to gel (g) and fluid (f) lipids. In the two-phase region (g + f), gel and fluid lipid phases coexist. Along a tie line at constant temperature (solid horizontal line, T), the chemical potentials of coexisting gel phase (composition $x_{P,g}$) and fluid phase (composition $x_{P,f}$) are equal. The *solidus* phase boundary is at temperature T_g and the *fluidus* phase boundary is at temperature T_f, for total mole fraction of protein X_P.

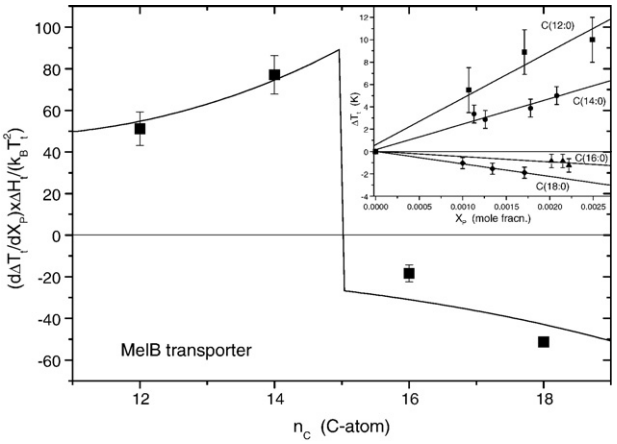

Fig. 18. Chainlength dependence of the shift, ΔT_t, in lipid chain-melting transition temperature with mole fraction, X_P, of the *E. coli* melibiose permease (MelB) in di$C_{n_C:0}$PC bilayers. The ordinate, $d\Delta T_t/dX_P$, is obtained from the linear regressions given in the inset (data from [242]) and is normalized by the factor: $\Delta H_t/k_B T_t^2$ obtained from calorimetric data for di$C_{n_C:0}$PCs from Lewis et al. [258]. Solid line: least-squares fit of Eqs. (36) and (31), with fixed value of $n_P = 15$ [245].

8.5. Adaptation of lipid length

Eq. (24) predicts that the fractional extension in length, $\Delta l/l_o$, of the lipid chains is independent of the extent of mismatch and lies in the range 5–10%. For the lysine-anchored transmembrane leucine–alanine oligopeptide Ac-GK_2(LA)$_8$LK_2A-amide (KALP23) and arginine or histidine analogues (RALP23 and HALP23), the extension of di$C_{14:0}$PC chains adjacent to the peptide is small [53,230], but those for the corresponding tryptophan-anchored peptides are appreciably larger.

Fig. 19 shows the change in hydrophobic thickness, $d_c - d_c^o$, of disaturated phosphatidylcholines that is induced by the Fm-AW_2(LA)$_5$W$_2$A-Etn (WALP16) and Fm-AW_2L(AL)$_m$W$_2$A-Etn ($m = 5$: WALP17; $m = 6$: WALP19) peptides. Values are obtained from the increase, $\Delta\langle S_{CD}(n_C)\rangle$, in mean chain segmental order parameter of the fluid-phase di$C_{n_C:0}$PC lipids [52], according to [245,259]:

$$d_c(n_C : 0) - d_c^o(n_C : 0) = -(0.254\text{nm}) \times \Delta\langle S_{CD}(n_C)\rangle n_C \tag{37}$$

where the length of an all-*trans* chain segment is 0.127 nm. The data are corrected to a common temperature of 30 °C, and are scaled up from average values for the whole bilayer to represent

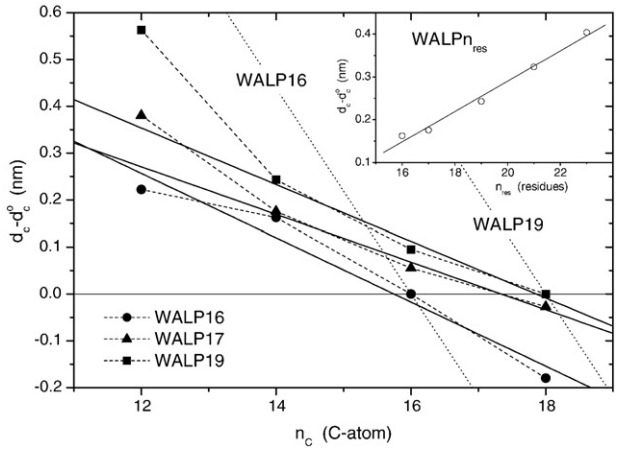

Fig. 19. Chainlength dependence of the maximal increase in hydrophobic thickness, $d_c - d_c^o$, for di$C_{n_C:0}$PC lipids directly adjacent to WALP16 (circles), WALP17 (triangles) or WALP19 (squares) peptides (^{2}H-NMR order parameters from [52]). Data from fluid-phase bilayers are corrected to 30 °C with $\alpha_d = -0.0033$ K^{-1}. Solid lines are linear regressions (omitting $n_C = 12$ for WALP17 and WALP19). Dotted lines are predictions for complete hydrophobic matching (see [245]). Inset: dependence on peptide length, n_{res}, for WALPn_{res} in di$C_{14:0}$PC (^{2}H-NMR order parameters from [52,53,230]).

the maximal extension of the lipids in immediate contact with the peptides according to Eq. (13) (see Section 4.1). Unlike the prediction of Eq. (24), the degree of extension of the lipid chains by the WALP peptides depends on the extent of mismatch. This is evident also from the dependence of the maximal lipid extension on hydrophobic length of the WALP peptides in a phosphatidylcholine of constant chainlength, $n_C = 14$ (see inset to Fig. 19).

Fig. 19 shows that hydrophobic matching is achieved at chainlengths of $n_C = 16$ and 18 for WALP16 and WALP19, respectively, and the zero-crossing for WALP17 is at $n_C \approx 17.3$. Predictions of the total hydrophobic mismatch, from the chainlength increment in thickness of protein-free bilayers, are given by the dotted lines in Fig. 19. The elastic distortion of the lipid chains compensates for 31±3, 23±4 and 28±6% of the total mismatch with the WALP16, WALP17 and WALP19 peptides, respectively. Hydrophobic thicknesses of $d_c = 2.77 \pm 0.13$, 2.94± 0.13 and 3.02±0.13 nm are deduced for the WALP16, WALP17 and WALP19 peptides, respectively from Fig. 19 [245]. For comparison, the geometrical lengths of WALP16, WALP17 and WALP19 are 2.55, 2.70 and 3.00 nm, respectively, counting the C-terminal ethanolamine as a residue and assuming regular α-helices.

Eq. (24) predicts a constant elastic distortion of the lipid chains that does not depend on the extent of mismatch. This is because a fixed free energy density of mismatch, Δg_{mis}, corresponds to a constant interfacial tension, which at equilibrium is balanced by an equal tension that is generated at a specific elastic extension, $l_L - l_o$, of the lipid chains. A chain extension that depends on the extent of hydrophobic mismatch requires that the excess free energy density of mismatch also depends on the extent of mismatch. A linear dependence, of the form $\Delta g_{\mathrm{mis}}(l_P/l_o - 1)$, would be consistent with the results in Fig. 19, but this predicts an excess free energy of lipid–protein interaction that depends harmonically of the extent of mismatch and therefore describes the chainlength dependence of lipid binding less well than does Eq. (25). A more detailed discussion can be found in Marsh [245].

9. Modulation by intrinsic lipid curvature

Spontaneous (or intrinsic) curvature was introduced originally by Helfrich [260] and Evans [261], within the framework of elasticity theory, to describe curvature that arises from transbilayer membrane asymmetry. It was later generalized to lipid monolayers to explain the tendency of particular lipids to form non-lamellar phases — see Section 7. Subsequently, various protein-associated membrane functions have been found to be controlled or modulated by the intrinsic curvature of the lipids that constitute the membrane bilayer environment [262–267].

Lipids that form non-lamellar phases, such as the inverted hexagonal (H_{II}) or normal micellar (M_I) phase, exist in a state of curvature frustration when constrained to be in a lamellar membrane configuration. Intrinsic curvature of membrane lipids therefore can favour conformational changes of embedded proteins, or facilitate incorporation of proteins in the membrane, if the shape of the protein tends to alleviate the curvature frustration of the adjacent lipids. A quantitative description, in terms of elasticity theory, has been given by Attard et al. [265] for the activation of CTP:cytidylyltransferase on binding to membranes that contain non-bilayer lipids.

Bending elasticity can also be described in terms of the inhomogeneous profile of lateral pressure across the lipid membrane [189,268,269]. Cantor [270] has proposed a mechanism whereby changes in the lateral pressure profile may induce transitions between protein conformations that differ in their intramembranous shape, and hence cause a dependence of function on lipid composition. Conceptually, this approach is very appealing. Uncertainties exist, however, as to the size of the various components that contribute to the lateral pressure profile, and this had led to questioning the quantitative significance of this mechanism [271]. It is not until recently that the equivalence of this approach to that based on spontaneous curvature and elasticity theory has been demonstrated [132]. Here, we describe the information that can be obtained from both approaches.

9.1. Curvature elasticity

For a membrane (or monolayer) of surface area A that is composed of lipids with intrinsic curvature c_o, the elastic free energy of bending is given by [260]:

$$\Delta G_c(\overline{c}, \overline{c}_G) = \tfrac{1}{2} k_c A (\overline{c} - c_o)^2 + \overline{k}_c A \, \overline{c}^{\,2}_G \qquad (38)$$

where, for principal curvatures $c_1 = 1/R_1$ and $c_2 = 1/R_2$ (see Fig. 20), the mean (or total) curvature is given by $\overline{c} = c_1 + c_2$ and the Gaussian curvature is given by $\overline{c}^{\,2}_G = c_1 c_2$. The elastic moduli (or bending rigidities) for mean and Gaussian curvature are k_c and $\overline{k}_c$, respectively. In the case of a flat (i.e., non-curved) reference surface, the elastic free energy is given by $\Delta G_c(0,0) = \tfrac{1}{2} k_c A c_o^2$, which represents the curvature frustration of the lipids when they are forced into a planar configuration. Thus,

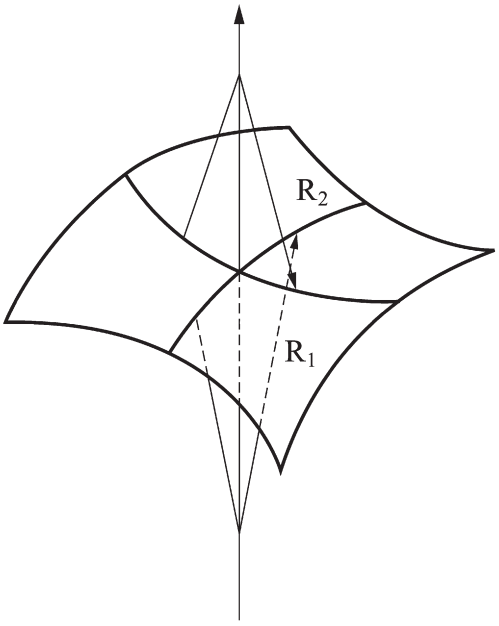

Fig. 20. Bending of a lipid monolayer with principal curvatures $c_1 = 1/R_1$ and $c_2 = 1/R_2$. The mean curvature is given by $\overline{c} = c_1 + c_2$ and the Gaussian curvature is given by $\overline{c}^2_G = c_1 c_2$. For cylindrical bending, $\overline{c} = c_1$ and $\overline{c}_G = 0$, and for a spherical vesicle/micelle, $\overline{c}/2 = c_1 = c_2 = \overline{c}_G$.

the chemical potential, μ_b, of a protein at mole fraction X_b in a planar membrane contains a contribution from the curvature elasticity of the lipids, and is given by [132]:

$$\mu_b = \mu_b^o + k_B T \ln(X_b) - N_L A_L k_C \left(\overline{c}_P c_o - \overline{c}_P^2/2 - \overline{k}_C \overline{c}^2_{G,P}/k_C \right) \quad (39)$$

where N_L is the number of lipids whose curvature is perturbed by the protein, and $\overline{c}_P$ and $\overline{c}_{G,P}$ are the mean and Gaussian curvatures, respectively, of the protein-associated lipids. Other symbols have their usual meanings.

In Eq. (39), the adaptation of the lipid curvature to the intramembranous shape of the protein is expressed in terms of $\overline{c}_P$ (and $\overline{c}_{G,P}$). As regards the dependence on lipid composition of the membrane, the contribution of curvature elasticity to the protein chemical potential is linear in the spontaneous curvature of the lipid mixture, plus a constant term. It should be noted that the elastic contribution refers to the alleviation of lipid curvature frustration at the protein surface and includes only implicitly any change in curvature of the actual membrane surface, such as might occur in the case of hydrophobic mismatch between protein and lipid (see Section 8 and [272,273]). The dependence on c_o in Eq. (39) demonstrates the direct sensitivity of protein conformations with different intramembrane shapes, i.e., different values of $\overline{c}_P$, to lipids with different intrinsic curvatures. This constitutes a mechanism whereby lipid composition can control conformational equilibria, and also insertion, of proteins in membranes.

9.2. Lateral pressure profile

Expressed alternatively in terms of the transmembrane lateral pressure profile, $p(z).dz$, the chemical potential of a protein in the membrane is given by [270]:

$$\mu_b = \mu_b^o + k_B T \ln(X_b) + \int A_P(z) p(z).dz \quad (40)$$

where $A_P(z)$ is the cross-sectional area of the protein at distance z from the membrane mid-plane (see Fig. 21). A conformational change that is accompanied by a change $\Delta A_P(z)$ in cross-sectional area profile will therefore cause a lipid-dependent change, $\Delta\mu_b$, in chemical potential of the protein. For lipid membranes that differ by an amount $\Delta p(z)$ in the lateral pressure profile, the difference in $\Delta\mu_b$ is then given by:

$$\Delta\Delta\mu_b = \int \Delta A_P(z) \Delta p(z).dz \quad (41)$$

As for the lipid spontaneous curvature in Eq. (39), transduction of $\Delta\mu_b$ in Eq. (41) is a means by which membrane lipid composition, via changes in the lateral pressure profile, can modulate the conformational equilibria of integral membrane proteins [270].

Contributions from the two apposing monolayers of the lipid membrane are additive in Eq. (41). For a symmetrical bilayer, the lateral pressure has reflection symmetry about the mid-plane $z = 0$, i.e., $p(-z) = p(z)$ (see Fig. 21). As illustrated in Fig. 22,

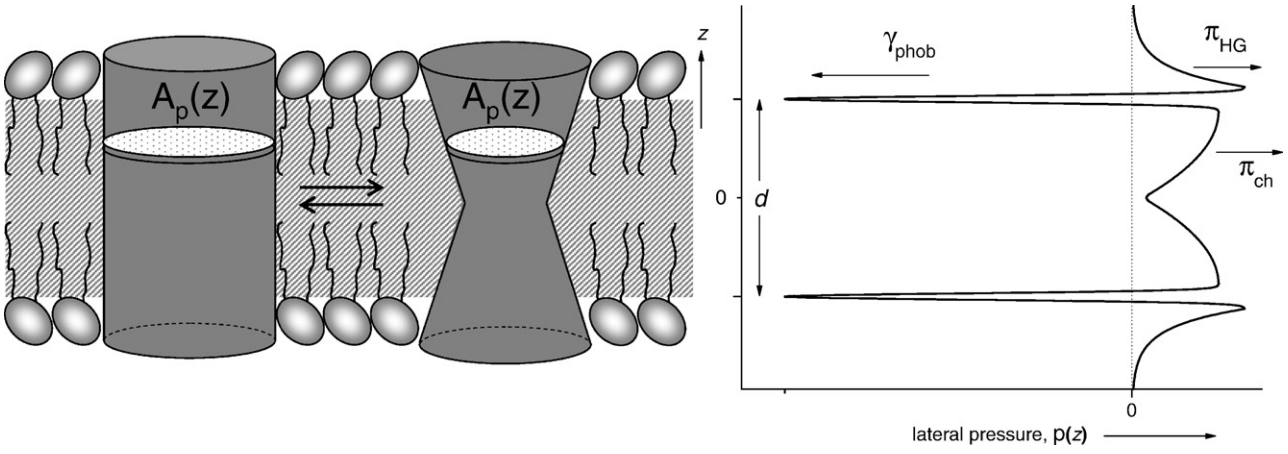

Fig. 21. Profile of lateral pressure, $p(z).dz$, with distance z from the bilayer mid-plane in a lipid membrane (right), and the cross-sectional profile, $A_P(z)$, of an inserted transmembrane protein (left). The protein is shown schematically in two conformations that differ in the shape of their transmembrane domain and therefore differently sense the lateral pressure profile.

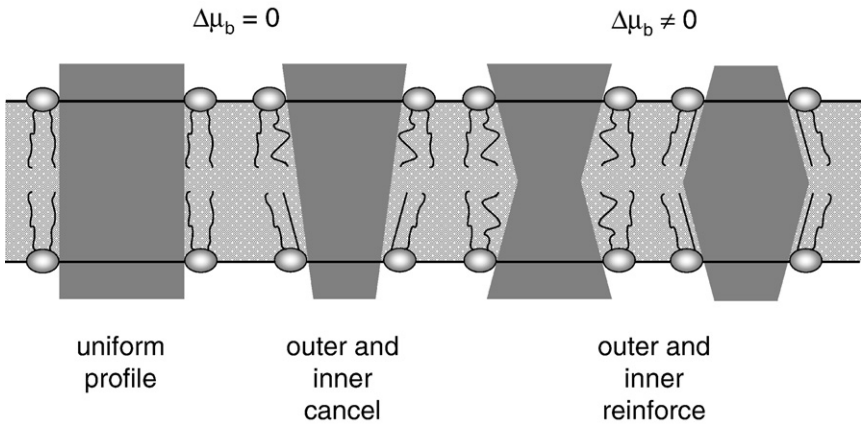

Fig. 22. Effect of protein shape profiles (or changes in profiles) on sensitivity to the lateral pressure profile of a symmetrical lipid bilayer. The two protein shapes on the left possess no net sensitivity to the lateral pressure profile, whereas the two monolayers reinforce in their effect on proteins with the two shapes shown on the right.

antisymmetric changes in cross-sectional area profile: $\Delta A_P(-z) = -A_P(z)$, e.g., of conical shape, then produce no net change in chemical potential of the protein. On the other hand, changes in cross-sectional area profile having reflection symmetry: $\Delta A_P(-z) = \Delta A_P(z)$, e.g., of an hour-glass shape, produce a net change in chemical potential, $\Delta\mu_b$, in symmetrical bilayers that is twice that for a single monolayer. A protein of uniform cross-sectional shape (i.e., $\Delta A_P(z)$=constant), such as on the extreme left in Fig. 22, possesses no net sensitivity to the lateral pressure profile, even in a lipid monolayer. This is because, at thermodynamic equilibrium, the membrane is free of tension and therefore the different contributions to the pressure profile must cancel exactly, i.e., $\overline{T} = \partial\mu_b/\partial A = \int p(z).dz = 0$ (cf. Fig. 21 and [189]).

The transmembrane profile of the cross-sectional area of the protein in Eq. (40) can be expanded in a Taylor series [274]:

$$A_P(z) = A_P(0) + a_{1,P}z + a_{2,P}z^2 + \ldots \tag{42}$$

where $a_{i,P}$ are the expansion coefficients. The reason for doing this is that the corresponding contributions to the chemical potential of the protein then depend on the moments of the lateral pressure profile:

$$\mu_b = \mu_b^o + k_BT\ln(X_b) + a_{1,p}\int z.p(z).dz + a_{2,P}\int z^2p(z).dz + \ldots \tag{43}$$

where the initial term, $A_P(0)$, in the area expansion does not enter because $\int p(z).dz = 0$. The moments of the lateral pressure profile relate directly to the experimental elastic constants for bending [268]. The spontaneous bending moment (per unit length), k_cc_o, is simply the first moment of the pressure profile:

$$k_cc_o = \int z.p(z).dz \tag{44}$$

which does not depend on the choice of origin for z, because $\int p(z).dz = 0$. The elastic modulus for Gaussian curvature, $\overline{k}_c$, is determined by the second moment of the pressure profile [268]:

$$\overline{k}_c = -\int (z-\delta)^2p(z).dz \tag{45}$$

where $z=\delta$ is the position of the neutral plane, i.e., that for bending without area extension. Eqs. (44) and (45) therefore allow the chemical potential of the protein in Eq. (43) to be rewritten as [132]:

$$\mu_b = \mu_b^o + k_BT\ln(X_b) + \left(a_{1,P} + 2a_{2,P}\delta\right)k_cc_o - a_{2,P}\overline{k}_c \tag{46}$$

Eq. (46) expresses the contribution from the lateral pressure profile to the chemical potential of the protein in terms of the experimentally accessible quantities, k_c, $\overline{k}_c$ and c_o. This expansion holds in so far as the profile of the cross-sectional area of the protein can be depicted adequately by the first three terms in Eq. (42). To this level of approximation, the contributions of the membrane lateral pressure profile to the chemical potential of the protein are given by a term that depends linearly on the intrinsic curvature of the lipids, plus a constant, just as in Eq. (39) that is derived from bending elasticity. However, the adaptation of the lipids to the protein surface is expressed differently in the two equivalent cases: either in terms of the cross-sectional profile of the protein (characterized by $a_{1,P}$ and $a_{2,P}$), or by the change in effective curvature of the lipids (characterized by $\overline{c}_P$).

9.3. Dependence of protein insertion or conformational change on lipid intrinsic curvature

Fig. 23 shows the dependence on membrane lipid composition, X(*B*-lipid), of the change in chemical potential, $\Delta\Delta\mu_b$, relative to that in the background lipid, for membrane insertion and/or conformational change of various proteins. These are examples of membrane proteins for which a well defined dependence on lipid spontaneous curvature has been established. The background lipid, referred to as *A*-lipid, is a PC whose intrinsic curvature is small: di$C_{18:1c}$PC, $C_{16:0}C_{18:1c}$PC, or di$C_{16:1c}$PC. The lipid whose mole fraction, X(*B*-lipid), increases in Fig. 23 is either the corresponding PE, which has pronounced negative intrinsic curvature, or PCs with short saturated chains (or saturated lysoPC) that are expected to have marked positive intrinsic curvature. The *B*-lipids with negative intrinsic curvature (i.e., water-in-oil configuration) are: di$C_{18:1c}$PE, $C_{16:0}C_{18:1c}$PE, or di$C_{16:1c}$PE. The *B*-lipids with positive intrinsic curvature (i.e., oil-in-water configuration) are: di$C_{10:0}$PC, di$C_{14:0}$PC, or $C_{16:0}$lysoPC. See also Section 7.

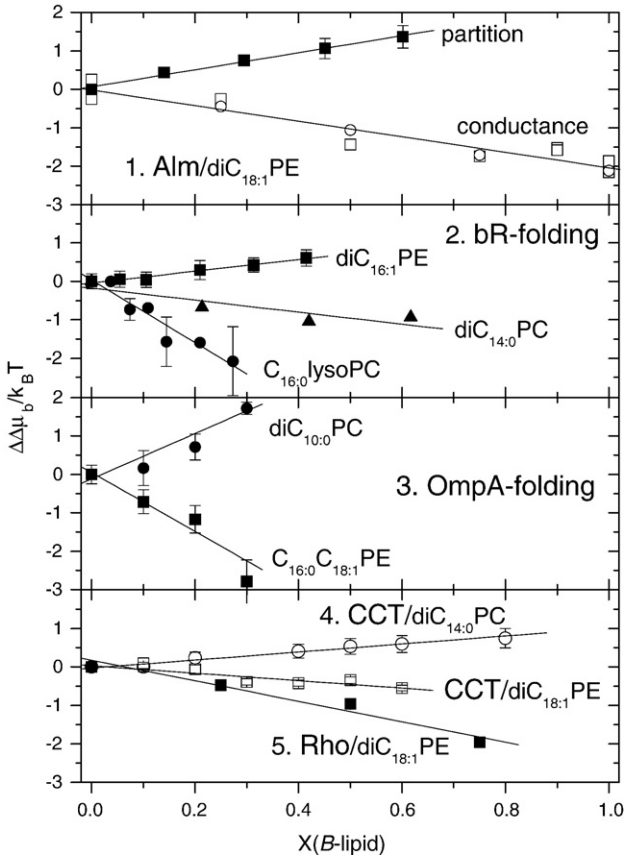

Fig. 23. Change in protein chemical potential, $\Delta\Delta\mu_b$, as a function of lipid composition, X(*B*-lipid), in binary mixtures of lipids *A* and *B* (see [132]). All values are referred to those of the *A*-lipid. From top to bottom: 1) Alm/diC$_{18:1c}$PE: alamethicin monomer partitioning into membranes (solid squares; [263]), and populations of the second (open squares) and third (open circles: scaled by 0.5×) channel conductance states [262]; *A*-lipid=diC$_{18:1c}$PC, *B*-lipid=diC$_{18:1c}$PE. 2) bR-folding: refolding yields of bacteriorhodopsin from SDS into membranes [275]; *A*-lipid=diC$_{16:1c}$PC; *B*-lipid=diC$_{16:1c}$PE (solid squares), diC$_{14:0}$PC (solid triangles) or C$_{16:0}$lysoPC (solid circles). 3) OmpA-folding: refolding yields of *E. coli* outer membrane protein A into membranes in the presence of urea [267]; *A*-lipid=C$_{16:0}$C$_{18:1c}$PC; *B*-lipid=diC$_{10:0}$PC (solid circles), or C$_{16:0}$C$_{18:1c}$PE (solid squares); all mixtures contained 7.5 mol% C$_{16:0}$C$_{18:1c}$PG. 4) CCT: CTP:phosphocholine cytidylyltransferase activation by binding to membranes [265]; *A*-lipid=diC$_{18:1c}$PC; *B*-lipid=diC$_{14:0}$PC (open circles), or diC$_{18:1c}$PE (open squares). 5) Rho/diC$_{18:1c}$PE: light-activated meta-II/meta-I state equilibrium in bovine rhodopsin (solid squares; [266]); *A*-lipid=diC$_{18:1c}$PC; *B*-lipid=diC$_{18:1c}$PE.

The equilibria for which the changes in chemical potential are given in Fig. 23, range from simple partitioning of the protein into the membrane (with or without protein activation), via a change in conformation or degree of oligomerisation of the protein in the membrane, to refolding of the protein on incorporation in the membrane. These comprise (see [132]): 1. The partitioning of monomeric alamethicin (Alm) into diC$_{18:1c}$PC-diC$_{18:1c}$PE membranes (solid squares) [263]. The changes in relative populations of ion conductance levels by incorporation of one or more monomers into alamethicin channel assemblies in diC$_{18:1c}$PC-diC$_{18:1c}$PE membranes (open squares and circles) [262]. 2. The yield of refolded bacteriorhodopsin (bR) on diluting SDS-solubilised protein into vesicles of diC$_{16:1c}$PC mixed with diC$_{16:1c}$PE (solid squares), diC$_{14:0}$PC (solid triangles), or C$_{16:0}$lysoPC (solid circles) [275]. 3. The refolding yields of *E. coli* outer membrane protein A (OmpA) in vesicles of C$_{16:0}$C$_{18:1c}$PC in the presence of various concentrations of aqueous urea, for mixtures with C$_{16:0}$C$_{18:1c}$PE (solid squares) or diC$_{10:0}$PC (solid circles) [267]. 4. The association of CTP:phosphocholine cytidylyltransferase (CCT) with membranes of diC$_{18:1c}$PC that is deduced from enzyme activation, for mixtures with diC$_{18:1c}$PE (open squares) or diC$_{14:0}$PC (open circles) [265]. 5. The light-driven conformational change from the meta-I state to the meta-II state that activates rhodopsin (Rho) in diC$_{18:1c}$PC–diC$_{18:1c}$PE membranes (solid squares) [266].

For each case in Fig. 23, the change in chemical potential is approximately linear in mole fraction of the *B*-lipid, which has non-vanishing intrinsic curvature. This is expected because the intrinsic curvature of these binary lipid mixtures depends approximately linearly on mole fraction of the components, according to Eq. (22) (see Section 7). For folding and membrane insertion of bR and of OmpA, and for activation of CCT, the change in chemical potential is of opposite sign (and $\partial\Delta\Delta\mu_b/\partial X$ is of opposite gradient) for lipids with opposite intrinsic curvatures. This clearly indicates that lipid intrinsic curvature is directly involved, in each case. For partitioning of Alm monomers [263], and for the populations of Alm channel states [262], mixtures of *N*-methyl diC$_{18:1c}$PE with diC$_{18:1c}$PC gave results similar to those from mixtures of diC$_{18:1c}$PE with diC$_{18:1c}$PC that have the same value of c_o but different lipid mole fractions. This shows that intrinsic curvature, and not chemical composition, is the controlling factor, also in these cases.

Fig. 24 shows the dependence on lipid intrinsic curvature, c_o, of the change in chemical potential, $\Delta\Delta\mu_b$, for the various proteins in the PC–PE mixtures that are presented in Fig. 23. The values of intrinsic curvature are obtained from fitting to X-ray data for H_{II} phases of diC$_{18:1c}$PE–diC$_{18:1c}$PC mixtures [199] by using linear additivity of component molecular volumes and molecular areas in Eq. (21) of Section 7 [197,198]. This procedure provides greater precision than the simple linear dependence on mole fraction (i.e., Eq. (22)) that is given in Fig. 23 [132]. In each case, an approximately linear dependence is found in accordance with the predictions of Eq. (39) or (46). From the gradients of the linear regressions in Fig. 24, values of $-N_L A_L \overline{c}_P \equiv a_{1,P} + 2a_{2,p}\delta \approx -0.75 \pm 0.11$ and $+0.35 \pm 0.10$ nm are obtained for membrane insertion of Alm and CCT, respectively. Similarly, in the case of conformational changes, values obtained for the difference, $-\Delta(N_L A_L \overline{c}_P) \equiv \Delta\left(a_{1,P} + 2a_{2,p}\delta\right)$, are: $+0.60 \pm 0.12$ and $+0.83 \pm 0.12$ nm for channel transitions of Alm, and M-I to M-II transitions of rhodopsin, respectively; and $+2.9 \pm 0.8$ and -0.55 ± 0.24 nm for the folding and membrane incorporation of OmpA and bR, respectively. An average value of $k_c/k_BT = 9.86 \pm 0.59$ for the mean curvature modulus of a monolayer, which is obtained from recent measurements on diC$_{18:1c}$PC and diC$_{18:1c}$PE (see [276]), is used in these calculations. It is notable that a considerably larger difference, $-\Delta(N_L A_L \overline{c}_P) \equiv \Delta\left(a_{1,P} + 2a_{2,p}\delta\right) \approx -4.4 \pm 0.3$ nm, is obtained for the conformational change associated with opening of the mechanosensitive ion channel, MscL [132,277], than for conformational changes of the proteins in Fig. 23. This is almost certainly because this involves the opening of a large

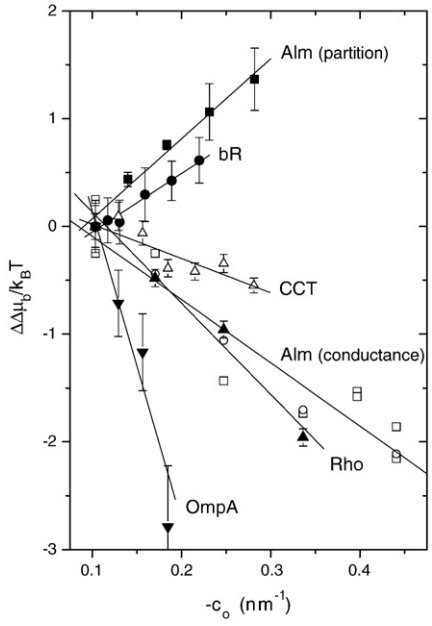

Fig. 24. Change in protein chemical potential, $\Delta\Delta\mu_b$, as a function of lipid intrinsic curvature, c_o, in binary mixtures of unsaturated PEs ($diC_{18:1c}$PE, $C_{16:0}C_{18:1c}$PE, or $diC_{16:1c}$PE) with the corresponding unsaturated PC (see [132]). All values are referred to those in PC. Intrinsic curvatures are those for $diC_{18:1c}$PE–$diC_{18:1c}$PC mixtures [199,197]. Alm: alamethicin monomer partitioning into membranes (solid squares; [263]), and populations of the channel conductance states (open squares and circles; [262]); bR: refolding yields of bacteriorhodopsin from SDS into membranes (solid circles; [275]); OmpA: refolding yields of *E. coli* outer membrane protein A into membranes in the presence of urea (inverted solid triangles; [267]); CCT: CTP:phosphocholine cytidylyltransferase activation by binding to membranes (open triangles; [265]); Rho: light-activated meta-II/meta-I state equilibrium in rhodopsin (solid triangles; [266]).

pore (~3 nm diameter) that is associated with the unusually high conductance of the MscL channel. For comparison, an approximate estimate for the KvAP K^+-channel, suggests a change of $-\Delta(N_L A_L \overline{c}_P) \equiv \Delta\left(a_{1,P} + 2a_{2,p}\delta\right) \approx 1.1 \pm 0.1$ nm occurs on opening of this voltage-gated channel [132,278].

By using the number, N_b, of first-shell lipids directly contacting the protein (see Table 1 and Section 2.1) as estimates for N_L, and average molecular areas of $diC_{18:1c}$ lipids, $A_L \approx 0.58-0.72$ nm^2 [197,279], it is possible to obtain values for the effective mean curvature, $\overline{c}_P$, of the lipids associated with an inserted protein, or for the change, $\Delta\overline{c}_P$, in effective curvature of the protein-associated lipids that accompanies a conformational change in the protein [see 132]. These values, which are listed in Table 8, represent the adaptation of the lipid curvature averaged over the first shell of perimeter lipids. If the perturbation of the lipid curvature by the protein extends beyond the first shell, then the values that are quoted will represent an upper limit for the first-shell average. EPR experiments with spin-labelled lipids, however, suggest that the lipid perturbation does not extend greatly beyond the first boundary shell [280,21].

A notable feature in Table 8 is that the largest absolute value (with the exception of MscL) is for the transmembrane insertion and folding of the β-barrel protein OmpA. The membrane association of CCT, on the other hand, is peripheral and causes less perturbation of the lipid. Interestingly, the membrane insertion of alamethicin monomers implies a relatively large value of shape asymmetry, but of the opposite sign to that of OmpA. The negative sign of $\overline{c}_P$ for OmpA is consistent with the hour-glass shape that is revealed by the 3-D structure [188,267]. The rather modest shape asymmetry revealed by bR is attributable to the fact that the transmembrane helices are relatively straight and untilted [281], as compared with those of Rho [282], for which the change in shape asymmetry at the M-I to M-II transition is comparable in absolute value to that on folding and membrane insertion of the entire bR protein. Overall, the values in Table 8 can be compared with the intrinsic curvatures determined for pure hydrated lipid systems from the application of dual solvent stress to H_{II} phases [199,200]. For lipids with negative intrinsic curvature, these vary from $c_o = -0.07$ nm^{-1} to -3.09 nm^{-1} for $diC_{18:1c}$PC and dioleoyl glycerol, respectively [197,198].

Unlike the application of Eq. (39) to determine the effective lipid curvature, application of Eq. (46) does not allow separate determination of the parameters $a_{1,P}$ and $a_{2,P}$ that govern the transmembrane shape of the protein. However, the composite quantity $a_{1,P}\delta + 2a_{2,P}\delta^2$ can be derived and provides an upper estimate for the magnitude of the effective difference, $A_P(\delta) - A_P(0) = a_{1,P}\delta + a_{2,P}\delta^2$, in cross-sectional area of the protein between the membrane mid-plane and the neutral plane (see Eq. (42)). This requires knowledge of δ, the position of the neutral surface, which is expected to lie close to the polar–apolar interface [283]. For the inverse bicontinuous cubic phase of a monolein, $diC_{18:1c}$PC and $diC_{18:1c}$PE mixture, $\delta = 1.29 \pm 0.005$ nm [284], and half the hydrocarbon thickness of a $diC_{18:1c}$PC bilayer is $l_C = 1.36 \pm 0.01$ nm [279]. Thus a reasonable estimate for lipids with $C_{18:1c}$ chains is $\delta = 1.35 \pm 0.1$ nm. Values of $a_{1,P}\delta + 2a_{1,P}\delta^2$ calculated in this way are also listed in Table 8. Interestingly, again with the exception of MscL, the absolute values for the shape changes are mostly in the region of 1 nm^2. It is tempting to assume that this might represent the general order of magnitude to be expected for area changes of embedded membrane proteins, other than those that undergo very large-scale conformational changes such as MscL.

Table 8
Changes in curvature, $\overline{c}_P$, of associated phospholipids, or in cross-sectional shape, $A_P(\delta)$-$A_P(0)$, on conformational changes, folding, or insertion of peptides or proteins in membranes[a] (see [132])

Protein/peptide[b]	$\overline{c}_P$ (nm^{-1})	$A_P(\delta) - A_P(0)$ (nm^2)
ALM monomer	+0.11±0.04	−1.0±0.2
isolated in channel	+0.07±0.06	+0.8±0.2
CCT	−0.035±0.015	+0.47±0.16
Rho	−0.06±0.02	+1.12±0.25
MscL	+0.24±0.04	−5.95±0.90
KvAP		1.50±0.30
OmpA	−0.21±0.06	
bR	+0.08±0.01	

[a] Deduced from dependence on intrinsic curvature of host lipids. $A_P(\delta) - A_P(0)$ is the difference in transverse cross-sectional area of the protein between the membrane mid-plane and the neutral plane of one bilayer half. The values given, viz., $(a_{1,P}+2a_{2,P}\delta)\times\delta$, are an upper estimate for this quantity.

[b] Alm, alamethicin; CCT, CTP:phosphocholine cytidylyltransferase; Rho, rhodopsin; MscL, mechanosensitive channel of large conductance; KvAP, voltage-dependent K^+-channel; OmpA, *E. coli* outer membrane protein A; bR, bacteriorhodopsin.

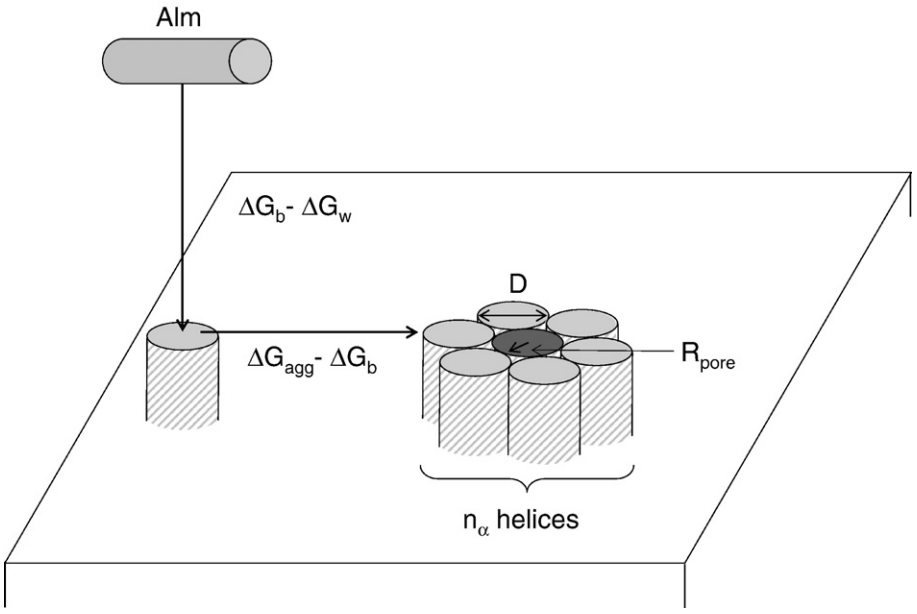

Fig. 25. Equilibria of alamethicin monomers in channel formation: partition into the membrane from the aqueous phase with free energy of transfer $\Delta G_b - \Delta G_w$, and incorporation into the channel within the membrane phase with transfer free energy $\Delta G_{agg} - \Delta G_b$. After ref. [132].

9.4. Alamethicin channels

Because of the success of interpreting the results for $diC_{18:1c}$PC–$diC_{18:1c}$PE lipid mixtures in terms of intrinsic curvature, and because there are two independent sets of data available for Alm, it is worthwhile to consider how these might be interpreted further in terms of the channel configuration. It is significant that the relative populations of channel conductance states have the opposite dependence on lipid intrinsic curvature to that of partitioning of Alm into the membrane (see Fig. 24). Changes in conductance must therefore occur via molecular rearrangements within the membrane, and not via partitioning of Alm from the aqueous phase.

The effective lipid curvature that is imposed by the Alm channel can be estimated by using the monomer reference state from the partitioning results (see Fig. 25). Referred to Alm in water, the free energy of an Alm monomer in the channel is equal to the free energy relative to a free monomer in the membrane, plus that of a free monomer in the membrane relative to that in water. This yields a value of $-N_L A_L \overline{c}_P \approx -(0.16 \pm 0.11)$ nm for a monomer in the channel assembly (see [132]). For a regular polygonal arrangement of $n_\alpha = 6$ transmembrane helices, the number of perimeter lipids per monomer from Eq. (3) is $N_L^{(1)} = \pi(D_\alpha/d_{ch} + 1)/n_\alpha + D_\alpha/d_{ch} \approx 3.7$ (see Section 2.1). Thus, the effective lipid curvature induced by the Alm channel is $\overline{c}_P \approx +0.07 \pm 0.05$ nm^{-1}. This relatively small value is consistent with a symmetrical arrangement of helices that are slightly bent.

From the data in Fig. 24 [262], the free energy of the ith conductance state, relative to the 1st state, depends linearly on the lipid intrinsic curvature with gradients of $+5.9 \pm 0.8\, k_BT \times$ nm and $+13.0 \pm 0.9\ k_BT \times$ nm for $i = 2$ and for $i = 3$ (data scaled by $0.5\times$ in Fig. 24), respectively. Therefore, it follows from Eqs. (39) and (46) that the ratio of the differences in $a_{1,P} + 2a_{2,P}\delta$, or in the products $N_L \overline{c}_P$ for the channel-associated lipids, in the two conductance states is $\sim 2.2 \pm 0.2$. This is consistent with conductance levels $i = 2$ and $i = 3$ being derived from level $i = 1$ by the incorporation of one and two monomers, respectively, in the channel assembly. An upper estimate for the change in cross-sectional area of the channel at the neutral surface, relative to that at the bilayer mid-plane, is $\Delta(a_{1,P} + 2\delta a_{2,P}) \times \delta \approx 0.8 \pm 0.2$ and 1.8 ± 0.3 nm^2 for the $i = 2$ and $i = 3$ conductance levels, respectively. This is comparable to the change in cross-sectional area of the internal pore ($R_{pore} = D_\alpha[\mathrm{cosec}(\pi/n_\alpha) - 1]/2$) on adding one or two monomers, respectively, to a regular hexagonal ($n_\alpha = 6$) arrangement of transmembrane helices (cf. [49]).

10. Conclusion

This is a wide ranging review that attempts to connect biophysical studies of the protein–lipid interface, and of curvature elasticity and the polymorphic potential of lipid assemblies, with those on the functional properties of membrane-embedded or surface-associated proteins. Both short-range molecular details and long-range cooperative properties of the lipid membrane are thus considered. The approach given is mostly thermodynamic, despite the fact that lipid membranes are dynamic at the molecular, mesoscopic and liquid-crystalline levels. Lipid dynamics can profoundly influence the function of membrane proteins, not least in dynamically differentiated and spatially separated in-plane membrane domains. A reminder should be given here that these further essential aspects have been only little touched upon.

References

[1] E. Pebay-Peyroula, C. Dahout-Gonzalez, R. Kahn, V. Trézéguet, G.J.M. Lauquin, G. Brandolin, Structure of mitochondrial ADP/ATP carrier in complex with carboxyatractyloside, Nature 426 (2003) 39–44.

[2] T. Páli, D. Bashtovyy, D. Marsh, Stoichiometry of lipid interaction with transmembrane proteins, deduced from the 3-D structures, Protein Sci. 15 (2006) 1153–1161.
[3] D. Marsh, A. Watts, Diffusible spin labels used to study lipid–protein interactions with rhodopsin and bacteriorhodopsin, Methods Enzymol. 88 (1982) 762–772.
[4] D. Marsh, A. Watts, R.D. Pates, R. Uhl, P.F. Knowles, M. Esmann, ESR spin label studies of lipid–protein interactions in membranes, Biophys. J. 37 (1982) 265–274.
[5] D. Marsh, Spin label answers to lipid–protein interactions, Trends Biochem. Sci. 8 (1983) 330–333.
[6] D. Marsh, Selectivity of lipid–protein interactions, J. Bioenerg. Biomembranes 19 (1987) 677–689.
[7] D. Marsh, G.L. Powell, Properties of cardiolipin and functional implications for cytochrome oxidase activity, Bioelectrochem. Bioenerg. 20 (1988) 73–82.
[8] D. Marsh, Lipid–protein interactions in membranes, FEBS Lett. 268 (1990) 371–375.
[9] P.F. Knowles, D. Marsh, Magnetic resonance of membranes, Biochem. J. 274 (1991) 625–641.
[10] D. Marsh, Role of lipids in membrane structures, Curr. Opin. Struct. Biol. 2 (1992) 497–502.
[11] D. Marsh, Lipid–protein interactions and heterogeneous lipid distribution in membranes, Mol. Membr. Biol. 12 (1995) 59–64.
[12] D. Marsh, Peptide models for membrane channels, Biochem. J. 315 (1996) 345–361.
[13] D. Marsh, Magnetic resonance of lipids and proteins in membranes, Curr. Opin. Colloid Interface Sci. 2 (1997) 4–14.
[14] D. Marsh, L.I. Horváth, Structure, dynamics and composition of the lipid–protein interface. Perspectives from spin-labelling, Biochim. Biophys. Acta 1376 (1998) 267–296.
[15] D. Marsh, L.I. Horváth, M.J. Swamy, S. Mantripragada, J.H. Kleinschmidt, Interaction of membrane-spanning proteins with peripheral and lipid-anchored membrane proteins. Perspectives from protein–lipid interactions, Mol. Membr. Biol. 19 (2002) 247–255.
[16] D. Marsh, T. Páli, The protein–lipid interface: perspectives from magnetic resonance and crystal structures, Biochim. Biophys. Acta 1666 (2004) 118–141.
[17] M. Esmann, D. Marsh, Lipid–protein interactions with the Na,K-ATPase, Chem. Phys. Lipids 141 (2006) 94–104.
[18] E. London, G.W. Feigenson, Fluorescence quenching in model membranes. 2. Determination of the local lipid environment of the calcium adenosine triphosphatase from sarcoplasmic reticulum, Biochemistry 20 (1981) 1939–1948.
[19] J.M. East, A.G. Lee, Lipid selectivity of the calcium and magnesium ion dependent adenosinetriphosphatase, studied with fluorescence quenching by a brominated phospholipid, Biochemistry 21 (1982) 4144–4151.
[20] A.G. Lee, Lipid–protein interactions in biological membranes: a structural perspective, Biochim. Biophys. Acta 1612 (2003) 1–40.
[21] P.F. Knowles, A. Watts, D. Marsh, Spin label studies of lipid immobilization in dimyristoylphosphatidylcholine-substituted cytochrome oxidase, Biochemistry 18 (1979) 4480–4487.
[22] J.H. Kleinschmidt, G.L. Powell, D. Marsh, Cytochrome *c*-induced increase of motionally restricted lipid in reconstituted cytochrome *c* oxidase membranes, revealed by spin-label ESR spectroscopy, Biochemistry 37 (1998) 11579–11585.
[23] J.F. Ellena, M.A. Blazing, M.G. McNamee, Lipid–protein interactions in reconstituted membranes containing acetylcholine receptor, Biochemistry 22 (1983) 5523–5535.
[24] S. Mantripragada, L.I. Horváth, H.R. Arias, G. Schwarzmann, K. Sandhoff, F.J. Barrantes, D. Marsh, Lipid–protein interactions and effect of local anesthetics in acetylcholine receptor-rich membranes from *Torpedo marmorata* electric organ, Biochemistry 42 (2003) 9167–9175.
[25] G.L. Powell, C.-A. Yu, D. Marsh, Stoichiometry and selectivity of lipid–protein interactions with bovine mitochondrial cytochrome *c* reductase, (in press).
[26] J.R. Brotherus, O.H. Griffith, M.O. Brotherus, P.C. Jost, J.R. Silvius, L.E. Hokin, Lipid–protein multiple binding equilibria in membranes, Biochemistry 20 (1981) 5261–5267.
[27] M. Esmann, A. Watts, D. Marsh, Spin-label studies of lipid–protein interactions in (Na^+,K^+)-ATPase membranes from rectal glands of *Squalus acanthias*, Biochemistry 24 (1985) 1386–1393.
[28] M. Esmann, K. Hideg, D. Marsh, A revised boundary lipid count for Na, K-ATPase from *Squalus acanthias*, in: J.C. Skou, J.G. Norby, A.B. Maunsbach, M. Esmann (Eds.), The Na^+,K^+-Pump, Part A: Molecular Aspects. Progress in Clinical and Biological Research, Vol. 268A, Alan Liss, New York, 1988, pp. 189–196.
[29] J.R. Silvius, D.A. McMillen, N.D. Saley, P.C. Jost, O.H. Griffith, Competition between cholesterol and phosphatidylcholine for the hydrophobic surface of sarcoplasmic reticulum Ca^{2+}-ATPase, Biochemistry 23 (1984) 538–547.
[30] D.D. Thomas, D.J. Bigelow, T.J. Squier, C. Hidalgo, Rotational dynamics of protein and boundary lipid in sarcoplasmic reticulum membrane, Biophys. J. 37 (1982) 217–225.
[31] A. Watts, I.D. Volotovski, D. Marsh, Rhodopsin–lipid associations in bovine rod outer segment membranes. Identification of immobilized lipid by spin labels, Biochemistry 18 (1979) 5006–5013.
[32] N.J.P. Ryba, L.I. Horváth, A. Watts, D. Marsh, Molecular exchange at the lipid–rhodopsin interface: spin-label electron spin resonance studies of rhodopsin–dimyristoyl phosphatidylcholine recombinants, Biochemistry 26 (1987) 3234–3240.
[33] R.D. Pates, A. Watts, R. Uhl, D. Marsh, Lipid–protein interactions in frog rod outer segment disc membranes. Characterization by spin labels, Biochim. Biophys. Acta 814 (1985) 389–397.
[34] L.I. Horváth, M. Drees, K. Beyer, M. Klingenberg, D. Marsh, Lipid–protein interactions in ADP–ATP carrier/egg phosphatidylcholine recombinants studied by spin-label ESR spectroscopy, Biochemistry 29 (1990) 10664–10669.
[35] P.J. Brophy, L.I. Horváth, D. Marsh, Stoichiometry and specificity of lipid–protein interaction with myelin proteolipid protein studied by spin-label electron spin resonance, Biochemistry 23 (1984) 860–865.
[36] T. Páli, M.E. Finbow, A. Holzenburg, J.B.C. Findlay, D. Marsh, Lipid–protein interactions and assembly of the 16-kDa channel polypeptide from *Nephrops norvegicus*. Studies with spin-label electron spin resonance spectroscopy and electron microscopy, Biochemistry 34 (1995) 9211–9218.
[37] S.J.C.J. Peelen, J.C. Sanders, M.A. Hemminga, D. Marsh, Stoichiometry, selectivity, and exchange dynamics of lipid–protein interaction with bacteriophage M13 coat protein studied by spin label electron spin resonance. Effects of protein secondary structure, Biochemistry 31 (1992) 2670–2677.
[38] R.L. Cornea, L.R. Jones, J.M. Autry, D.D. Thomas, Mutation and phosphorylation change the oligomeric structure of phospholamban in lipid bilayers, Biochemistry 36 (1997) 2960–2967.
[39] A. Arora, I.M. Williamson, A.G. Lee, D. Marsh, Lipid–protein interactions with cardiac phospholamban studied by spin-label electron spin resonance, Biochemistry 42 (2003) 5151–5158.
[40] C.B. Karim, C.G. Marquardt, J.D. Stamm, G. Barany, D.D. Thomas, Synthetic null-cysteine phospholamban analogue and the corresponding transmembrane domain inhibit the Ca-ATPase, Biochemistry 39 (2000) 10892–10897.
[41] Z. Kóta, T. Páli, D. Marsh, Orientation and lipid–peptide interactions of gramicidin A in lipid membranes: polarized ATR infrared spectroscopy and spin-label electron spin resonance, Biophys. J. 86 (2004) 1521–1531.
[42] L.I. Horváth, P.F. Knowles, P. Kovachev, J.B.C. Findlay, D. Marsh, A single-residue deletion alters the lipid selectivity of a K^+ channel-associated peptide in the β-conformation: spin label electron spin resonance studies, Biophys. J. 73 (1997) 2588–2594.
[43] L.I. Horváth, T. Heimburg, P. Kovachev, J.B.C. Findlay, K. Hideg, D. Marsh, Integration of a K^+ channel-associated peptide in a lipid bilayer: conformation, lipid–protein interactions, and rotational diffusion, Biochemistry 34 (1995) 3893–3898.
[44] C.J.A.M. Wolfs, L.I. Horváth, D. Marsh, A. Watts, M.A. Hemminga, Spin-label ESR of bacteriophage M13 coat protein in mixed lipid bilayers. Characterization of molecular selectivity of charged phospholipids for the bacteriophage coat protein in lipid bilayers, Biochemistry 28 (1989) 9995–10001.

[45] M. Ramakrishnan, C.L. Pocanschi, J.H. Kleinschmidt, D. Marsh, Association of spin-labelled lipids with β-barrel proteins from the outer membrane of *Escherichia coli*, Biochemistry 43 (2004) 11630–11636.
[46] V. Anbazhagan, J. Qu, J. H. Kleinschmidt, D. Marsh, Incorporation of outer membrane protein OmpG in lipid membranes. Protein–lipid interactions and β-barrel orientation, Biochemistry (in press).
[47] V. Anbazhagan, V. Narasimhan, J. H. Kleinschmidt, D. Marsh, Protein–lipid interactions with *E. coli* outer membrane protein FomA: spin-label EPR and polarised infrared spectroscopy, (in press).
[48] D. Marsh, Stoichiometry of lipid–protein interaction and integral membrane protein structure, Eur. Biophys. J. 26 (1997) 203–208.
[49] D. Marsh, Spin label ESR spectroscopy and FTIR spectroscopy for structural/dynamic measurements on ion channels, Methods Enzymol. 294 (1999) 59–92.
[50] N.J.P. Ryba, M.A. Hoon, J.B.C. Findlay, H.R. Saibil, J.R. Wilkinson, T. Heimburg, D. Marsh, Rhodopsin mobility, structure, and lipid–protein interaction in squid photoreceptor membranes, Biochemistry 32 (1993) 3298–3305.
[51] J. Pérez-Gil, C. Casals, D. Marsh, Interactions of hydrophobic lung surfactant proteins SP-B and SP-C with dipalmitoylphosphatidylcholine and dipalmitoylphosphatidylglycerol bilayers studied by electron spin resonance spectroscopy, Biochemistry 34 (1995) 3964–3971.
[52] M.R.R. de Planque, D.V. Greathouse, R.E. Koeppe II, H. Schäfer, D. Marsh, J.A. Killian, Influence of lipid/peptide hydrophobic mismatch on the thickness of diacylphosphatidylcholine bilayers. A ^{2}H NMR and ESR study using designed transmembrane α-helical peptides and gramicidin A, Biochemistry 37 (1998) 9333–9345.
[53] M.R.R. de Planque, J.A.W. Kruijtzer, R.M.J. Liskamp, D. Marsh, D.V. Greathouse, R.E. Koeppe II, B. De Kruijff, J.A. Killian, Different membrane anchoring positions of tryptophan and lysine in synthetic transmembrane α-helical peptides, J. Biol. Chem. 274 (1999) 20839–20846.
[54] D. Marsh, Infrared dichroism of twisted β-sheet barrels. The structure of *E. coli* outer membrane proteins, J. Mol. Biol. 297 (2000) 803–808.
[55] R.D.B. Fraser, T.P. MacRae, Conformation in Fibrous Proteins and Related Synthetic Peptides, Academic Press, New York, 1973.
[56] D. Marsh, The nature of the lipid–protein interface and the influence of protein structure on protein–lipid interactions, in: A. Watts (Ed.), New Comprehensive Biochemistry, Protein–Lipid Interactions, vol. 25, Elsevier, Amsterdam, 1993, pp. 41–66.
[57] H. Görrissen, D. Marsh, A. Rietveld, B. De Kruijff, Apocytochrome *c* binding to negatively charged lipid dispersions studied by spin-label electron spin resonance, Biochemistry 25 (1986) 2904–2910.
[58] A. Rietveld, G.A.E. Ponjee, P. Schiffers, W. Jordi, P.J.F.M. Van de Coolwijk, R.A. Demel, D. Marsh, B. De Kruijff, Investigations on the insertion of the mitochondrial precursor protein apocytochrome *c* into model membranes, Biochim. Biophys. Acta 818 (1985) 398–409.
[59] A. Rietveld, T.A. Berkhout, A. Roenhorst, D. Marsh, B. De Kruijff, Preferential association of apocytochrome *c* with negatively charged phospholipids in mixed model membranes, Biochim. Biophys. Acta 858 (1986) 38–46.
[60] W. Jordi, B. De Kruijff, D. Marsh, Specificity of the interaction of amino- and carboxy-terminal fragments of the mitochondrial precursor protein apocytochrome *c* with negatively charged phospholipids. A spin-label electron spin resonance study, Biochemistry 28 (1989) 8998–9005.
[61] M.M.E. Snel, D. Marsh, Membrane location of apocytochrome *c* and cytochrome *c* determined from lipid–protein spin exchange interactions by continuous wave saturation electron spin resonance, Biophys. J. 67 (1994) 737–745.
[62] M.B. Sankaram, P.J. Brophy, D. Marsh, Spin label ESR studies on the interaction of bovine spinal cord myelin basic protein with dimyristoyl-phosphatidylglycerol dispersions, Biochemistry 28 (1989) 9685–9691.
[63] M.B. Sankaram, P.J. Brophy, D. Marsh, Interaction of two complementary fragments of the bovine spinal cord myelin basic protein with phospholipid bilayers. An ESR spin label study, Biochemistry 28 (1989) 9692–9698.
[64] M.B. Sankaram, P.J. Brophy, D. Marsh, Selectivity of interaction of phospholipids with bovine spinal cord myelin basic protein studied by spin-label electron spin resonance, Biochemistry 28 (1989) 9699–9707.
[65] R.C.A. Keller, D. ten Berge, N. Nouwen, M.M.E. Snel, J. Tommassen, D. Marsh, B. De Kruijff, Mode of insertion of the signal sequence of a bacterial precursor protein into phospholipid bilayers as revealed by cysteine-based site-directed spectroscopy, Biochemistry 35 (1996) 3063–3071.
[66] R.C.A. Keller, M.M.E. Snel, B. De Kruijff, D. Marsh, SecA restricts, in a nucleotide-dependent manner, acyl chain mobility up to the center of a phospholipid bilayer, FEBS Lett. 358 (1995) 251–254.
[67] M.M.E. Snel, A.I.P.M. de Kroon, D. Marsh, Mitochondrial presequence inserts differently into membranes containing cardiolipin and phosphatidylglycerol, Biochemistry 34 (1995) 3605–3613.
[68] G.G. Montich, D. Marsh, Interaction of α-lactalbumin with phosphatidylglycerol. Influence of protein binding on the lipid phase transition and lipid acyl chain mobility, Biochemistry 34 (1995) 13139–13145.
[69] G.G. Montich, C. Montecucco, E. Papini, D. Marsh, Insertion of diphtheria toxin in lipid bilayers studied by spin label ESR, Biochemistry 34 (1995) 11561–11567.
[70] M. Ramakrishnan, V. Anbazhagan, T.V. Pratap, D. Marsh, M.J. Swamy, Membrane insertion and lipid–protein interactions of bovine seminal plasma protein PDC-109 investigated by spin-label electron spin resonance spectroscopy, Biophys. J. 81 (2001) 2215–2225.
[71] M.J. Swamy, D. Marsh, V. Anbazhagan, M. Ramakrishnan, Effect of cholesterol on the interaction of seminal plasma protein, PDC-109 with phosphatidylcholine membranes, FEBS Lett. 528 (2002) 230–234.
[72] M.B. Sankaram, P.J. Brophy, D. Marsh, Lipid–protein and protein–protein interactions in double recombinants of myelin proteolipid apoprotein and myelin basic protein with dimyristoylphosphatidylglycerol, Biochemistry 30 (1991) 5866–5873.
[73] J.E. Mahaney, J. Kleinschmidt, D. Marsh, D.D. Thomas, Effects of melittin on lipid–protein interactions in sarcoplasmic reticulum membranes, Biophys. J. 63 (1992) 1513–1522.
[74] M.J. Swamy, D. Marsh, Specific surface association of avidin with *N*-biotinylphosphatidylethanolamine membrane assemblies: effect on lipid phase behavior and acyl-chain dynamics, Biochemistry 40 (2001) 14869–14877.
[75] M.J. Swamy, D. Marsh, Spin-label studies on the anchoring and lipid–protein interactions of avidin with *N*-biotinylphosphatidylethanolamines in lipid bilayer membranes, Biochemistry 36 (1997) 7403–7407.
[76] M.J. Swamy, D. Marsh, Spin-label electron spin resonance studies on the dynamics of the different phases of *N*-biotinylphosphatidylethanolamines, Biochemistry 33 (1994) 11656–11663.
[77] M.J. Swamy, D. Marsh, Interaction of avidin with spin-labelled *N*-biotinyl phosphatidylethanolamine in a lipid membrane, FEBS Lett. 324 (1993) 56–58.
[78] M.J. Swamy, L.I. Horváth, P.J. Brophy, D. Marsh, Interactions between lipid-anchored and transmembrane proteins. Spin-label ESR studies on avidin-biotinyl phosphatidylethanolamine in membrane recombinants with myelin proteolipid protein, Biochemistry 38 (1999) 16333–16339.
[79] M. Ramakrishnan, P.H. Jensen, D. Marsh, α-synuclein association with phosphatidylglycerol probed by lipid spin labels, Biochemistry 42 (2003) 12919–12926.
[80] M. Ramakrishnan, P.H. Jensen, D. Marsh, Association of α-synuclein and mutants with lipid membranes: spin-label ESR and polarized IR, Biochemistry 45 (2006) 3386–3395.
[81] J.H. Kleinschmidt, D. Marsh, Spin-label electron spin resonance studies on the interactions of lysine peptides with phospholipid membranes, Biophys. J. 73 (1997) 2546–2555.
[82] J.H. Kleinschmidt, J.E. Mahaney, D.D. Thomas, D. Marsh, Interaction of bee venom melittin with zwitterionic and negatively charged phospholipid bilayers: a spin-label electron spin resonance study, Biophys. J. 72 (1997) 767–778.
[83] M.J. Swamy, D. Marsh, Spin-label electron paramagnetic resonance studies on the interaction of avidin with dimyristoyl-phosphatidylglycerol membranes, Biochim. Biophys. Acta 1513 (2001) 122–130.
[84] R. Bartucci, M. Pantusa, D. Marsh, L. Sportelli, Interaction of human serum albumin with membranes containing polymer-grafted lipids: spin-label ESR studies in the mushroom and brush regimes, Biochim. Biophys. Acta 1564 (2002) 237–242.

[85] F. De Simone, R. Guzzi, L. Sportelli, D. Marsh, R. Bartucci, Electron spin-echo studies of spin-labelled lipid membranes and free fatty acids interacting with human serum albumin, Biochim. Biophys. Acta 1768 (2007) 1541–1549.
[86] D. Cheneval, E. Carafoli, G.L. Powell, D. Marsh, A spin-label electron spin resonance study of the binding of mitochondrial creatine kinase to cardiolipin, Eur. J. Biochem. 186 (1989) 415–419.
[87] M.B. Sankaram, B. De Kruijff, D. Marsh, Selectivity of interaction of spin-labelled lipids with peripheral proteins bound to dimyristoylphosphatidylglycerol bilayers, as determined by ESR spectroscopy, Biochim. Biophys. Acta 986 (1989) 315–320.
[88] M.B. Sankaram, P.J. Brophy, W. Jordi, D. Marsh, Fatty acid pH titration and the selectivity of interaction with extrinsic proteins in dimyristoylphosphatidylglycerol dispersions. Spin label ESR studies, Biochim. Biophys. Acta 1021 (1990) 63–69.
[89] T. Heimburg, D. Marsh, Protein surface-distribution and protein–protein interactions in the binding of peripheral proteins to charged lipid membranes, Biophys. J. 68 (1995) 536–546.
[90] T. Heimburg, B. Angerstein, D. Marsh, Binding of peripheral proteins to mixed lipid membranes: effect of lipid demixing upon binding, Biophys. J. 76 (1999) 2575–2586.
[91] L.I. Horváth, P.J. Brophy, D. Marsh, Influence of polar residue deletions on lipid–protein interactions with the myelin proteolipid protein. Spin-label ESR studies with DM-20/lipid recombinants, Biochemistry 29 (1990) 2635–2638.
[92] A. Arora, M. Esmann, D. Marsh, Selectivity of lipid–protein interactions with trypsinized Na,K-ATPase studied by spin-label EPR, Biochim. Biophys. Acta 1371 (1998) 163–167.
[93] K.A. Dalton, J.M. East, S. Mall, S. Oliver, A.P. Starling, A.G. Lee, Interaction of phosphatidic acid and phosphatidylserine with the Ca^{2+}-ATPase of sarcoplasmic reticulum and the mechanism of inhibition, Biochem. J. 329 (1998) 637–646.
[94] R.J. Froud, C.R.A. Earl, J.M. East, A.G. Lee, Effects of lipid fatty acyl chain structure on the activity of the (Ca^{2+} + Mg^{2+})-ATPase, Biochim. Biophys. Acta 860 (1986) 354–360.
[95] P.F. Knowles, A. Watts, D. Marsh, Spin label studies of headgroup specificity in the interaction of phospholipids with yeast cytochrome oxidase, Biochemistry 20 (1981) 5888–5894.
[96] D.E. Raines, K.W. Miller, The role of charge in lipid selectivity for the nicotinic acetylcholine receptor, Biophys. J. 64 (1993) 632–641.
[97] K.P. Datema, C.J.A.M. Wolfs, D. Marsh, A. Watts, M.A. Hemminga, Spin-label electron spin resonance study of bacteriophage M13 coat protein incorporation into mixed lipid bilayers, Biochemistry 26 (1987) 7571–7574.
[98] A. Hubert, P.J.F. Henderson, D. Marsh, Lipid–protein interactions in *Escherichia coli* membranes overexpressing the sugar-H^+ symporter, GalP. EPR of spin-labelled lipids, Biochim. Biophys. Acta 1611 (2003) 243–248.
[99] A.H. O'Keeffe, J.M. East, A.G. Lee, Selectivity in lipid binding to the bacterial outer membrane protein OmpF, Biophys. J. 79 (2000) 2066–2074.
[100] S.J. Alvis, I.M. Williamson, J.M. East, A.G. Lee, Interactions of anionic phospholipids and phosphatidylethanolamine with the potassium channel KcsA, Biophys. J. 85 (2003) 3828–3838.
[101] D. Marsh, F.J. Barrantes, Immobilized lipid in acetylcholine receptor-rich membranes from *Torpedo Marmorata*, Proc. Natl. Acad. Sci. U. S. A. 75 (1978) 4329–4333.
[102] D. Marsh, A. Watts, F.J. Barrantes, Phospholipid chain immobilization and steroid rotational immobilization in acetylcholine receptor-rich membranes from *Torpedo marmorata*, Biochim. Biophys. Acta 645 (1981) 97–101.
[103] G. Schwarzmann, P. Hoffmann-Bleihauer, J. Schubert, K. Sandhoff, D. Marsh, Incorporation of ganglioside analogues into fibroblast cell membranes. A spin-label study, Biochemistry 22 (1983) 5041–5048.
[104] M. Esmann, D. Marsh, G. Schwarzmann, K. Sandhoff, Ganglioside-protein interactions: spin-label electron spin resonance studies with (Na^+, K^+)-ATPase membranes, Biochemistry 27 (1988) 2398–2403.
[105] G. Li, P.F. Knowles, D.J. Murphy, I. Nishida, D. Marsh, Spin-label ESR studies of lipid–protein interactions in thylakoid membranes, Biochemistry 28 (1989) 7446–7452.
[106] G. Li, L.I. Horváth, P.F. Knowles, D.J. Murphy, D. Marsh, Spin label saturation transfer ESR studies of protein–lipid interactions in photosystem II-enriched membranes, Biochim. Biophys. Acta 987 (1989) 187–192.
[107] G. Li, P.F. Knowles, D.J. Murphy, D. Marsh, Lipid–protein interactions in thylakoid membranes of chilling-resistant and -sensitive plants studied by spin label electron spin resonance spectroscopy, J. Biol. Chem. 265 (1990) 16867–16872.
[108] G.L. Powell, P.F. Knowles, D. Marsh, Spin label studies on the specificity of interaction of cardiolipin with beef heart cytochrome oxidase, Biochemistry 26 (1987) 8138–8145.
[109] M. Esmann, G.L. Powell, D. Marsh, Spin label studies on the selectivity of lipid–protein interaction of cardiolipin analogues with the Na^+/K^+-ATPase, Biochim. Biophys. Acta 941 (1988) 287–292.
[110] M. Esmann, K. Hideg, D. Marsh, Novel spin-labels for the study of lipid-protein interactions. Application to (Na^+,K^+)-ATPase membranes, Biochemistry 27 (1988) 3913–3917.
[111] G.L. Powell, P.F. Knowles, D. Marsh, Association of spin-labelled cardiolipin with dimyristoylphosphatidylcholine-substituted bovine heart cytochrome *c* oxidase. A generalized specificity increase rather than highly specific binding sites, Biochim. Biophys. Acta 816 (1985) 191–194.
[112] A. Watts, D. Marsh, P.F. Knowles, Lipid-substituted cytochrome oxidase: no absolute requirement of cardiolipin for activity, Biochem. Biophys. Res. Commun. 81 (1978) 397–402.
[113] T. Tsukihara, H. Aoyama, E. Yamashita, T. Tomizaki, H. Yamaguchi, K. Shinzawa-Itoh, R. Nakashima, R. Yaono, S. Yoshikawa, The whole structure of the 13-subunit oxidized cytochrome *c* oxidase at 2.8 Å, Science 272 (1996) 1136–1144.
[114] T. Tsukihara, K. Shimokata, Y. Katayama, H. Shimada, K. Muramoto, H. Aoyama, M. Mochizuki, K. Shinzawa-Itoh, A. Yamashita, M. Yao, Y. Ishimura, S. Yoshikawa, The low-spin heme of cytochrome *c* oxidase as the driving element of the proton-pumping process, Proc. Natl. Acad. Sci. U. S. A. 100 (2003) 15304–15309.
[115] D.A. Abramovitch, D. Marsh, G.L. Powell, Activation of beef heart cytochrome oxidase by cardiolipin and analogues of cardiolipin, Biochim. Biophys. Acta 1020 (1990) 34–42.
[116] A.M. Powl, J.M. East, A.G. Lee, Heterogeneity in the binding of lipid molecules to the surface of a membrane protein: hot spots for anionic lipids on the mechanosensitive channel of large conductance MscL and effects on conformation, Biochemistry 44 (2005) 5873–5883.
[117] P. Marius, S.J. Alvis, J.M. East, A.G. Lee, The interfacial lipid binding site on the potassium channel KcsA is specific for anionic phospholipids, Biophys. J. 89 (2005) 4081–4089.
[118] C. Tanford, The Hydrophobic Effect, Wiley, New York, 1980.
[119] L.I. Horváth, P.J. Brophy, D. Marsh, Influence of lipid headgroup on the specificity and exchange dynamics in lipid–protein interactions. A spin label study of myelin proteolipid apoprotein–phospholipid complexes, Biochemistry 27 (1988) 5296–5304.
[120] M. Esmann, D. Marsh, Spin-label studies on the origin of the specificity of lipid–protein interactions in Na^+,K^+-ATPase membranes from *Squalus acanthias*, Biochemistry 24 (1985) 3572–3578.
[121] J. Miyazaki, K. Hideg, D. Marsh, Interfacial ionization and partitioning of membrane-bound local anaesthetics, Biochim. Biophys. Acta 1103 (1992) 62–68.
[122] L.I. Horváth, H.R. Arias, H.O. Hankovszky, K. Hideg, F.J. Barrantes, D. Marsh, Association of spin-labeled local anaesthetics at the hydrophobic surface of acetylcholine receptor in native membranes from *Torpedo marmorata*, Biochemistry 29 (1990) 8707–8713.
[123] N. Dixon, T. Páli, S. Ball, M.A. Harrison, D. Marsh, J.B.C. Findlay, T.P. Kee, New biophysical probes for structure-activity analyses of vacuolar-H^+-ATPase enzymes, Org. Biomol. Chem. 1 (2003) 4361–4363.
[124] N. Dixon, T. Páli, T.P. Kee, D. Marsh, Spin-labelled vacuolar-ATPase inhibitors in lipid membranes, Biochim. Biophys. Acta 1665 (2004) 177–183.
[125] N. Dixon, T. Páli, T.P. Kee, S. Ball, M.A. Harrison, J.B.C. Findlay, J. Nyman, H.K. Väänänen, M.E. Finbow, D. Marsh, Interaction of spin-labelled inhibitors of the vacuolar H^+-ATPase with the transmembrane V_0-sector, Biophys. J. 94 (2008) 506–514.

[126] N.J.P. Ryba, D. Marsh, Protein rotational diffusion and lipid/protein interactions in recombinants of bovine rhodopsin with saturated diacylphosphatidylcholines of different chain lengths studied by conventional and saturation transfer electron spin resonance, Biochemistry 31 (1992) 7511–7518.
[127] N.J.P. Ryba, D. Marsh, R. Uhl, The kinetics and thermodynamics of bleaching of rhodopsin in dimyristoylphosphatidylcholine. Identification of meta-I, meta-II, and meta-III intermediates, Biophys. J. 64 (1993) 1801–1812.
[128] M. Caffrey, G.W. Feigenson, Fluorescence quenching in model membranes. 3. Relationship between calcium adenosinetriphosphatase enzyme activity and the affinity of the protein for phosphatidylcholines with different acyl chain characteristics, Biochemistry 20 (1981) 1949–1961.
[129] D.M. Small, The Physical Chemistry of Lipids. From Alkanes to Phospholipids, Plenum Press, New York and London, 1986.
[130] I. Pascher, M. Lundmark, P.-G. Nyholm, S. Sundell, Crystal structures of membrane lipids, Biochim. Biophys. Acta 1113 (1992) 339–373.
[131] D.C. Teller, T. Okada, C.A. Behnke, K. Palczewski, R.E. Stenkamp, Advances in determination of a high-resolution three-dimensional structure of rhodopsin, a model of G-protein-coupled receptors (GPCRs), Biochemistry 40 (2001) 7761–7772.
[132] D. Marsh, Lateral pressure profile, spontaneous curvature frustration, and the incorporation and conformation of proteins in membranes, Biophys. J. 93 (2007) 3884–3899.
[133] A. Watts, J. Davoust, D. Marsh, P.F. Devaux, Distinct states of lipid mobility in bovine rod outer segment membranes. Resolution of spin label results, Biochim. Biophys. Acta 643 (1981) 673–676.
[134] M.A. Lomize, A.L. Lomize, I. Pogozheva, H.I. Mosberg, OPM: orientations of proteins in membranes database, Bioinformatics 22 (2006) 623–625.
[135] P.V. Attwood, H. Gutfreund, The application of pressure relaxation to the study of the equilibrium between metarhodopsin I and II from bovine retinas, FEBS Lett. 119 (1980) 323–326.
[136] P.A. Baldwin, W.L. Hubbell, Effects of lipid environment on the light-induced conformational changes of rhodopsin. 2. Roles of lipid chain length, unsaturation, and phase state, Biochemistry 24 (1985) 2633–2639.
[137] L.I. Horváth, P.J. Brophy, D. Marsh, Microwave frequency dependence of ESR spectra from spin labels undergoing two-site exchange in myelin proteolipid membranes, J. Magn. Reson. B105 (1994) 120–128.
[138] D. Marsh, D. Kurad, V.A. Livshits, High-field electron spin resonance of spin labels in membranes, Chem. Phys. Lipids 116 (2002) 93–114.
[139] J.-H. Sachse, M.D. King, D. Marsh, ESR determination of lipid diffusion coefficients at low spin-label concentrations in biological membranes, using exchange broadening, exchange narrowing, and dipole–dipole interactions, J. Magn. Reson. 71 (1987) 385–404.
[140] M.D. King, J.-H. Sachse, D. Marsh, Unconstrained optimization method for interpreting the concentration and temperature dependence of the linewidths of interacting nitroxide spin labels. Application to the measurement of translational diffusion coefficients of spin-labeled phospholipids in membranes, J. Magn. Reson. 72 (1987) 257–267.
[141] L.I. Horváth, P.J. Brophy, D. Marsh, Exchange rates at the lipid–protein interface of myelin proteolipid protein studied by spin-label electron spin resonance, Biochemistry 27 (1988) 46–52.
[142] J.M. East, D. Melville, A.G. Lee, Exchange rates and numbers of annular lipids for the calcium and magnesium ion dependent adenosinetriphosphatase, Biochemistry 24 (1985) 2615–2623.
[143] T. Páli, M.E. Finbow, D. Marsh, Membrane assembly of the 16-kDa proteolipid channel from *Nephrops norvegicus* studied by relaxation enhancements in spin-label ESR. Biochemistry 38 (1999) 14311–14319.
[144] T. Páli, J.H. Kleinschmidt, G.L. Powell, D. Marsh, Nonlinear electron paramagnetic rsonance studies of the interaction of cytochrome *c* oxidase with spin-labeled lipids in gel-phase membranes, Biochemistry 39 (2000) 2355–2361.
[145] A. Arora, D. Marsh, Protein-induced vertical lipid dislocation in a model membrane system: spin-label relaxation studies on avidin-biotinylphosphatidylethanolamine interactions. Biophys. J. 75 (1998) 2915–2922.
[146] A. Arora, M. Esmann, D. Marsh, Microsecond motions of the lipids associated with trypsinized Na,K-ATPase membranes. Progressive saturation spin-label electron spin resonance studies, Biochemistry 38 (1999) 10084–10091.
[147] L.I. Horváth, P.J. Brophy, D. Marsh, Exchange rates at the lipid–protein interface of the myelin proteolipid protein determined by saturation transfer electron spin resonance and continuous wave saturation studies, Biophys. J. 64 (1993) 622–631.
[148] L.I. Horváth, P.J. Brophy, D. Marsh, Spin label saturation transfer EPR determinations of the stoichiometry and selectivity of lipid–protein interactions in the gel phase, Biochim. Biophys. Acta 1147 (1993) 277–280.
[149] P. Meier, J.-H. Sachse, P.J. Brophy, D. Marsh, G. Kothe, Integral membrane proteins significantly decrease the molecular motion in lipid bilayers: a deuteron NMR relaxation study of membranes containing myelin proteolipid apoprotein, Proc. Natl. Acad. Sci. U. S. A. 84 (1987) 3704–3708.
[150] M. Hayer-Hartl, P.J. Brophy, D. Marsh, A. Watts, Interaction of two complementary fragments of the bovine spinal cord myelin basic protein with phosphatidylglycerol bilayers, studied by ^{2}H and ^{31}P NMR spectroscopy, Biochemistry 32 (1993) 9709–9713.
[151] S.Y. Kang, H.S. Gutowsky, J.C. Hsung, R. Jacobs, T.E. King, D. Rice, E. Oldfield, Nuclear magnetic resonance investigation of the cytochrome oxidase-phospholipid interaction: A new model for boundary lipid, Biochemistry 18 (1979) 3257–3267.
[152] E. Oldfield, NMR of protein–lipid interactions in model and biological membrane systems, in: E.N. Martonosi (Ed.), Membranes and Transport, vol. 1, Plenum Press, New York, 1982, pp. 115–123.
[153] J. Seelig, A. Seelig, L. Tamm, Nuclear magnetic resonance and lipid–protein interactions, in: P.C. Jost, O.H. Griffith (Eds.), Lipid–Protein Interactions, vol. 2, John Wiley & Sons, New York, 1982, pp. 127–148.
[154] M. Bloom, I.C.P. Smith, Manifestations of lipid–protein interactions in deuterium NMR, in: A. Watts, J.J.H.H.M. de Pont (Eds.), Progress in Protein–Lipid Interactions, vol. 1, Elsevier, Amsterdam, 1985, pp. 61–88.
[155] A. Bienvenue, M. Bloom, J.H. Davis, P.F. Devaux, Evidence for protein-associated lipids from deuterium nuclear magnetic resonance studies of rhodopsin-dimyristoylphosphatidylcholine recombinants, J. Biol. Chem. 257 (1982) 3032–3038.
[156] D. Marsh, A. Watts, I.C.P. Smith, Dynamic structure and phase behaviour of dimyristoylphosphatidylethanolamine bilayers studied by deuterium nuclear magnetic resonance, Biochemistry 22 (1983) 3023–3026.
[157] K. Schorn, D. Marsh, Dynamic chain conformations in dimyristoyl glycerol-dimyristoyl phosphatidylcholine mixtures. ^{2}H-NMR studies, Biophys. J. 71 (1996) 3320–3329.
[158] R.D. Pates, D. Marsh, Lipid mobility and order in bovine rod outer segment disk membranes. A spin-label study of lipid-protein interactions, Biochemistry 26 (1987) 29–39.
[159] D. Marsh, T. Páli, Lipid conformation in crystalline bilayers and in crystals of transmembrane proteins, Chem. Phys. Lipids 141 (2006) 48–65.
[160] D. Marsh, Lipid-binding proteins: structure of the phospholipid ligands, Protein Sci. 12 (2003) 2109–2117.
[161] R.D. Kornberg, H.M. McConnell, Inside–outside transitions of phospholipids in vesicle membranes, Biochemistry 10 (1971) 1111–1120.
[162] B. De Kruijff, E.J.J. Van Zoelen, Effect of the phase transition on transbilayer movement of dimyristoyl phosphatidylcholine in unilamellar vesicles, Biochim. Biophys. Acta 511 (1978) 105.
[163] W.C. Wimley, T.E. Thompson, Exchange and flip-flop of dimyristoylphosphatidylcholine in liquid-crystalline, gel, and two-component, two-phase large unilamellar vesicles, Biochemistry 29 (1990) 1296–1303.
[164] M.A. Kol, A.I.P.M. de Kroon, J.A. Killian, B. De Kruijff, Transbilayer movement of phospholipids in biogenic membranes, Biochemistry 43 (2004) 2673–2681.
[165] M.A. Kol, A.I.P.M. de Kroon, D.T.S. Rijkers, J.A. Killian, B. De Kruijff, Membrane-spanning peptides induce phospholipid flop: a model for phospholipid translocation across the inner membrane of *E. coli*, Biochemistry 40 (2001) 10500–10506.
[166] A.T.M. van der Steen, W.A.C. de Jong, B. De Kruijff, L.L.M. van Deenen, Lipid dependence of glycophorin-induced transbilayer movement of lysophosphatidylcholine in large unilamellar vesicles, Biochim. Biophys. Acta 647 (1981) 63–72.
[167] M.A. Kol, A. van Dalen, A.I.P.M. de Kroon, B. De Kruijff, Translocation of phospholipids is facilitated by a subset of membrane-spanning proteins of the bacterial cytoplasmic membrane, J. Biol. Chem. 278 (2003) 24586–24593.

[168] M.A. Kol, A.N.C. van Laak, D.T.S. Rijkers, J.A. Killian, A.I.P.M. de Kroon, B. De Kruijff, Phospholipid flop induced by transmembrane peptides in model membranes is modulated by lipid composition, Biochemistry 43 (2003) 231–237.
[169] W. Helfrich, Out-of-plane fluctuations of lipid bilayers, Z. Naturforsch 30 (1975) 841–842.
[170] E.A. Evans, W. Rawicz, Entropy-driven tension and bending elasticity in condensed-fluid membranes, Phys. Rev. Lett. 64 (1990) 2094–2097.
[171] D. Marsh, Renormalization of the tension and area expansion modulus in fluid membranes, Biophys. J. 73 (1997) 865–869.
[172] F. Brochard, J.F. Lennon, Frequency spectrum of flicker phenomenon in erythrocytes, J. de Phys. 36 (1975) 1035–1047.
[173] H. Engelhardt, H.P. Duwe, E. Sackmann, Bilayer bending elasticity measured by Fourier analysis of thermally excited surface undulations of flaccid vesicles, J. Phys. Lett. 46 (1985) L395–L400.
[174] W. Helfrich, Steric interaction of fluid membranes in multilayer systems, Z. Naturforsch. 33a (1978) 305–315.
[175] E.A. Evans, V.A. Parsegian, Thermal-mechanical fluctuations enhance repulsion between bimolecular layers, Proc. Natl. Acad. Sci. U. S. A. 83 (1986) 7132–7136.
[176] E. Rommel, F. Noack, P. Meier, G. Kothe, Proton spin relaxation dispersion studies of phospholipid membranes, J. Phys. Chem. 92 (1988) 2981–2987.
[177] J. Stohrer, G. Gröbner, D. Reimer, K. Weisz, C. Mayer, G. Kothe, Collective lipid motions in bilayer membranes studied by transverse deuteron spin relaxation, J. Chem. Phys. 95 (1991) 672–678.
[178] E.A. Evans, R. Skalak, Mechanics and Thermodynamics of Biomembranes, CRC Press, Boca Raton, FL, 1980.
[179] G. Cevc, D. Marsh, Phospholipid Bilayers. Physical Principles and Models, Wiley-Interscience, New York, 1987.
[180] J.H. Kleinschmidt, L.K. Tamm, Secondary and tertiary structure formation of the β-barrel membrane protein OmpA is synchronized and depends on membrane thickness, J. Mol. Biol. 324 (2002) 319–330.
[181] C.L. Pocanschi, G.J. Patel, D. Marsh, J.H. Kleinschmidt, Curvature elasticity and refolding of OmpA in large unilamellar vesicles, Biophys. J. 91 (2006) L75–L77.
[182] C.L. Pocanschi, H.J. Apell, P. Puntervoll, B. Hogh, H.B. Jensen, W. Welte, J.H. Kleinschmidt, The major outer membrane protein of *Fusobacterium nucleatum* (FomA) folds and inserts into lipid bilayers via parallel folding pathways, J. Mol. Biol. 355 (2006) 548–561.
[183] M. Ramakrishnan, J. Qu, C.L. Pocanschi, J.H. Kleinschmidt, D. Marsh, Orientation of β-barrel proteins OmpA and FhuA in lipid membranes. Chainlength dependence from infrared dichroism, Biochemistry 44 (2005) 3515–3523.
[184] P.C.A. van der Wel, E. Strandberg, J.A. Killian, R.E. Koeppe II, Geometry and intrinsic tilt of a tryptophan-anchored transmembrane α-helix determined by ^{2}H NMR, Biophys. J. 83 (2002) 1479–1488.
[185] S. Özdirekcan, D.T.S. Rijkers, R.M.J. Liskamp, J.A. Killian, Influence of flanking residues on tilt and rotation angles of transmembrane peptides in lipid bilayers. A solid-state ^{2}H NMR study, Biochemistry 44 (2005) 1004–1012.
[186] D. Marsh, M. Jost, C. Peggion, C. Toniolo, Lipid chainlength dependence for incorporation of alamethicin in membranes: EPR studies on TOAC-spin labelled analogues, Biophys. J. 92 (2007) 4002–4011.
[187] D. Marsh, M. Jost, C. Peggion, C. Toniolo, TOAC spin labels in the backbone of alamethicin: EPR studies in lipid membranes, Biophys. J. 92 (2007) 473–481.
[188] D. Marsh, B. Shanmugavadivu, J.H. Kleinschmidt, Membrane elastic fluctuations and the insertion and tilt of β-barrel proteins, Biophys. J. 91 (2006) 227–232.
[189] D. Marsh, Lateral pressure in membranes, Biochim. Biophys. Acta 1286 (1996) 183–223.
[190] J.M. Seddon, G. Cevc, D. Marsh, Calorimetric studies of the gel–fluid (L_β-L_α) and lamellar-inverted hexagonal (L_α-H_{II}) phase transitions in dialkyl- and diacylphosphatidylethanolamines, Biochemistry 22 (1983) 1280–1289.
[191] J.M. Seddon, G. Cevc, R.D. Kaye, D. Marsh, X-ray diffraction study of the polymorphism of hydrated diacyl- and dialkylphosphatidylethanolamines, Biochemistry 23 (1984) 2634–2644.
[192] P.R. Cullis, B. De Kruijff, Lipid polymorphism and the functional roles of lipids in biological membranes, Biochim. Biophys. Acta 559 (1979) 399–420.
[193] D. Marsh, General features of phospholipid phase transitions, Chem. Phys. Lipids 57 (1991) 109–120.
[194] D. Marsh, Handbook of Lipid Bilayers, CRC Press, Boca Raton FL, 1990.
[195] J.N. Israelachvili, D.J. Mitchell, B.W. Ninham, Theory of self-assembly of hydrocarbon amphiphiles into micelles and bilayers, J. Chem. Soc. (Faraday II) 72 (1976) 1525–1568.
[196] S.M. Gruner, Intrinsic curvature hypothesis for biomembrane lipid composition: a role for non-bilayer lipids, Proc. Natl. Acad. Sci. U. S. A. 82 (1985) 3665–3669.
[197] D. Marsh, Intrinsic curvature in normal and inverted lipid structures and in membranes, Biophys. J. 70 (1996) 2248–2255.
[198] D. Marsh, Nonlamellar packing parameters for diacylglycerols, Biophys. J. 72 (1997) 2834–2836.
[199] R.P. Rand, N.L. Fuller, S. Gruner, V.A. Parsegian, Membrane curvature, lipid segregation, and structural transitions for phospholipids under dual-solvent stress, Biochemistry 29 (1990) 76–87.
[200] S. Leikin, M.M. Kozlov, N.L. Fuller, R.P. Rand, Measured effects of diacylglycerol on structural and elastic properties of phospholipid membranes, Biophys. J. 71 (1996) 2623–2632.
[201] G.L. Powell, D. Marsh, Polymorphic phase behaviour of cardiolipin derivatives studied by ^{31}P NMR and X-ray diffraction, Biochemistry 24 (1985) 2902–2908.
[202] J.M. Seddon, R.D. Kaye, D. Marsh, Induction of the lamellar-inverted hexagonal phase transition in cardiolipin by protons and monovalent cations, Biochim. Biophys. Acta 734 (1983) 347–352.
[203] M.B. Sankaram, G.L. Powell, D. Marsh, Effect of acyl chain composition on salt-induced lamellar to inverted hexagonal phase transitions in cardiolipin, Biochim. Biophys. Acta 980 (1989) 389–392.
[204] D. Marsh, J.M. Seddon, Gel-to-inverted hexagonal (L_β–H_{II}) phase transitions in phosphatidylethanolamines and fatty acid-phosphatidylcholine mixtures, demonstrated by ^{31}P NMR spectroscopy and X-ray diffraction, Biochim. Biophys. Acta 690 (1982) 117–123.
[205] G. Cevc, J.M. Seddon, D. Marsh, The mechanism of regulation of membrane phase behaviour, structure and interactions by lipid headgroups and electrolyte solution, Faraday Discuss. Chem. Soc. 81 (1986) 179–189.
[206] J.M. Seddon, R.H. Templer, N.A. Warrender, Z. Huang, G. Cevc, D. Marsh, Phosphatidylcholine-fatty acid membranes: effects of headgroup hydration on the phase behaviour and structural parameters of the gel and inverse hexagonal (H_{II}) phases, Biochim. Biophys. Acta 1327 (1997) 131–147.
[207] Y.V.S. Rama Krishna, D. Marsh, Spin label ESR and ^{31}P-NMR studies of the cubic and inverted hexagonal phases of dimyristoylphosphatidylcholine/myristic acid (1:2, mol/mol) mixtures, Biochim. Biophys. Acta 1024 (1990) 89–94.
[208] T. Heimburg, N.J.P. Ryba, U. Würz, D. Marsh, Phase transition from a gel to a fluid phase of cubic symmetry in dimyristoylphosphatidylcholine/myristic acid (1:2, mol/mol) bilayers, Biochim. Biophys. Acta 1025 (1990) 77–81.
[209] T. Heimburg, U. Würz, D. Marsh, Binary phase diagram of hydrated dimyristoylglycerol-dimyristoyl phosphatidylcholine mixtures, Biophys. J. 63 (1992) 1369–1378.
[210] M.J. Swamy, M. Ramakrishnan, D. Marsh, U. Würz, Miscibility and phase behaviour of binary mixtures of *N*-palmitoylethanolamine and dipalmitoylphosphatidylcholine, Biochim. Biophys. Acta 1616 (2003) 174–183.
[211] R. Kamlekar, S. Satyanarayana, D. Marsh, M.J. Swamy, Miscibility and phase behavior of *N*-acylethanolamine/diacylphosphatidylethanolamine binary mixtures of matched acyl chainlengths (n = 14, 16), Biophys. J. 92 (2007) 3968–3977.
[212] M.J. Swamy, U. Würz, D. Marsh, Structure of vitaminylated lipids in aqueous dispersion: X-ray diffraction and ^{31}P NMR studies of *N*-biotinyl phosphatidylethanolamines, Biochemistry 32 (1993) 9960–9967.
[213] M.J. Swamy, U. Würz, D. Marsh, Phase polymorphism, molecular interactions, and miscibility of binary mixtures of dimyristoyl-*N*-biotinylphosphatidylethanolamine with dimyristoyl phosphatidylcholine, Biochemistry 34 (1995) 7295–7302.

[214] D. Marsh, M.J. Swamy, Derivatised lipids in membranes. Physicochemical aspects of *N*-biotinyl phosphatidylethanolamines, *N*-acyl phosphatidylethanolamines and *N*-acyl ethanolamines, Chem. Phys. Lipids 105 (2000) 43–69.
[215] K. Schorn, D. Marsh, Lipid chain dynamics and molecular location of diacylglycerol in hydrated binary mixtures with phosphatidylcholine: spin label ESR studies, Biochemistry 35 (1996) 3831–3836.
[216] M.D. King, D. Marsh, Polymorphic phase behaviour of lysopalmitoylphosphatidylcholine in poly(ethylene glycol)-water mixtures, Biochemistry 28 (1989) 5643–5647.
[217] D. Marsh, Scaling and mean-field theories applied to polymer brushes, Biophys. J. 86 (2004) 2630–2633.
[218] M. Esmann, N.U. Fedosova, D. Marsh, Osmotic stress and viscous retardation of the Na,K-ATPase ion pump, Biophys. J. (in press). doi:10.1529/biophysj.106.101774
[219] D. Marsh, Water adsorption isotherms and hydration forces for lysolipids and diacyl phospholipids, Biophys. J. 55 (1989) 1093–1100.
[220] T.F. Taraschi, B. De Kruijff, A.J. Verkleij, C.J.A. Van Echteld, Effect of glycophorin on lipid polymorphism: A ^{31}P NMR study, Biochim. Biophys. Acta 685 (1982) 153–161.
[221] T.F. Taraschi, B. De Kruijff, A.J. Verkleij, The effect of an integral membrane protein on lipid polymorphism in the cardiolipin Ca^{2+} system, Eur. J. Biochem. 129 (1983) 621–625.
[222] A. Rietveld, T.J.J.M. Van Kemenade, T. Hak, A.J. Verkleij, B. De Kruijff, The effect of cytochrome *c* oxidase on lipid polymorphism of model membranes containing cardiolipin, Eur. J. Biochem. 164 (1987) 137–140.
[223] G.L. Powell, P.F. Knowles, D. Marsh, Incorporation of cytochrome oxidase into cardiolipin bilayers and induction of non-lamellar phases, Biochemistry 29 (1990) 5127–5132.
[224] W.J. de Grip, E.H.S. Drenthe, C.J.A. Van Echteld, B. De Kruijff, A.J. Verkleij, Possible role of rhodopsin in maintaining bilayer structure in the photoreceptor membrane, Biochim. Biophys. Acta 558 (1979) 330–337.
[225] L.C.P.J. Mollevanger, W.J. de Grip, Phase behavior of isolated photoreceptor membrane lipids is modulated by bivalent cations, FEBS Lett. 169 (1984) 256–260.
[226] M. Esmann, D. Marsh, Influence of Na,K-ATPase on membrane lipid polymorphism, (in press).
[227] I. Ekiel, D. Marsh, B.W. Smallbone, M. Kates, I.C.P. Smith, The state of the lipids in the purple membrane of *Halobacterium cutirubrum* as seen by ^{31}P-NMR, Biochem. Biophys. Res. Commun. 100 (1981) 105–110.
[228] J.A. Killian, I. Salemink, M.R.R. de Planque, G. Lindblom, R.E. Koeppe II, D.V. Greathouse, Induction of nonbilayer structures in diacylphosphatidylcholine model membranes by transmembrane α-helical peptides: importance of hydrophobic mismatch and proposed role of tryptophans, Biochemistry 35 (1996) 1037–1045.
[229] P.C.A. van der Wel, T. Pott, S. Morein, D.V. Greathouse, R.E. Koeppe II, J.A. Killian, Tryptophan-anchored transmembrane peptides promote formation of nonlamellar phases in phosphatidylethanolamine model membranes in a mismatch-dependent manner, Biochemistry 39 (2000) 3124–3133.
[230] M.R.R. de Planque, J.-W.P. Boots, D.T.S. Rijkers, R.M.J. Liskamp, D.V. Greathouse, J.A. Killian, The effects of hydrophobic mismatch between phosphatidylcholine bilayers and transmembrane alpha-helical peptides depend on the nature of interfacially exposed aromatic and charged residues, Biochemistry 41 (2002) 8396–8404.
[231] B. De Kruijff, P.R. Cullis, Cytochrome *c* specifically induces non bilayer structures in cardiolipin-containing model membranes, Biochim. Biophys. Acta 602 (1980) 477–490.
[232] P.J.R. Spooner, A. Watts, Reversible unfolding of cytochrome *c* upon interaction with cardiolipin bilayers. 2. Evidence from phosphorus-31 NMR measurements, Biochemistry 30 (1991) 3880–3885.
[233] T. Heimburg, P. Hildebrandt, D. Marsh, Cytochrome *c*–lipid interactions studied by resonance Raman and ^{31}P NMR spectroscopy. Correlation between the conformational changes of the protein and the lipid bilayer, Biochemistry 30 (1991) 9084–9089.
[234] T. Heimburg, R.L. Biltonen, Thermotropic behavior of dimyristoylphosphatidylglycerol and its interaction with cytochrome c,, Biochemistry 33 (1994) 9477–9488.
[235] M.F. Schneider, D. Marsh, W. Jahn, B. Kloesgen, T. Heimburg, Network formation of lipid membranes: triggering structural transitions by chain melting, Proc. Natl. Acad. Sci. U. S. A. 96 (1999) 14312–14317.
[236] P. Mariani, V. Luzzati, H. Delacroix, Cubic phases of lipid-containing systems—structure analysis and biological implications, J. Mol. Biol. 204 (1988) 165–188.
[237] P. Hildebrandt, T. Heimburg, D. Marsh, Quantitative conformational analysis of cytochrome *c* bound to phospholipid vesicles studied by resonance Raman spectroscopy, Eur. Biophys. J. 18 (1990) 193–201.
[238] T. Heimburg, D. Marsh, Investigation of secondary and tertiary structural changes of cytochrome *c* in complexes with anionic lipids using amide hydrogen exchange measurements: an FTIR study, Biophys. J. 65 (1993) 2408–2417.
[239] A. Johannsson, C.A. Keightley, G.A. Smith, C.D. Richards, T.R. Hesketh, J.C. Metcalfe, The effect of bilayer thickness and *n*-alkanes on the activity of the (Ca^{2+}+Mg^{2+})-dependent ATPase of sarcoplasmic reticulum, J. Biol. Chem. 256 (1981) 1643–1650.
[240] A. Johannsson, G.A. Smith, J.C. Metcalfe, The effect of bilayer thickness on the activity of Na^++K^+-ATPase, Biochim. Biophys. Acta 641 (1981) 416–421.
[241] C. Montecucco, G.A. Smith, F. Dabbeni-Sala, A. Johannsson, Y.M. Galante, R. Bisson, Bilayer thickness and enzymatic activity in the mitochondrial cytochrome *c* oxidase and ATPase complex, FEBS Lett. 144 (1982) 145–148.
[242] F. Dumas, J.F. Tocanne, G. Leblanc, M.C. Lebrun, Consequences of hydrophobic mismatch between lipids and melibiose permease on melibiose transport, Biochemistry 39 (2000) 4846–4854.
[243] F. Cornelius, Modulation of Na,K-ATPase by phospholipids and cholesterol. I. Steady-state kinetics, Biochemistry 40 (2001) 8842–8851.
[244] E. Perozo, A. Kloda, D.M. Cortes, B. Martinac, Physical principles underlying the transduction of bilayer deformation forces during mechanosensitive channel gating, Nat. Struct. Biol. 9 (2002) 696–703.
[245] D. Marsh, Energetics of hydrophobic matching in lipid–protein interactions, Biophys. J. 94 (2008) 3996–4013.
[246] I.M. Williamson, S.J. Alvis, J.M. East, A.G. Lee, Interactions of phospholipids with the potassium channel KcsA, Biophys. J. 83 (2002) 2026–2038.
[247] A.M. Powl, J.M. East, A.G. Lee, Lipid–protein interactions studied by introduction of a tryptophan residue: the mechanosensitive channel MscL, Biochemistry 42 (2003) 14306–14317.
[248] N. Kučerka, S. Tristram-Nagle, J.F. Nagle, Structure of fully hydrated fluid phase lipid bilayers with monounsaturated chains, J. Membr. Biol. 208 (2005) 193–202.
[249] D. Marsh, Comment on interpretation of mechanochemical properties of lipid bilayer vesicles from the equation of state or pressure–area measurement of the monolayer at the air–water or oil–water interface, Langmuir 22 (2006) 2916–2919.
[250] M.D. King, D. Marsh, Headgroup and chain length dependence of phospholipid self-assembly studied by spin-label electron spin resonance, Biochemistry 26 (1987) 1224–1231.
[251] M.M. Sperotto, O.G. Mouritsen, Dependence of lipid-membrane phase transition temperature on the mismatch of protein and lipid hydrophobic thickness, Eur. Biophys. J. Biophys. Lett. 16 (1988) 1–10.
[252] E. Perozo, D.M. Cortes, P. Sompornpisut, A. Kloda, B. Martinac, Open channel structure of MscL and the gating mechanism of mechanosensitive channels, Nature 318 (2002) 942–948.
[253] S.I. Sukharev, W.J. Sigurdson, C. Kung, F. Sachs, Energetic and spatial parameters for gating of the bacterial large conductance mechanosensitive channel, MscL, J. Gen. Physiol. 113 (1999) 525–539.
[254] N. Kučerka, Y. Liu, N. Chu, H.I. Petrache, S. Tristram-Nagle, J.F. Nagle, Structure of fully hydrated fluid phase DMPC and DLPC lipid bilayers using x-ray scattering from oriented multilamellar arrays and from unilamellar vesicles, Biophys. J. 88 (2005) 2626–2637.
[255] N. Kučerka, S. Tristram-Nagle, J.F. Nagle, Structure of fully hydrated fluid phase lipid bilayers with monounsaturated chains, J. Membr. Biol. 208 (2006) 193–202.
[256] A.L. Lomize, I.D. Pogozheva, M.A. Lomize, H.I. Mosberg, Positioning of proteins in membranes: a computational approach, Protein Sci. 15 (2006) 1318–1333.

[257] D. Marsh, Polarity and permeation profiles in lipid membranes, Proc. Natl. Acad. Sci. U. S. A. 98 (2001) 7777–7782.
[258] R.N.A.H. Lewis, N. Mak, R.N. McElhaney, A differential scanning calorimetric study of the thermotropic phase behavior of model membranes composed of phosphatidylcholines containing linear saturated fatty acyl chains, Biochemistry 26 (1987) 6118–6126.
[259] H. Schindler, J. Seelig, Deuterium order parameters in relation to thermodynamic properties of a phospholipid bilayer—statistical mechanical interpretation, Biochemistry 14 (1975) 2283–2287.
[260] W. Helfrich, Elastic properties of lipid bilayers: theory and possible experiments, Z. Naturforsch. 28c (1973) 693–703.
[261] E.A. Evans, Bending resistance and chemically induced moments in membrane bilayers, Biophys. J. 14 (1974) 923–931.
[262] S.L. Keller, S.M. Bezrukov, S.M. Gruner, M.W. Tate, I. Vodyanoy, V.A. Parsegian, Probability of alamethicin conductance states varies with nonlamellar tendency of bilayer phospholipids, Biophys. J. 65 (1993) 23–27.
[263] J.R. Lewis, D.S. Cafiso, Correlation between the free energy of a channel-forming voltage-gated peptide and the spontaneous curvature of bilayer lipids, Biochemistry 38 (1999) 5932–5938.
[264] A.R. Curran, R.H. Templer, P.J. Booth, Modulation of folding and assembly of the membrane protein bacteriorhodopsin by intermolecular forces within the lipid bilayer, Biochemistry 38 (1999) 9328–9336.
[265] G.S. Attard, R.H. Templer, W.S. Smith, A.N. Hunt, S. Jackowski, Modulation of CTP:phosphocholine cytidylyltransferase by membrane curvature elastic stress, Proc. Natl. Acad. Sci. U. S. A. 97 (2000) 9032–9036.
[266] A.V. Botelho, N.J. Gibson, R.L. Thurmond, Y. Wang, M.F. Brown, Conformational energetics of rhodopsin modulated by nonlamellar-forming lipids, Biochemistry 41 (2002) 6354–6368.
[267] H. Hong, L.K. Tamm, Elastic coupling of integral membrane protein stability to lipid bilayer forces, Proc. Natl. Acad. Sci. U. S. A. 101 (2004) 4065–4070.
[268] W. Helfrich, Amphiphilic mesophases made of defects, in: R. Balian, M. Kléman, J.P. Poirier (Eds.), Physics of Defects, North-Holland Publishing Company, Amsterdam, 1981, pp. 716–755.
[269] D. Marsh, Elastic constants of polymer-grafted lipid membranes, Biophys. J. 81 (2001) 2154–2162.
[270] C.R. Cantor, Lateral pressures in cell membranes: a mechanism for modulation of protein function, J. Phys. Chem., B 101 (1997) 1723–1725.
[271] A.G. Lee, How lipids affect the activities of integral membrane proteins, Biochim. Biophys. Acta 1666 (2004) 62–87.
[272] C. Nielsen, M. Goulian, O.S. Andersen, Energetics of inclusion-induced bilayer deformations, Biophys. J. 74 (1998) 1966–1983.
[273] T.A. Harroun, W.T. Heller, T.M. Weiss, L. Yang, H.W. Huang, Theoretical analysis of hydrophobic matching and membrane-mediated interactions in lipid bilayers containing gramicidin, Biophys. J. 76 (1999) 3176–3185.
[274] C.R. Cantor, The influence of membrane lateral pressures on simple geometric models of protein conformational equilibria, Chem. Phys. Lipids 101 (1999) 45–56.
[275] S.J. Allen, A.R. Curran, R.H. Templer, W. Meijberg, P.J. Booth, Controlling the folding efficiency of an integral membrane protein, J. Mol. Biol. 342 (2004) 1293–1304.
[276] D. Marsh, Elastic curvature constants of lipid monolayers and bilayers, Chem. Phys. Lipids 144 (2006) 146–159.
[277] P. Moe, P. Blount, Assessment of potential stimuli for mechano-dependent gating of MscL: effects of pressure, tension, and lipid headgroups, Biochemistry 44 (2005) 12239–12244.
[278] D. Schmidt, Q.X. Jiang, R. MacKinnon, Phospholipids and the origin of cationic gating charges in voltage sensors, Nature 444 (2006) 775–779.
[279] Y.F. Liu, J.F. Nagle, Diffuse scattering provides material parameters and electron density profiles of biomembranes, Phys. Rev. E 69 (2004) 040901–1–040901-4.
[280] D. Marsh, A. Watts, W. Maschke, P.F. Knowles, Protein-immobilized lipid in dimyristoylphosphatidylcholine-substituted cytochrome oxidase: evidence for both boundary and trapped-bilayer lipid, Biochem. Biophys. Res. Commun. 81 (1978) 403–409.
[281] D. Marsh, T. Páli, Infrared dichroism from the x-ray structure of bacteriorhodopsin, Biophys. J. 80 (2001) 305–312.
[282] R.E. Stenkamp, S. Filipek, C.A.G.G. Driessen, D.C. Teller, K. Palczewski, Crystal structure of rhodopsin: a template for cone visual pigments and other G protein-coupled receptors, Biochim. Biophys. Acta 1565 (2002) 168–182.
[283] W. Rawicz, K.C. Olbrich, T. McIntosh, D. Needham, E. Evans, Effect of chain length and unsaturation on elasticity of lipid bilayers, Biophys. J. 79 (2000) 328–339.
[284] R.H. Templer, B.J. Khoo, J.M. Seddon, Gaussian curvature modulus of an amphiphilic monolayer, Langmuir 14 (1998) 7427–7434.